TRACTION IN EHL-CONTACTS - THE INFLUENCE OF LOCAL FLUID RHEOLOGY AND TEMPERATURES

Von der Fakultät für Maschinenbau
der Gottfried Wilhelm Leibniz Universität Hannover
zur Erlangung des akademischen Grades
Doktor-Ingenieur
genehmigte Dissertation

von

Dipl.-Ing.
NORBERT FRITZ BADER

geboren am 01.05.1985
in Pretoria

2018

ABSTRACT

The traction in concentrated contacts is governed by the fluid rheology. While the film formation has been well understood and its relation to the physical lubricant properties have been shown, the rheology governing the lubricant behaviour within elastohydrodynamic lubricated (EHL) contacts still poses numerous challenges.

The limit of the traction transferable through a concentrated contact is governed by the lubricant property limiting shear stress. The behaviour of the limiting shear stress is evaluated by examining data from traction experiments. It is found that a linear relationship of pressure and maximum shear stress exists. The problem of using an integral contact is addressed by using data gained from a specialised experiment with homogeneous pressure. This shows the same pressure limiting shear stress relation. Thus the traction experiments are assumed a valid basis for extracting pressure limiting shear stress data.

From the observations in the experiments a limiting shear stress relation is formulated and abstracted for several lubricants. This relation is subsequently implemented in a computational routine.

The temperature dependence of the limiting shear stress is investigated by measurements of body temperature and by obtaining temperature maps of the contact through thermography. It can be found, that a small temperature dependence of the limiting shear stress may be present. However, when including the temperature maps into computations it is shown that the effect of temperature on viscosity outweighs possible influences of temperature on the limiting shear stress. Furthermore, the knowledge of local temperatures makes the solution of the energy equation for a local temperature calculation unnecessary thus allowing for faster computations with the real temperatures.

This is backed further by implementing several different viscosity models which are all based on identical high pressure viscometry data. It can be shown that the viscosity model influences the traction results substantially.

Thus this work aims to achieve the following goals: Shed light on the true fluid behaviour in the EHL contact, point out the influence of temperature on the limiting shear stress, and further enhance a simple numerical model of the limiting shear stress for use in computations.

ZUSAMMENFASSUNG

Die Reibung in hochbelasteten elastohydrodynamisch geschmierten Kontakten (EHD) wird von der Schmierstoffrheologie beherrscht. Während die Mechanismen die zur Schmierfilmbildung führen und die Zusammenhänge mit physikalischen Schmierstoffeigenschaften bereits erforscht und zufriedenstellend geklärt sind, ist das rheologische Verhalten der Schmierstoffe in den Kontakten weiterhin nicht ausreichend geklärt.

Die maximale Schubspannung/Traktion die durch den Schmierfilm eines hochbelasteten EHD Kontaktes transferiert wird ist eine Schmierstoffabhängige Größe: Die Grenzschubspannung. Das Verhalten der Grenzschubspannung wurde mithilfe von Traktionsversuchen untersucht. Ein linearer Zusammenhang zwischen Druck und Grenzschubspannung konnte bestätigt werden. Da es sich bei der Traktionsmessung um eine Messung an einem integrierenden EHD Kontakt handelt wurden die Ergebnisse mit Versuchen aus einem Experiment mit homogener Druckverteilung abgeglichen. Es konnte gezeigt werden, dass die Ergebnisse aus Traktionsmessungen und Laborexperiment diesselben Werte liefern. Daraus wurde abgeleitet, dass eine Nutzung von Traktionsexperimenten zulässig ist um die Grenzschubspannung zu ermitteln.

Aus den Messwerten wird eine Druckabhängigkeit der Grenzschubspannung abstrahiert und diskutiert. Weiterhin wird diese Relation in einer Berechungsroutine umgesetzt.

Die Temperaturabhängigkeit der Grenzschubspannung wird mittels Massentemperaturmessungen und flächigen Thermografiemessungen untersucht. Es kann eine kleine Temperaturabhängigkeit der Grenzschubspannung ermittelt werden. Durch die Thermografiemessungen zeigen sich jedoch die Einflüsse auf Viskosität dominant. Durch die Kenntnis der lokalen Temperaturen kann eine schnelle Berechnungsroutine entwickelt werden, die es ermöglicht zeitsparend mit den vorliegenden Temperaturen zu rechnen.

Weiterhin wurden weiter Viskositätsmodelle rechnerisch betrachtet und stützen die Beobachtung, dass die maximal Schubspannung im Kontakt vornehmlich durch das Viskositäts Temperatur Verhalten begrenzt werden, die Grenzschubspannung aber davon unberührt bleibt.

Diese Arbeit bildet einen Beitrag bei der Beantwortung der Frage wie sich das Fluid im EHD Kontakt verhält, sie zeigt den Einfluss der Temperatur auf die Grenzschubspannung und entwickelt eine einfache Berechnungsvorschrift zur überschlägigen Traktionsberechnung weiter.

*All we have to decide is
what to do with the time that is given us.*

— Gandalf
— J. R. R. Tolkien,
The Fellowship of the Ring (Tolkien, 1954)

ACKNOWLEDGMENTS

CONTENTS

LIST OF FIGURES

LIST OF TABLES

NOMENCLATURE

A_{HERTZ} HERTZian contact area in m^2

a greater half-width of contact ellipse in m

α^* pressure viscosity coefficient in Pa^{-1}

α_ϱ density temperature coefficient in kg/m^{3}K

b lesser half-width of contact ellipse in m

β_{th} temperature viscosity coefficient

C_{th} thermal correction factor

C_a, C_b pressure coefficients for density model Eq. 2.30 in Pa^{-1}

C_{RS} correction factor for minimum film thickness for full film lubrication

De DEBORAH number

δ mutual approach in m

E^*, E' equivalent elastic modulus in Pa

E elastic modulus in Pa

E_A activation energy in J/mol

$\mathcal{E}$ complete elliptical integral of second order

η viscosity in Pas

F force in N

f friction coefficient sometimes in German literature denominated as μ

$\mathcal{F}$ complete elliptical integral of first order

G dimensionless material parameter

G shear modulus in Pa (Note: in literature in the CARREAU equation the parameter G is sometimes used. In this work this parameter is always refered to as τ_c)

G'' component of the dynamic shear modulus in phase with the shear strain in Pa. Sometimes denoted as G' in literature.

G_∞ limiting high rate shear modulus of the liquid in Pa

g_E, g_V elasticity and viscosity parameter

Γ inlet WEISSENBERG number

γ shear

$\dot{\gamma}$ shear rate in 1/s

H dimensionless film thickness

h film thickness in m

K isothermal bulk modulus in Pa

K_0 isothermal bulk modulus at $p = 0$ in Pa

K_0' pressure rate of change of isothermal bulk modulus at $p = 0$

k ratio of half-widths or ellipticity parameter

k_{th} thermal conductivity in W/mK

L_{th} thermal load factor

l length of line contact in m

Λ hydrodynamic roughness parameter

λ film thickness ratio

λ characteristic time of a molecule to realign due to Brownian motion

n power law exponent of the fluid

ν Poisson's ratio

μ_0 low shear viscosity at ambient pressure in Pas

μ_2 second Newtonian viscosity in Pas

P, P_e dimensionless pressure

$\bar{p}, p_0$ mean pressure in Pa

p_Hertz Hertzian pressure in Pa

ϕ_st shear thinning correction factor

Q load on contact in N

R composite radius in m

R_g universal gas constant $8.314\,459\,8\,\mathrm{J/molK}$

R_q root mean squared roughness in µm

R_K core roughness in µm

R_vk reduced valley depth in µm

R_pk reduced peak height in µm

R_Z average maximum height in µm

r curvature radius in m

ρ curvature in $1/\mathrm{m}$

ϱ density in $\mathrm{kg/m^3}$

ϱ_0 density at $15\,°\mathrm{C}$ and ambient pressure in $\mathrm{kg/m^3}$

SRR, S slide to roll ratio

σ composite root mean square roughness in µm

T temperature in K

τ shear stress in $\mathrm{N/m^2}$

τ_c critical shear stress in Pa

τ_E	EYRING stress in Pa
τ_{lim}	limiting shear stress in Pa
$\bar{\tau}$	integral shear stress in EHL contact
τ_{max}	maximum shear stress from integral EHL contact
U	dimensionless speed parameter
V	sum of speeds in entrainment direction and perpendicular to entrainment
V	volume at T and p in m^3
V_0	volume at $p = 0$ in m^3
$v, \bar{u}$	entrainment velocity in m/s
W	dimensionless load parameter
Wi	WEISSENBERG number

SUBSCRIPTS

cen	central
e	effective
el	elastic
fric	friction
isoth	isothermal
max	maximum
min	minimum
rol	rolling
sl	sliding
sol	solid
th	thermal
x	in x direction
y	in y direction

ABREVIATIONS

EHL	elastohydrodynamic lubrication
HPC	high pressure chamber

INTRODUCTION

The use of lubrication makes machinery operate and can lower energy consumption and reduce wear. Ever since humans have used technical systems (e. g., during building of the pyramids (Dowson, 1998)) lubrication has been used to reduce friction. However, the study and understanding of the mechanisms occurring in lubricated contacts is still a field with a number of unanswered questions. While the mechanism responsible for the build up of lubricant films in highly loaded non-conformal contacts (e. g., rolling element bearings, gears) has only been understood in the midtwentieth century, engineers always strived towards a reduction of wear and losses in these contacts. This mode of lubrication is called elastohydrodynamic lubrication (EHL) and is explained in Sec. 1.2.1.

The wear can be greatly reduced by enabling a lubricant film to form, which is thick enough to separate the rubbing surfaces. The reduction of the losses (termed friction or traction in elastohydrodynamic lubricated contacts) can be influenced by changing the lubricant rheology. However, to enable a prediction of changes and help understand the expected losses and wear during the design process models of the behaviour of the lubricated contacts are needed. Furthermore, during an optimisation process the interaction of the mechanisms must be understood to allow for a full system optimisation without causing interference in one direction, e. g., having low friction through low viscosity lubricants while then causing thin films leading to excessive wear.

1.1 FORMULATION OF PROBLEM

One of the most striking features of EHL contacts is that the film thickness and the traction are independent. The reason being that the film thickness is governed by the inlet region, whilst the traction is dominated by the lubricant properties in the middle of the contact. This leads to the phenomenon that numerous precise models for the film thickness exist whilst models for traction calculation are still debated.

The calculation of traction in these EHL contacts relies on the rheological models used. In this work, results from traction experiments, which form an integration over Hertzian contacts with strongly inhomogeneous conditions, are presented (Sec. 5.1). They are compared to data from laboratory measurements with homogeneous conditions (Sec. 5.2). Due to the fact that the integral data do not directly rep-

resent local rheological fluid properties, further investigations are presented. Here, thermographic measurements are used to discern the contact temperature locally. Furthermore, a model for the maximum shear stress depending on pressure is proposed and compared to existing models. By using these parameters in a simple calculation routine an influence of the parameters is shown, ultimately enabling a further insight into the rheological behaviour of the investigated lubricants.

1.2   CONCENTRATED LUBRICATED CONTACTS

In lubricated contacts, the formation of a separating lubricant film is achieved by hydrodynamic mechanisms (Sec. 2.1). The viscous lubricant is pulled into the contact by the relative movement of the contact partners. Due to a converging gap a pressure builds up in the film in the contact, leading to formation of a film carrying parts or all of the normal load. The lubricating film build-up is influenced substantially by the macroscopic shape of the contact. In the case of conformal conjunctions, found for example in journal bearings, the load and contact shape often do not lead to significant elastic deformation of the contacting bodies, so that the lubricant film formation can be said to be purely hydrodynamic.

In the case of non-conformal or concentrated contacts, found for example in rolling element bearing contacts and gear teeth, the load leads to elastic deformations of the bodies in an order of magnitude of the resulting lubricant film thickness. Furthermore, the pressures encountered in these contacts are significantly higher, in the range of up to 4 GPa. The resulting contact shape is thus governed by the elastic deformation of the contacting bodies as well as the lubricant behaviour. This mechanism is termed elastohydrodynamic lubrication (EHL). The friction in these contacts is the subject of this work.

In the following sections at first the dry contact of non-conformal bodies without tangential forces is introduced. Subsequently, the models governing EHL contacts are discussed.

Contact of non-conforming surfaces

When two bodies with non-conforming surfaces are brought into contact they initially touch in a line (e. g., cylinder on a plane or two cylinders with parallel axes) or in a point (e. g., ball on flat or any two ellipsoids). However, as soon as a load is applied these contact areas turn into finite contact areas.

A well known analytical solution for the contact problem of two non-conforming elastic ellipsoid bodies was presented by HERTZ (1881). A great number of solutions for contact problems are still based on these equations.

When two elastic ellipsoids are pressed together with a normal force Q an elliptical contact forms. This elliptical contact can be described by the major and minor half-width a and b of the ellipse. For the definition of the coordinate system the following conventions are used: The x-y plane is the common tangent plane of the two surfaces and the z axis points into the lower body on the normal of that plane. This coincides with the load direction. The direction of the x axis is chosen so that the radii of curvature are maximised as shown in Fig. 1.2.1, so that:

$$\frac{1}{r_{1y}} + \frac{1}{r_{2y}} > \frac{1}{r_{1x}} + \frac{1}{r_{2x}} \ . \tag{1.1}$$

HERTZ regarded the bodies as elastic half-spaces. He further used the following simplifications to reach a solution of the problem. The dimensions of the contact area must be small compared to the dimensions of the bodies and the relative radii of curvature. The second assumption is based on the necessity of small strains to stay within the scope of linear elastic behaviour. Furthermore, the surfaces are assumed to be frictionless and only normal forces are transmitted between them. The whole system is assumed to be in a state of equilibrium.

The contacting bodies are assumed as isotropic and homogeneous. The following equations are from HAMROCK and DOWSON (1981). The equivalent elastic modulus E^* is then defined as:

$$\frac{1}{E^*} = \frac{1}{2} \left(\frac{1 - \nu_1^2}{E_1} + \frac{1 - \nu_2^2}{E_2} \right) \ , \tag{1.2}$$

whilst the curvature of the bodies $\sum \rho$ (which is the reciprocal composite radius R) is defined as:

$$\sum \rho = \frac{1}{R} = \frac{1}{R_x} + \frac{1}{R_y} = \frac{1}{r_{1x}} + \frac{1}{r_{2x}} + \frac{1}{r_{1y}} + \frac{1}{r_{2y}} \tag{1.3}$$

with convex curvatures defined as negative. The half-widths of the contact area are then:

$$a = \sqrt[3]{\frac{6k^2 \mathcal{E} Q}{\pi \sum \rho E^*}} \tag{1.4}$$

$$b = \sqrt[3]{\frac{6 \mathcal{E} Q}{\pi k \sum \rho E^*}} \tag{1.5}$$

with the elliptic integrals $\mathcal{E}$ and $\mathcal{F}$. The ratio of half-widths or ellipticity parameter:

$$k = \frac{a}{b} \tag{1.6}$$

whilst the mutual approach δ is:

$$\delta = \mathcal{F} \cdot \sqrt[3]{\frac{9\sum\rho}{2\mathcal{E}} \cdot \left(\frac{Q}{\pi k E^*}\right)^2} .$$ (1.7)

From the contact size the mean contact pressure p_0 is:

$$p_0 = \bar{p} = \frac{Q}{A_{\text{HERTZ}}} = \frac{Q}{\pi a b} .$$ (1.8)

The pressure distribution is then:

$$p(x,y) = p_0 \cdot \sqrt{1 - \left(\frac{x}{a}\right)^2 - \left(\frac{y}{b}\right)^2}$$ (1.9)

following from this:

$$p_{\text{HERTZ}} = p_{\text{max}} = \frac{3}{2} \cdot p_0 .$$ (1.10)

The calculation necessitates solving the complete elliptical integrals $\mathcal{F}$ and $\mathcal{E}$ of first and second order.

$$\mathcal{F} = \int_0^{\pi/2} \left[1 - \left(1 - \frac{1}{k^2}\right)\sin^2\varphi\right]^{-1/2} \mathrm{d}\varphi$$ (1.11)

$$\mathcal{E} = \int_0^{\pi/2} \left[1 - \left(1 - \frac{1}{k^2}\right)\sin^2\varphi\right]^{1/2} \mathrm{d}\varphi$$ (1.12)

To speed up numerical solution and avoid lengthy calculations several methods have been proposed. One of these is the use of values looked up from tables (e. g. COOPER, 1969; SCHMELZ and MÜLLER, 2001) making use of parameters dependent on $\cos(\tau)$:

$$\cos(\tau) = \left|\frac{r_{1x} - r_{1y} + r_{2x} - r_{2y}}{\sum\rho}\right| .$$ (1.13)

Another approach was taken by several authors who proposed approximate algebraic expressions in terms of a/b to replace the elliptic integrals (DYSON, 1965; BREWE and HAMROCK, 1977). The method proposed by BREWE and HAMROCK is presented. By using the relation stated by (HARRIS, 1966):

$$J(k) = \sqrt{\frac{2\mathcal{F} - \mathcal{E}(1+\Gamma)}{\mathcal{E}(1-\Gamma)}}$$ (1.14)

and through iteration gaining the ellipticity parameter from:

$$k_{n+1} = J(k_n)$$ (1.15)
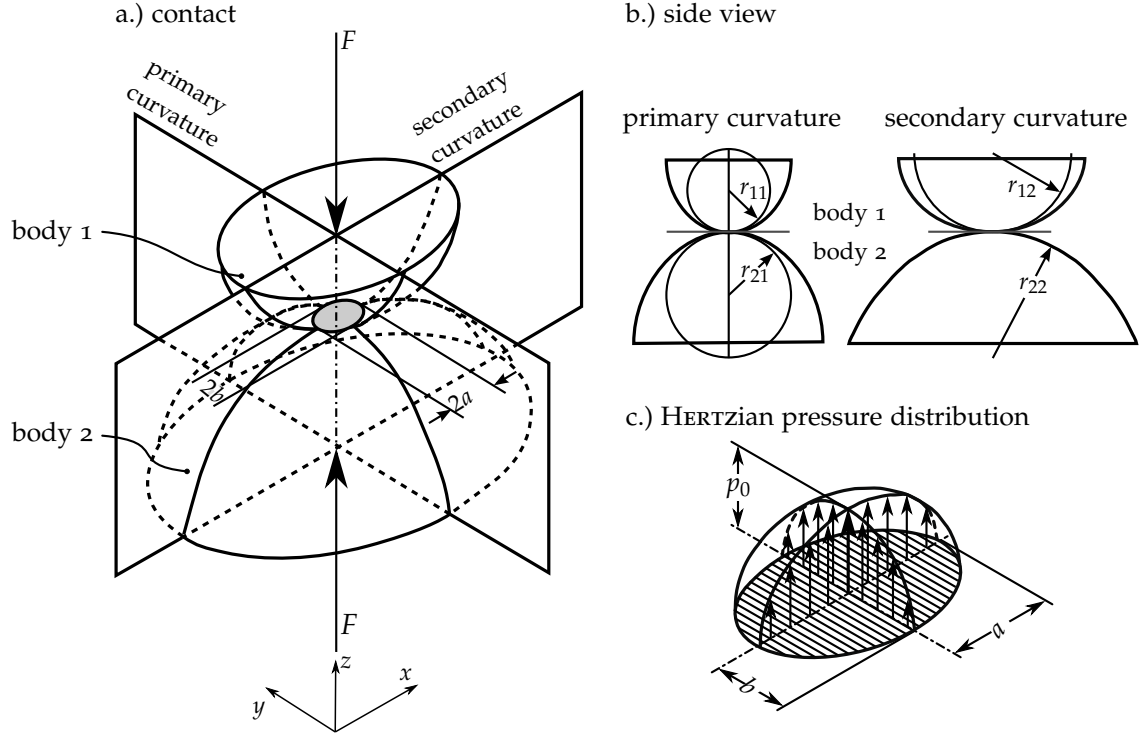
Figure 1.2.1: Contact of two ellipsoids as described by HERTZ

with

$$\Gamma = R \left(\frac{1}{R_x} - \frac{1}{R_y} \right) ,$$

(1.16)

using the composite radius defined in Eq. 1.3. The provided fits for $k, \mathcal{E},$ and $\mathcal{F}$ are denoted by $\bar{k}, \bar{\mathcal{E}}, \bar{\mathcal{F}}$:

$$\bar{k} = 1.0339 \cdot \left(\frac{R_y}{R_x} \right)^{0.6360}$$

(1.17)

$$\bar{\mathcal{E}} = 1.0003 + \frac{0.5968}{R_y/R_x}$$

(1.18)

$$\bar{\mathcal{F}} = 1.5277 + 0.6023 \cdot \ln \frac{R_y}{R_x}$$

(1.19)

These fits are often used in calculations where a solution of the elliptic integrals is deemed too time consuming (e. g. BALY, 2005; BARZ, 1996; WANG, 2015).

1.2.1 *Fundamentals of EHL Contacts*

The lubrication mechanism of contacts in the presence of lubricants can be described by determining the behaviour of the lubricant viscosity as well as the deformation behaviour of the solid surfaces. These can be grouped into four regimes (JOHNSON, 1970):

- *Isoviscous rigid*: The pressure in the film (i.e., contact) is insufficient to cause a notable elastic deformation of the solid. The pressure furthermore does not change the viscosity of the lubricant notably. Typically this regime is encountered in lightly loaded contacts operating at high speeds. The solid can thus be regarded as rigid body.

- *Piezoviscous rigid*: The pressure in the film increases the viscosity of the lubricant, however it is not sufficient to deform the solid bodies. This regime is possible with lubricants that vary viscosity with low pressure changes and relatively high speed (BAIR, 2007).

- *Isoviscous elastic*: The pressure in the film changes the shape of the solids, however the viscosity of the lubricant does not change. This behaviour is encountered if the solids have a low elastic modulus and is referred to as *soft EHL*. The pressure thus changes the shape of the solids but not the viscosity of the lubricant.

- *Pieziviscous elastic*: The pressure within the film both deforms solids and changes the viscosity of the liquid. This regime is called *full elastohydrodynamic* or EHL respectively EHD. This is present in most systems with concentrated contacts lubricated with organic lubricants, e.g., rolling element bearings, traction drives, and gears. This is the regime forming the focus of this work.

To divide these regimes JOHNSON (1970) devised the dimensionless viscosity and elasticity parameters g_V and g_E respectively. For line contacts these are:

$$g_V^2 = \frac{8 \cdot \pi^3 \cdot \alpha^{*2} \cdot p_H^6 \cdot R}{E'^3 \cdot \bar{u} \cdot \mu_0} \tag{1.20}$$

$$g_E^2 = \frac{4 \cdot \pi^2 \cdot p_H^4 \cdot R}{E'^3 \cdot \bar{u} \cdot \mu_0} \tag{1.21}$$

and for point contacts these can be written as:

$$g_V = \frac{\left(\frac{2}{3} \cdot \pi^3\right)^3 \cdot \alpha^* \cdot p_H^9 \cdot R^2}{E'^6 \cdot \bar{u}^2 \cdot \mu_0^2} \tag{1.22}$$

$$g_E = \frac{\left(\frac{2}{3} \cdot \pi^3\right)^{\frac{8}{3}} \cdot p_H^8 \cdot R^2}{E'^6 \cdot \bar{u}^2 \cdot \mu_0^2}. \tag{1.23}$$

With the parameters:

α^* pressure viscosity coefficient (as defined in Eq. 2.56)

E' reduced elastic modulus (Eq. 1.2)

$\bar{u}$ velocity

μ_0 viscosity at ambient pressure $\mu(p = 0)$ (see Sec. 2.3)

p_{H} HERTZian pressure (Eq. 1.10)

R the composite radius (Eq. 1.3)

For point contacts, the ellipticity ratio must also be taken into account as it influences the film formation through flow to the sides of the contact.

Figure 1.2.2 shows these regimes for the line contact depending on the parameters. It must be noted that the borders of the regimes are not strict and thus transition zones between the regimes are indicated. It is visible that with increasing elasticity parameter g_{E} the behaviour changes from rigid to elastic. This transition can happen due to rising HERTZian pressure or decreasing elastic modulus E'. At a rise of the viscosity parameter g_{V} the behaviour changes towards piezoviscous. Here not only the HERTZian pressure and the elastic modulus but also the pressure viscosity coefficient, i. e., viscosity change with pressure, plays an important role.

The focus of the work presented is on elastohydrodynamicly lubricated contacts between bodies with high elastic modulus and thus the piezoviscous regime is the centre of the focus in the following sections.

1.2.2 *Film Thickness and contact geometry*

The flow of the lubricant in EHL contacts can be described by the NAVIER-STOKES equation and the continuity equation. The NAVIER-STOKES equations pose a great challenge to solve and analytical solutions do not exist.

REYNOLDS (1886) deduced from the NAVIER-STOKES equation a usable formulation which could be solved to determine the pressure profile in the lubricating gap. The NAVIER-STOKES equations encompass surface, body, and inertia forces (HAMROCK, 1991). The surface forces act on the surface of a fluid element, whilst the body forces result from external force fields like gravity. The inertia forces are result of the acceleration of the fluid element.

The flow in an EHL contact can be described as slow viscous motion for which REYNOLDS showed that only the pressure and viscous terms are of importance. Thus the NAVIER-STOKES equation is simplified to the REYNOLDS equation when certain assumptions are valid:

$$\frac{\partial}{\partial x}\left(h^3\frac{\partial p}{\partial x}\right) + \frac{\partial}{\partial y}\left(h^3\frac{\partial p}{\partial y}\right) = 6\eta\left(u_1 + u_2\right)\frac{\partial h}{\partial x} + 12\eta\frac{\partial h}{\partial t}. \qquad (1.24)$$

The assumptions limiting the application are:
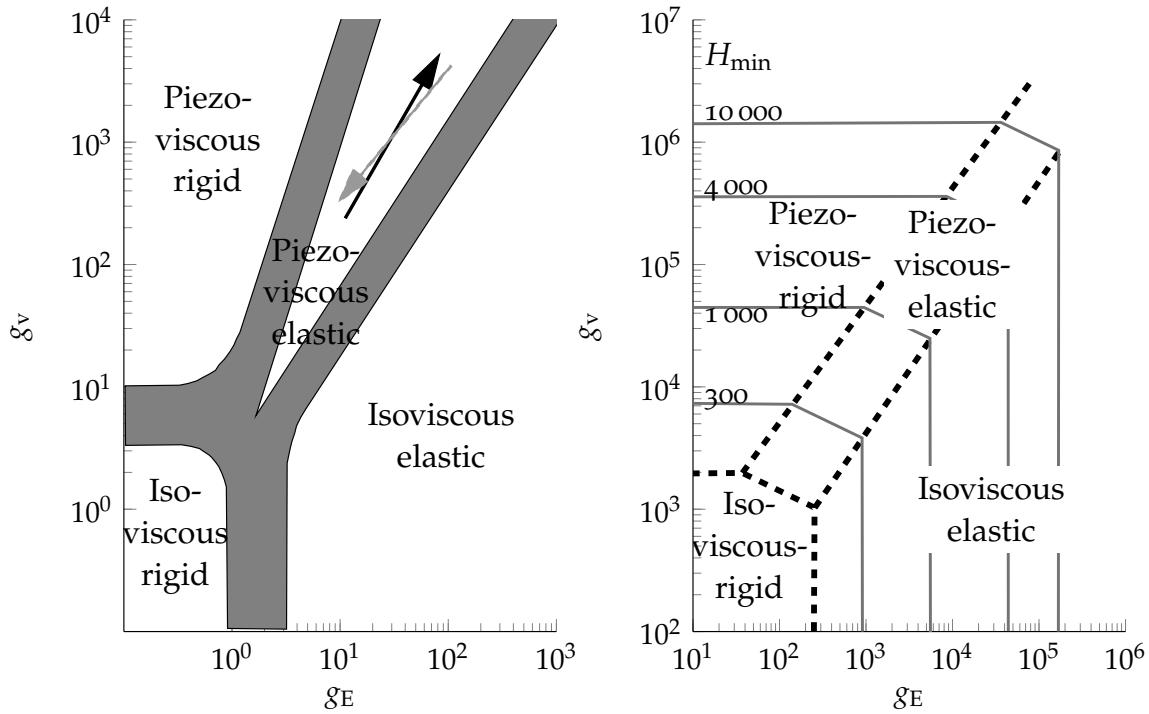
Figure 1.2.2: Regimes of lubrication according to JOHNSON (1970). Left: Diagram for line contacts from WINER and CHENG (1980) and BAIR (2007). The grey arrow (downward pointing) represents a velocity increase from 0.1 to 10 m/s at $p_H = 1$ GPa. The black arrow (upward pointing) shows an increase in HERTZian pressure from 0.6 to 1.6 GPa at 1 m/s. Right: Regimes for point contact with ellipticity ratio $k = 1$ from HAMROCK and DOWSON (1983). Lines of identical dimensionless minimum film thickness are shown.

- constant viscosity and a NEWTONian fluid,

- height of the film thin compared to its length,

- homogeneous properties across height of the lubricant,

- the lubricant is incompressible,

- and the flow is laminar.

The left terms of Eq. 1.24 are often referred to as the POISEUILLE or pressure term and the right side is often referred to as COUETTE term for the first term of the sum and squeeze term for the second.

Formulations have been proposed to incorporate Non-NEWTONian properties, thermal behaviour, and compressibility (DOWSON, 1962; PEIRAN and SHIZHU, 1990b; PEIRAN and SHIZHU, 1990a), thus over-

coming REYNOLD's limitations. Written according to PEIRAN and SHIZHU (1990a):

$$
\frac{\partial}{\partial x}\left[\left(\frac{\varrho}{\eta}\right)_{ey} h^3 \frac{\partial p}{\partial x}\right] + \frac{\partial}{\partial y}\left[\left(\frac{\varrho}{\eta}\right)_{ey} h^3 \frac{\partial p}{\partial y}\right] = \dots
$$
$$
\dots 12\frac{\partial}{\partial x}\left(\varrho_x^* \bar{u} h\right) + 12\frac{\partial}{\partial y}\left(\varrho_y^* \bar{u} h\right) + 12\frac{\partial}{\partial t}\left(\varrho_e h\right) . \tag{1.25}
$$

The local deformations $\delta(x,y)$ of the elastic half space can be described by the BOUSSINESQ equation depending on the local stress (HAMROCK, 1991):

$$
\delta(x,y) = \frac{2}{\pi E'} \int \int_S \frac{p\left(x',y'\right) \mathrm{d}x' \mathrm{d}y'}{\sqrt{\left(x - x'\right)^2 + \left(y - y'\right)^2}}. \tag{1.26}
$$

The film thickness including deformation is given as (LUGT and MORALES-ESPEJEL, 2011):

$$
h(x,y) = h_0 + \frac{x^2}{2R_x} + \frac{y^2}{2R_y} + \delta(x,y) \tag{1.27}
$$

where the second and third term are an approximation of the gap shape and the constant h_0 is the mutual distance of approach found by solving the force balance equation:

$$
m\frac{\partial^2 h_0}{\partial t^2} + \int \int_S p\left(x,y\right) \mathrm{d}x\mathrm{d}y = F(t). \tag{1.28}
$$

To solve the EHL contact problem, i. e., determine $p(x,y)$ and $h(x,y)$, the REYNOLDS equation (Ee. 1.25), the deformation equation (Eq. 1.26), the film shape equation (Eq. 1.27), and the force balance (Eq. 1.28) need to be solved simultaneously. The solution of the coupled system of equations has led to several methods being used. First numerical calculations used GAUSS-SEIDEL iteration schemes (HAMROCK and DOWSON, 1976; CHITTENDEN et al., 1985a; CHITTENDEN et al., 1985b). Subsequent use of the NEWTON-RHAPHSON method saw an increase in computing speed. Further methods used include multi-grid techniques (LUBRECHT, 1987; VENNER, 1991) coupled with multilevel integration (VENNER and LUBRECHT, 2000). Another way to solve the problem has been proposed using computational fluid dynamics (CFD) to solve the NAVIER-STOKES equations instead of the REYNOLDS equation (HARTINGER, 2007; HARTINGER et al., 2008; HAJISHAFIEE, 2013; SRIRATTAYAWONG, 2014). However, these methods require a significant amount of computing power and time and are thus not useful for standard applications yet. Due to rising computing power this method of solving the contact may be applied in greater scale in future. Further methods include finite element, or finite difference schemes applied to the coupled equations. HABCHI (2008) has applied a full system finite element approach, which solves the equations in
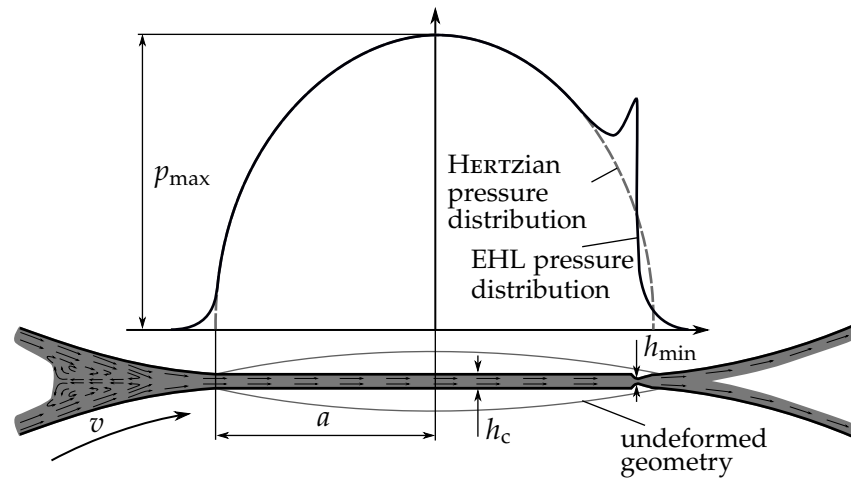
Figure 1.2.3: Results of EHL contact solution showing film profile and pressure. From MEYER (2010b)

an iterative loop where the elastic deformation is replaced by a full body elasticity. Further work presented was focused on the order reduction of the finite element problem enabling a more economic computation (HABCHI and ISSA, 2017).

The solution of the EHL conjunction for a point contact is shown in Fig. 1.2.3 in the mid-plane of the contact. The characteristic difference of the EHL pressure distribution when compared to the HERTZian pressure distribution is the PETRUSEVICH pressure spike caused by the closing gap at the outlet (HAMROCK, 1991). The closing gap results from the observation that the steep gradient of the pressure spike would increase flow rate and thus cause continuity problems if the gap closure was not present. However, the HERTZian pressure distribution is quite similar to the EHL pressure distribution. This can be taken advantage of when very fast calculations with a focus on qualitative behaviour are carried out.

Film Thickness Formulae

A first solution for the central film thickness was presented by ERTEL GRUBIN (1949).

DOWSON and HIGGINSON (1966) used the results obtained from numerical solutions (DOWSON and HIGGINSON, 1959) to develop analytical formulae for the calculation of the central film thickness h_c and the minimum film thickness h_{min} for line contacts with entrainment parallel to the minor half-width of the contact. They assumed the lubricant to be NEWTONian and used an equation of state discussed in Sec. 2.3.1 (Eq. 2.29). Based on this work further analytical formulae have been developed to include point contacts as well as higher

pressure regimes and thermal effects. The following dimensionless constants are used. The speed parameter U is:

$$U = \frac{\eta_0 V}{E'R} \tag{1.29}$$

where the speed V is:

$$V = \sqrt{\bar{u}^2 + \bar{v}^2} \,,$$

and the material parameter G can be written as:

$$G = \alpha E' \,. \tag{1.30}$$

The load parameter W is for point contacts:

$$W = \frac{Q}{E'R_x^2} \quad \text{, and} \quad W = \frac{Q}{lE'R} \tag{1.31}$$

for line contacts. The dimensionless pressure P_e is:

$$P_e = \frac{p}{E'} \,. \tag{1.32}$$

Thus the dimensionless minimum film thickness $H_{\min}$ was defined as:

$$H_{\min} = \frac{h_{\min}}{R_x} = 3.63 U^{0.68} G^{0.49} W^{-0.073} \left(1 - e^{-0.68k}\right). \tag{1.33}$$

With the central film thickness (HAMROCK and DOWSON, 1981):

$$H_c = 2.69 U^{0.67} G^{0.53} W^{-0.067} \left(1 - 0.61 e^{-0.73k}\right). \tag{1.34}$$

CHITTENDEN et al. (1985a) and CHITTENDEN et al. (1985b) derived a formula for arbitrary entrainment direction.

$$H_{\min} = 3.68 \cdot U_e^{0.68} \cdot G^{0.49} \cdot W^{-0.073} \cdot \left\{1 - \exp\left[-0.67 \cdot \left(\frac{R_s}{R_e}\right)^{\frac{2}{3}}\right]\right\} \tag{1.35}$$

$$H_{\text{cen}} = 4.31 \cdot U_e^{0.68} \cdot G^{0.49} \cdot W^{-0.073} \cdot \left\{1 - \exp\left[-1.23 \cdot \left(\frac{R_s}{R_e}\right)^{\frac{2}{3}}\right]\right\} \tag{1.36}$$

where

$$\frac{1}{R_e} = \frac{\cos^2 \theta}{R_x} + \frac{\sin^2 \theta}{R_y} \quad \text{and} \quad \frac{1}{R_s} = \frac{\sin^2 \theta}{R_x} + \frac{\cos^2 \theta}{R_y}$$

whith the effective entrainment velocity u_e

$$u_e = \frac{u}{\cos\theta} = \frac{v}{\sin\theta} \quad \text{and} \quad U_e = \frac{\eta_0 \cdot u_e}{E' \cdot R_e} \ .$$

The equations have been compared to interferometric film thickness measurements and show reasonable agreement for most lubricants (DYSON, NAYLOR and WILSON, 1965; CHAOMLEFFEL, DALMAZ and VERGNE, 2007). However, deviations observed showed lower experimental film thickness than expected for some conditions. This led to an investigation into the inlet shear heating (GREENWOOD and KAUZLARICH, 1973). MURCH and WILSON (1975) used an equation taking into account the viscous heating of the inlet zone to develop a method to corrected the isothermal film thickness using a correction factor C_{th}:

$$h_{0,th} = C_{th} \cdot h_{0,isoth} \tag{1.37}$$

$$h_{min,th} = C_{th} \cdot h_{min,isoth} \tag{1.38}$$

with the correction factor defined as function of the thermal load factor L_{th} from HARRIS (1991):

$$C_{th} = \frac{1}{1 + 0.182 \cdot L_{th}^{0.548}} \tag{1.39}$$

MURCH WILSON give it as

$$C_{th} = \frac{3.94}{3.94 + L_{th}^{0.62}} \tag{1.40}$$

$$L_{th} = \eta_0 \cdot \frac{\beta_{th} \cdot u^2}{k_{th}} \tag{1.41}$$

With β_{th}, k_{th} being the temperature viscosity coefficient and the thermal conductivity of the lubricant respectively and u denominating the surface velocity.

During the formulation of the models NEWTONIAN fluid behaviour was assumed. In the inlet the pressures and the shear rates are still low making this assumption valid for a number of fluids. However, several lubricants exist that already exhibit shear thinning (see Sec. 2.1.4) in the inlet. Thus the the film thickness is influenced by the shear thinning. A factor ϕ_{st} similar to the thermal correction factor to consider the non-NEWTONIAN behaviour was discussed (BAIR and WINER, 1997; BAIR and QURESHI, 2003; BAIR, 2004a) and finally proposed by BAIR (2005) as:

$$\phi_{st}(S, \Gamma) = \left\{ 1 + 0.79 \left[(1 + S)\,\Gamma \right]^{1/(1+0.2S)} \right\}^{3.6(1-n)^{1.7}} \tag{1.42}$$

With Γ the inlet WEISSENBERG[1] number:

$$\Gamma = \frac{\mu_0 u}{h_N G} \qquad (1.43)$$

and n is the power-law exponent for the liquid, h_N the film thickness, S the slide to roll ratio, and G the modulus in Pa. This correction should work for values of $\Gamma < 25$, $\phi_{st} < 8$, and $0 < S < 1$. The values of n are restricted as well and can be taken from BAIR (2005). The parameter was determined in an analysis based on the method of ERTEL-GRUBIN and is thus valid for line contacts. However, based on solutions of the EHL problem factors have been developed for point contacts (KUMAR and KHONSARI, 2008) and second NEWTONIAN viscosities (JANG, KHONSARI and BAIR, 2008; ANURADHA and KUMAR, 2011). From HABCHI et al. (2013) the correction factor is given as:

$$\frac{1}{\phi_{st}} = \left(\frac{\mu_2}{\mu}\right)^a + \left(1 - \left(\frac{\mu_2}{\mu}\right)^a\right)[1 + b\Gamma]^{n-1} \qquad (1.44)$$

for point contacts and lubricants exhibiting shear thinning and a second NEWTONIAN plateau. The parameters a and b were fit to data from two gear oils, three not nearer described oils, and eight motor oils allowing the determination of μ_2/μ. This lead to $a = 0.7589$ and $b = 1.929$ for the central correction factor and $a = 0.9069$ and $b = 2.189$ for minimum correction factor.

STÅHL and JACOBSON (2003) numerically analysed the influence of a variation of the limiting shear stress on the film thickness and found little influence on the minimum film thickness. The film profile in the central region was found to change, however, without influencing the mean central film thickness which agreed with the values predicted by the equations.

CHAOMLEFFEL, DALMAZ and VERGNE (2007) compared measurements with film thickness formulae and found a reasonable agreement for h_c even when using non-NEWTONIAN lubricants and applying the film thickness equations outside their stated domains. However, the minimum film thickness outside the proposed domain of the equations was greatly influenced and could not be predicted for all conditions.

Several further models taking into account different lubricant rheology have been proposed and are still being considered (ANURADHA and KUMAR, 2013).

WHEELER et al. (2016) compare a number of film thickness equations to computations solving the REYNOLDS equation. They state that the agreement for the central film thickness h_c is reasonable for nearly all investigated film thickness formulations. Some shortcomings for heavily loaded contacts with slow entrainment velocity (i. e., low film thickness) were found. They recommend the use of

---

1 Note that the WEISSENBERG number is similar to the DEBORAH number and sometimes used to characterise the visco-elastic regime as being predominantly viscous or elastic.

the CHITTENDEN formulation for h_c and of the NIJENBANNING model for h_{min}. Although the equations describing the film thickness have been developed several decades ago their use is still widespread and reasonable due to the fact that good predictions of film thickness are possible with negligible computing time.

Typical central film thickness values for EHL contacts are in the range of 100 nm to 2 µm in hard EHL contacts.

2

FRICTION AND LUBRICANT BEHAVIOUR

2.1 FRICTION IN LUBRICATED CONTACTS

The determination of friction forces has been investigated for a long time. The friction occurring in tribological contacts can be classified by the contact pairs and mechanisms involved. It is normally divided into three categories in lubricated systems. Dry friction (direct contact exists between asperities of the solid bodies in contact), boundary friction (i. e., friction between boundary layers or ultra thin films of lubricant) and fluid film lubrication, i. e., friction originates within a fluid film separating the surfaces of the contact bodies. When the film separation does not suffice to prevent all asperity contact the condition is referred to as mixed friction and models often use a sum of dry and lubricated friction models.
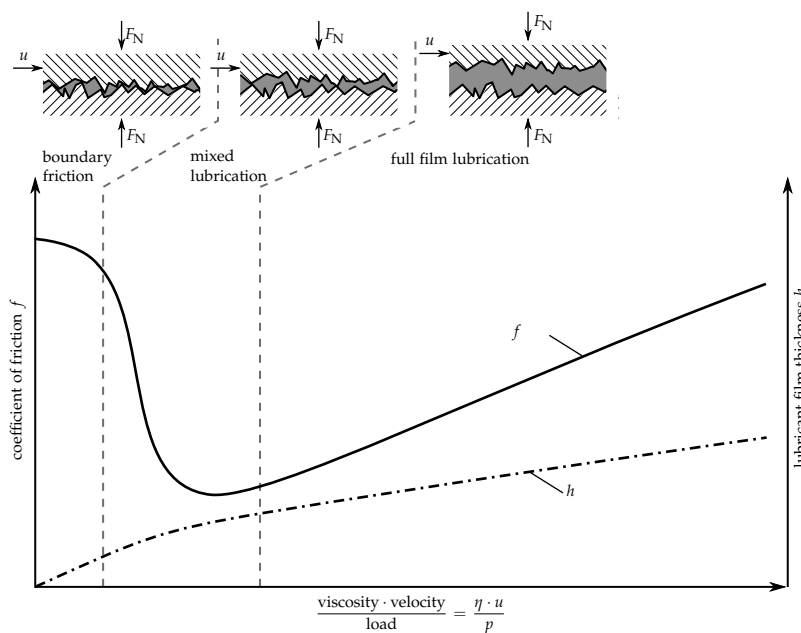
Figure 2.1.1: The STRIBECK curve

The friction coefficient f in the three regimes is usually depicted dependent of entrainment speed v, viscosity η, and the inverse contact pressure p in the STRIBECK curve which is shown in Fig. 2.1.1. The dimensionless parameter $v \cdot \eta / p$ is directly related to the hydrodynamic film thickness h in the contact provided there is a wedge shaped geometry. The friction regimes are characterised as follows:

- Boundary friction: The contact takes place between the roughness asperities of the boundary layers. The lubricant has not yet formed a load carrying hydrodynamic film. The friction is governed by mechanical interaction between the boundary layers and possibly the shearing of very thin lubricant films between asperities.

- Mixed friction: A hydrodynamic film is formed, however, asperity contacts still occur. The load of the contact is shared between the asperity contacts and the lubricant film. The friction is determined by both shearing losses in the lubricant and mechanical interactions of the asperities.

- Full film or fluid friction: The fluid film supports the contact load. The friction is only the result of shearing of the lubricant. No asperity contacts occur.

A special case of friction occurs when absolutely no lubricant is present. The so called dry friction between the asperities of the surfaces is then a result of adhesive forces and deformations.

2.1.1 *Lambda ratio*

To determine the lubrication regime a lubricated contact is running in, often the film thickness ratio λ is used. This ratio is defined as the ratio of the average film thickness h_a and the composite root mean square roughness σ or standard deviation of the roughness profiles (ZHU and WANG, 2012).

$$\lambda = \frac{h_a}{\sigma} \tag{2.1}$$

where

$$\sigma = \sqrt{R_{q1}^2 + R_{q2}^2} \tag{2.2}$$

for statistically independent roughness profiles. It needs to be pointed out that often the hydrodynamic roughness parameter Λ is used interchangeably:

$$\Lambda = \frac{h_{cs}}{\sigma} \tag{2.3}$$

where h_{cs} is the central film thickness of ideally smooth surfaces, e.g g., determined from one of the equations in Sec. 1.2.2. Sometimes the minimal film thickness is used as well (KREIL, 2007; BARTEL, 2010; MAYER, 2013). Several authors also use different definitions of σ using the arithmetical mean rather than the root mean squared roughness R_a (WALBECK, 2004; MEYER, 2010a; MAYER, 2013). Even with the different definitions and use of λ and Λ both values are close to each

other. Thus the deductions should be comparable independently of the definition used.

A well accepted definition of full lubrication is $\Lambda > 3$ (JOHNSON, GREENWOOD and POON, 1972; SPIKES, 1997; SPIKES and OLVER, 2003). This is derived from the observation that at three sigma, 99.3 % of roughness asperities are not in contact. SPIKES (1997) states that at $\lambda > 5$ true full lubrication with no asperity contacts is to be expected and below 0.5 boundary lubrication with negligible load support by the lubricant film is present.

ZHU and WANG (2012) argue that from experiments and simulations for $\Lambda = 0.05 \ldots 0.1$ a considerable portion of the load is still supported by the lubricant. While for $\Lambda = 0.6 \ldots 1.2$ no asperity contact is observed any more. Thus already from values greater than 1.2 the regime can be assumed to be fully lubricated. This coincides with the value of $\Lambda = 1.25$ for which most bearing life calculations assume that no surface distress occurs and life is limited by fatigue.

CANN et al. (1994) point out that not only the macroscopic film formation needs to be understood, but that the micro EHL at the asperity level greatly influences the film formation. They point out that even for values of $\Lambda \approx 20$ occasional metallic contacts have been observed, while run-in surfaces sometimes show no contact from $\Lambda = 0.3$ onwards. Thus for a true understanding the surface structure and roughness geometry should be considered.

A different approach was followed by SCHMIDT (1985) who investigated the influence of the roughness form on the EHL film formation. He came to the conclusion that the surface structure with low amounts of deep grooves is advantageous for the film thickness, whilst deep valleys lead to lower films. (SCHMIDT, 1985) thus introduces a correction factor C_{RS} based on the surface profile (SCHMIDT, 1985; KUHLMANN, 2009):

$$C_{\text{RS}} = 0.8 \cdot \left(\frac{R_{\text{K}}}{R_{\text{z}}} \right)^{0.61} \cdot \left(\frac{R_{\text{pk}}}{R_{\text{vk}}} \right)^{0.25} \tag{2.4}$$

which incorporates the core roughness R_{k}, average maximum height R_{z}, reduced valley depth R_{vk}, and reduced peak height R_{pk} of the ABBOTT-FIRESTONE curve. A low value of the parameter C_{RS} is beneficial for the film formation. From twin-disc measurements with different surface structures SCHMIDT (1985) deduces that the minimum film thickness where no contacts occur is:

$$h_{\text{min}}^* = R_{\text{z}} \cdot C_{\text{RS}} . \tag{2.5}$$

KUHLMANN (2009) states, that this leads to the necessary minimum full film lubrication thickness of:

$$h_{\text{full,min}} \approx h_{\text{min,1}}^* + h_{\text{min,2}}^* \tag{2.6}$$

which he states is equivalent to $\Lambda \approx 3$.

The influence of the roughness structure on the film formation has been discussed and pointed out, e. g. by PEKLENIK (1967). However, apart from formulations like the above the effect has not yet been incorporated into film thickness equations directly. It is often only considered in simulations solving the REYNOLDS equation by introducing shear and pressure flow factors as proposed by PATIR and CHENG (1978) and PATIR and CHENG (1979).

BARTEL (2001) uses a different approach, which is based on interaction of roughness and pressure in the lubricant film. In his view, the criteria are pressure fluctuations in the fluid film caused by roughness. A value of $\lambda > 3 \ldots 5$ is required to make these fluctuations vanish. Below, he speaks of mixed lubrication even when no direct asperity contact exists.

From an engineering point of view, the use of a definition based on the macroscopic surface parameters (e. g., R_q values) are often the only viable option due to the information of the surface micro structure being unavailable.

Being based on the theoretical film thickness (see Sec. 1.2.2), Λ can be easily used in most practical applications to describe the lubrication regime. This is also the parameter applied in this thesis, with σ as defined in Eq. 2.2. While this approach neglects before mentioned aspects it is found to be a useful method to describe the lubrication regime.

2.1.2 *Losses in elastohydrodynamic contacts*

The losses in fully flooded EHL contacts comprise of two mechanisms: The friction force due to rolling F_{rol} and the friction due to sliding F_{sl}. In this context the forces depict the resulting tangential forces in the contact.

The rolling friction results from the pressure profile of the EHL contact (see Sec. 1.2.2) and compression losses. The asymmetric pressure profile causes the resulting force to act off contact center, thus causing a moment around the axis of rotation (GOHAR, 1988).

The sliding component causes shearing of the lubricant. Thus, the losses occurring due to this motion are governed by the rheological properties of the lubricant. According to GOHAR (1988):

$$F_{fric} = F_{rol} \mp F_{sl} = \int\int_{A_{contact}} \frac{h}{2} \cdot \frac{\partial p}{\partial x} \mathrm{d}x\mathrm{d}y \mp \int\int_{A_{contact}} \Delta u \cdot \frac{\eta}{h} \mathrm{d}x\mathrm{d}y \quad (2.7)$$

The plus '+' and minus '−' describe the upper or lower contact surface. It must be pointed out that even if the sum is zero, i. e., the tangential friction force is zero, friction is still present and a moment would be necessary to overcome this friction and keep the system running at constant velocity. However the extra tangential force in the contact would have disappeared. This behaviour is somewhat similar to the effect of the losses due to deformation.

For the determination of the rolling friction several analytical models have been proposed (GOKSEM and HARGREAVES, 1978a; GOKSEM and HARGREAVES, 1978b; GOHAR, 1988).

This work focusses on the traction resulting from lubricant shearing. The rolling friction is thus not considered and has been eliminated from measurements where possible.

2.1.3 *Dry and Boundary Friction*

The COULOMB [1] law of friction for dry friction is characterised by a friction coefficient μ which links the friction force F_{fric} to the normal force F_{N}:

$$F_{\text{fric}} = \mu \cdot F_{\text{N}} \quad \text{or} \quad F_{\text{fric}} = f \cdot F_{\text{N}}. \tag{2.8}$$

With the friction coefficient μ or f. Typical values for f in dry contacts are between 0.1...1, however, may in the lower range $(0.1\ldots0.3)$ be the result of boundary friction[2]. [3] This model is often also applied in the calculation of mixed friction. The lubricant friction is calculated separately and in the areas of direct asperity contact a dry model is applied (XI et al., 2016). Complementing explanations of the contribution of the asperities is through very thin films incurring high local shear rates and high local pressures (see Sec. 2.1.4) in a lubricant present (e. g. SCHIPPER et al., 1990).

2.1.4 *Fluid Friction*

The friction in lubricated contacts under full film lubrication is determined by the losses within the lubricant film. A simple shear flow, with a linear velocity-height profile, is shown in Fig. 2.1.2. The first models assumed a linear dependence of the shear stress τ on the shear rate $\dot{\gamma}$, i. e., ratio of velocity difference $(v_1 - v_2)$ to film thickness h, and the dynamic viscosity μ[4] indicates the resistance of the lubricant against shear flow. This rheological behaviour is called NEWTONian. The resulting in the shear stress is thus:

$$\tau = \mu \cdot \dot{\gamma} \tag{2.9}$$

---

1 COULOMB (1821) published work regarding this behaviour founded on experiments. LEONARDO DA VINCI also experimented and gave a friction coefficient of 0.25 for all materials, which might be attributed to boundary friction rather than real dry friction shown by PITENIS, DOWSON and SAWYER (2014).

2 which should yield values of $0.03\ldots0.1$

3 When using Eq. 2.8 to describe friction in fully lubricated contacts values of f of 0.001...0.01 are stated.

4 The low shear viscosity shall be referred to as μ. It is often also referred to as η_0 according to German conventions. However, this was may lead to confusion with the viscosity at ambient pressure. Also, there may be a confusion with the coefficient of friction which is called μ in German literature. Therefore, f, which is common in international literature, is to be preferred

with

$$\dot{\gamma} = \frac{\partial v}{\partial y} \; .$$
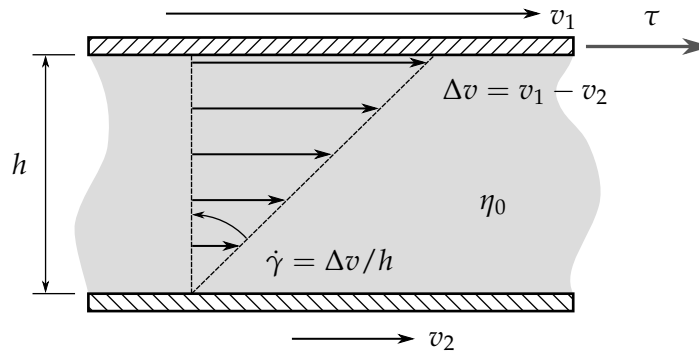
Figure 2.1.2: Flow in film of NEWTONian fluid under shearing

The equation above can be used to determine the low shear viscosity if shear stress and shear rate can be determined. The viscometers utilised can be of different types:

- *falling body*, i.e., a sinker falls in the lubricant and falling time or velocity of the sinker, slowed by the shear stress resulting from the fluid flowing past it, are measured.

- COUETTE, i.e., a cylinder rotates with a defined gap. Rotational velocity and gap width determine shear rate, while the torque on the stationary wall is measured to determine the shear stress.

- *vibrating quartz type*, i.e., an oscillating quarz is excited to vibrate and the damping measured.

Furthermore, a standard method to measure the kinematic viscosity v using capillary viscometers is well established. The dynamic viscosity and the kinematic viscosity are linked through the density ϱ:

$$v = \frac{\eta}{\varrho} \; . \tag{2.10}$$

In lubricated contacts, the temperatures and pressures vary quite significantly. This causes a change of the physical lubricant properties discussed in Sec. 2.3.

Under shearing[5] most lubricants do not exhibit a linear relationship (as shown in Eq. 2.9) between shear rate and viscosity over an unlimited range of shear stress respective shear rate. More widely spread is a lubricant behaviour as depicted in Fig. 2.1.3. Under moderate shear rates the linear, i.e., NEWTONian behaviour is visible. From

---

[5] It must be noted that the shear rates in typical EHL contacts, in combination with rapid pressure and temperature changes, are severe and thus lead to this behaviour.

a critical shear stress τ_c[6] –sometimes regarded as equivalent to the EYRING stress τ_E– the effective lubricant viscosity decreases, leading to a degressive slope of the shear stress as well. This behaviour is called *shear thinning*.

Furthermore, the fluids may also exhibit a rise in viscosity with rising shear rate (grey curves in Fig. 2.1.3). The fluids used as lubricants in technical systems however mostly exhibit only shear thinning.
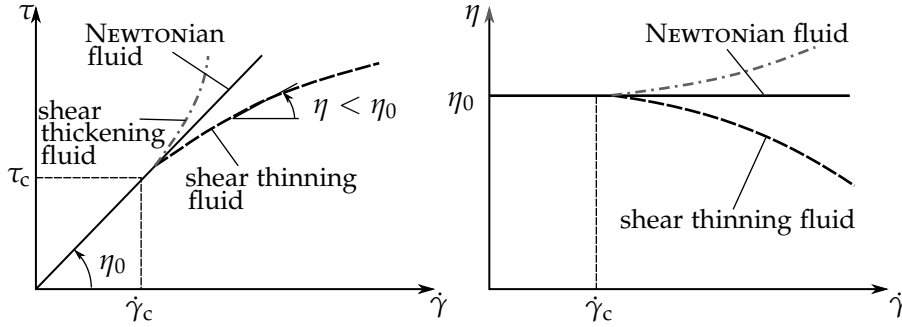
Figure 2.1.3: Shear stress (left) and dynamic viscosity (right) of NEWTONIAN and Non-NEWTONIAN fluids.

Several models exist to describe shear thinning, which is attributed to the molecules aligning during shearing thus leading to a drop in viscosity (TANNER, 2000; BAIR, 2007). The viscosity to be applied is now not the limiting low shear viscosity μ any more but the shear dependent viscosity η. Thus the shear stress viscosity relation from Eq. 2.9 needs to be rewritten as:

$$\tau = \eta(\dot{\gamma}) \cdot \dot{\gamma} \tag{2.11}$$

or dependent of shear stress (which is physically more sensible)

$$\tau = \eta(\tau) \cdot \dot{\gamma} . \tag{2.12}$$

The onset of the shear thinning at the characteristic shear stress τ_c is to be expected when the dimensionless WEISSENBERG number Wi, describing the ratio of elastic to viscous forces, reaches unity (TANNER, 2000; BAIR, 2007). It is defined as:

$$Wi = \lambda \cdot \dot{\gamma} . \tag{2.13}$$

λ here describes the characteristic time a liquid molecule needs to realign through the BROWNIAN motion and reach thermodynamic equilibrium. If Wi is higher than unity the time for realignment is not sufficient thus leading to a change in fluid structure and a viscosity η lower than the low shear viscosity μ. Below a WEISSENBERG number

---

6 τ_c is sometimes referred to as τ_0 (GOHAR, 1988, e. g.) or τ_E (HOUPERT, 1980, e. g.) in literature. The critical shear stress shall always be referred to as τ_c in this work.

of one the relaxation time is sufficient for the molecules to realign. The viscosity thus remains constant at the low shear viscosity μ and the behaviour of the lubricant is NEWTONian. A comparison of the WEISSENBERG and DEBORAH number is given in Sec. 2.3.

GRUNTFEST (1965) attributed shear thinning to thermal effects. However, while thermal effects do play a role in traction experiments, non-thermal shear thinning has been shown to exist in temperature controlled viscometer measurements. However, extreme care needs to be taken in experiments if a shear thinning behaviour is to be investigated, that the temperature and shear heating are well controlled or known.

The shear stress in Fig. 2.1.4, which depicts typical behaviour of shear stress under shearing, reaches a maximum value τ_{lim}[7] the limiting shear stress. When the shear rate is increased further thermal effects lead to a decrease in shear stress. This is attributed to an increase in temperature leading to a decrease in viscosity and possibly a decrease in limiting shear stress. A more detailed discussion of the limiting shear stress τ_{lim} is presented in Sec. 2.5.3.

Models for the shear rate dependent lubricant behaviour are discussed in Sec. 2.4 while Sec. 2.3 gives an overview of models of the physical properties of lubricants.
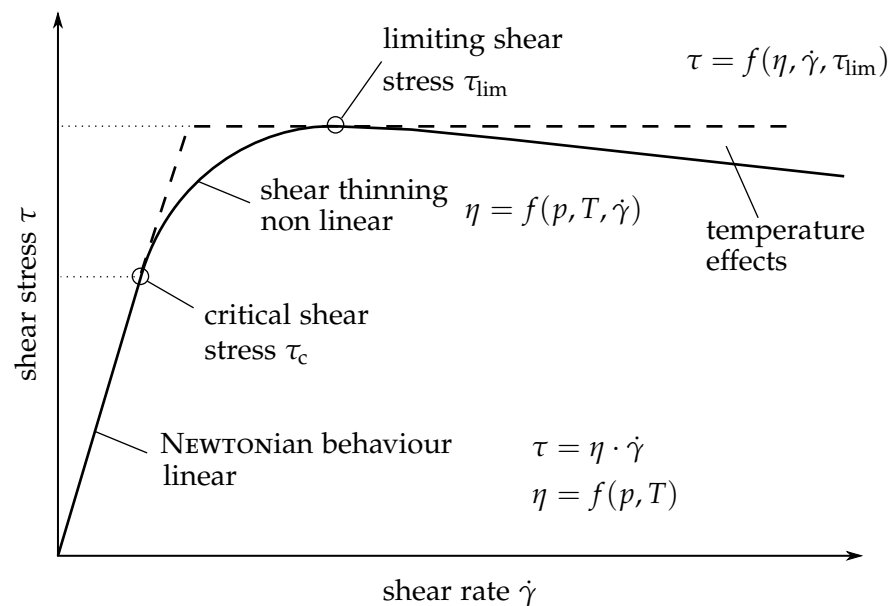
Figure 2.1.4: Fluid model as described e. g. by BAIR (2007)

---

7 τ_{lim} is sometimes referred to as τ_{c} in literature (GOHAR, 1988). However to avoid confusion this work uses τ_{lim} for the limiting shear stress whilst τ_{c} is used exclusively for the critical shear stress.

It is notable, that this behaviour is found in the lubricant under steady shear. The shear stress shear rate plot is quite similar to the plot of a traction curve (either coefficient of friction versus slide to roll ration or shear stress slide to roll ratio, see e. g., Sec. 4.1). Whilst the behaviour of the traction curve is dominated by the lubricant rheology, the traction curve represents the integral behaviour of the EHL contact. Thus the extraction of physical lubricant properties from traction measurements has to be viewed with caution. Several methods have been proposed in literature (JOHNSON and CAMERON, 1967). These have however also been criticised (VERGNE and BAIR, 2014).

2.1.5 *Elastic slip of solids*

The rolling sliding motion occurring in EHL contacts can be described by the slide to roll ratio *SRR* or just *S*:

$$S = \frac{v_1 - v_2}{0.5 \cdot (v_1 + v_2)} \tag{2.14}$$

where v_1, v_2 are the speeds of body 1 and 2 respectively. From there it follows that for pure sliding $S = 2$, e. g., $v_2 = 0 \Rightarrow S = v_1/0.5 \cdot v_1$. In the EHL contacts of rolling element bearings values of $S < 0.02$ occur while worm gears may exhibit values close to 2.

In all contacts between solids friction leads to a tangential elastic deformation of the solids. Due to this elastic deformation slip occurs within the contact. This is termed elastic or micro slip of the solids (REYNOLDS, 1876; CARTER, 1926; MINDLIN, 1949; JOHNSON, 1955; POLL, 1983). This needs to be considered when interpreting traction data due to the fact that the raw traction data contains fluid behaviour as well as the elastic slip of the solids (BAIR and KOTZALAS, 2006; MEYER, 2010b; WANG and POLL, 2013)

Figure 2.1.5 shows the effect of the micro slip. The two rolling elements are loaded with a normal force and run with the constant speeds $\omega_1 > \omega_2$. In the contact area the frictional force (acting tangentially) shears the elements A and B of the solid boundary zone. The element A of the faster body is compressed while the element B of the slower body is stretched. These deformations cause a shear stress between the elements. If this shear stress remains below the static friction in the element's surface no slip occurs. However, the strain increases as the elements pass on through the contact. At this point a speed difference, i. e., slip, is result of solely elastic deformation. The resulting slip is thus $S_{\mathrm{el,sol}}$. If the shear stress within the element exceeds the static friction in the element's surface (in case of lubricated contacts governed by the lubricant), sliding occurs. This portion of the slip is $S_{\mathrm{sl,sol}}$. The total slip S_{sol} measured in such a contact is thus

$$S_{\mathrm{sol}} = S_{\mathrm{el,sol}} + S_{\mathrm{sl,sol}}. \tag{2.15}$$
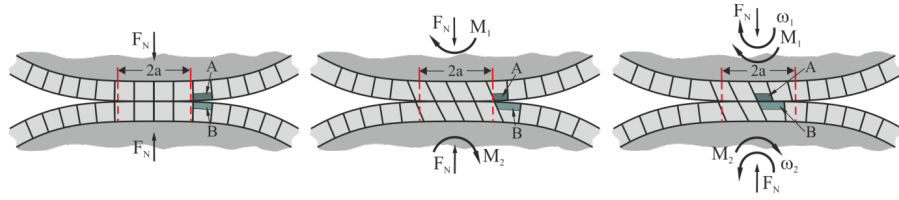
Figure 2.1.5: Elastic slip of solids as described by (POLL, 1983) from (MEYER, 2010a)

Due to the HERTZian pressure distribution micro slip always occurs as at the borders of the contact ellipse where the pressure is zero, i.e., static friction force transferable is also zero. If the speed difference is increased the friction force of the contact increases, however the area encountering sliding increases. If the whole contact area is sliding a further increase in slip will not lead to higher friction forces. Figure 2.1.6 shows the traction behaviour of the dry contact[8].

The behaviour of the dry contact may be calculated using the deformation theory by CARTER (1926) or finite element models (used e.g., by MEYER (2010b)).

The slip S_{sol} is for line contacts (CARTER, 1926):

$$S_{sol} = 2 \cdot f_{max} \cdot \bar{p} \cdot \frac{1 - \nu_{poisson}}{G} \cdot \frac{4}{\pi} \cdot \left(1 - \sqrt{1 - \frac{f}{f_{max}}}\right). \quad (2.16)$$

The gradient of the curve in Fig. 2.1.6 can be found as:

$$\frac{df}{dS} = \frac{E}{2 \cdot p_{max} \cdot \left(1 - \nu_{poisson}^2\right)}, \quad (2.17)$$

which can be used to determine the elastic component of the slip of the solid (Eq. 2.15).

When measuring traction in lubricated contacts the measured slip S_{total} is the result of the slip occurring in the lubricant, i.e., shearing, and the elastic slip in the solids.

$$S_{total} = S_{fluid} + S_{el,sol} \quad (2.18)$$

Thus, when investigating the lubricant behaviour alone the relation between lubricant slip S_{fluid} and traction coefficient f (or shear stress) is of interest. Thus a correction of the measured slip S_{total} is necessary.

$$S_{fluid} = S_{total} - S_{el,sol} = S_{total} - f \cdot \frac{2 \cdot p_{max} \cdot \left(1 - \nu_{poisson}^2\right)}{E}. \quad (2.19)$$

The gradient can not only be found using deformation theory but also using finite element modeling or measurements of the behaviour

---

8 This behaviour is quite similar to the traction behaviour of a lubricated contact (Fig. 4.1.2).

of the dry contact. NEUBAUER (2007) and MEYER (2010b) showed that all models yield gradients which are in good agreement. Thus the traction data in this work is corrected by the above mentioned method which was described by WANG (2015). The method is summarised in Fig. 2.1.7.
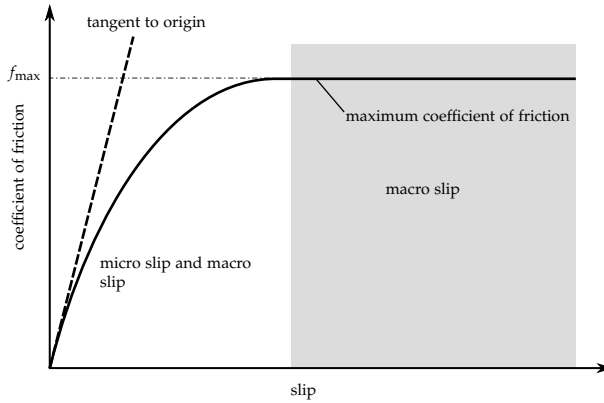
Figure 2.1.6: Coefficient of friction over slip for a dry contact from (POLL, 1983)
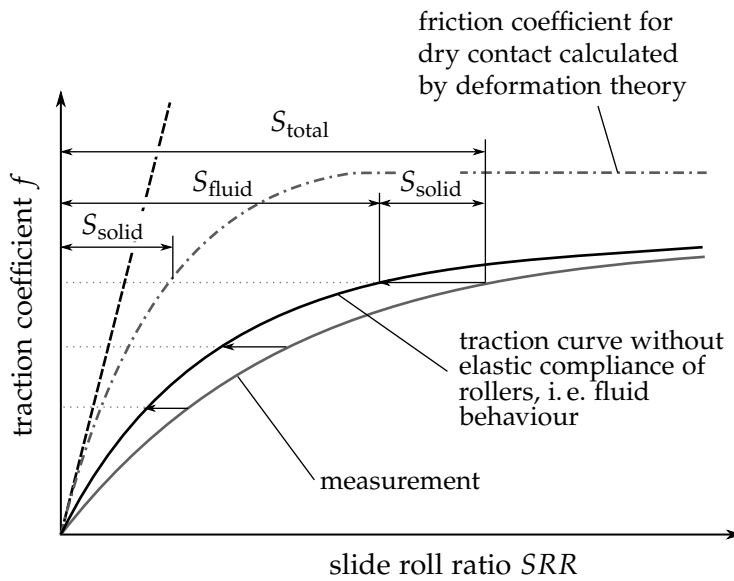
Figure 2.1.7: Correction of the measured data by elastic slip MEYER, 2010a

2.2 MAXWELL MODEL

To model the lubricant behaviour in transient shear the assumption is made that the lubricant behaves not only viscous but also exhibits elastic properties (TANNER, 1960; HIRST and MOORE, 1974; JOHNSON and ROBERTS, 1974; TEVAARWERK and JOHNSON, 1975; HIRST and MOORE, 1979; EVANS and JOHNSON, 1986). As was shown in Sec. 2.3 the DEBORAH number exceeds unity for most highly loaded contacts. To describe visco-elastic behaviour often mechanical models are used. These models, consisting of springs and dashpots, represent the shear-stress strain and strain rate relation. Models used are the MAXWELL (1867), the KELVIN-VOIGT –mostly applied to solids–, the PHAN-THIEN-TANNER (PHAN THIEN and TANNER, 1977; PHAN THIEN, 1978), and the OLDROYD model (OLDROYD, 1950). In these models, the elastic and viscous strains are summed resulting in the total strain. AKYILDIZ, JONES and WALTERS (1990) point out that some models represent a mechanical analogue, however make use of not sound parameters, e. g., negative viscosities. If however, the models satisfy the condition that the work done by deformation is positive they principally correctly model the overall behaviour.

Figure 2.2.1 visualises a MAXWELL model with an added dry sliding element corresponding to the limiting shear stress (see Sec. 2.5.3). The viscous behaviour is represented by the dashpot and the elastic component by the spring.

Sometimes elasticity is confused with time dependence of pressure-viscosity or temperature-viscosity behaviour due to the short times of passage through an EHL contact. While this has been mentioned as an explanation of lubricant behaviour under small shear rates, indications from laboratory measurements exist that for an EHL time scale these effects should not be noticeable (BAIR, 2001; BAIR, JARZYNSKI and WINER, 2001). While this explanation cannot be ruled out definitely at this time a time dependence is not seen as a likely explanation of the lubricant behaviour. Thus in this work it is assumed that elastic fluid behaviour is responsible for the lubricant behaviour under small strains.

The total shear in the simplified MAXWELL model is:

$$\gamma_{\text{total}} = \gamma_{\text{elastic}} + \gamma_{\text{viscous}} \tag{2.20}$$

differentitation and inserting the terms for the elastic and viscous part yields the shear rate:

$$\dot{\gamma} = \frac{1}{G} \cdot \frac{\mathrm{d}\tau}{\mathrm{d}t} + \frac{\tau}{\eta\left(p, T, \dot{\gamma}\right)} \tag{2.21}$$

with τ/η signifying the viscous part whilst the second term $\mathrm{d}\tau/G\mathrm{d}t$ signifies the elastic behaviour. BAIR (1990) points out that the shear modulus G needs to be taken into the time derivative. This is due to
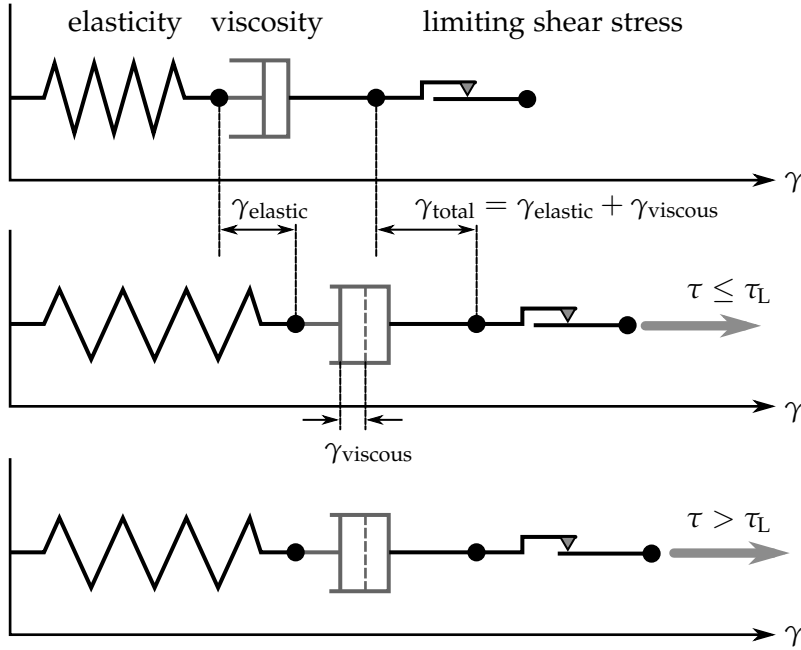
Figure 2.2.1: MAXWELL model incorporating limiting shear stress. The spring reperexents the elastic part of the deformation, whilst the dashpot represents the viscous part. The limiting shear stress is visualised by the dry sliding element.

the temperature and pressure dependence of G (see Sec. 2.5) which vary with the position and thus time. Thus more precisely the MAXWELL equation should be written as:

$$\dot{\gamma} = \frac{\mathrm{d}\left(\tau/G(p,T)\right)}{\mathrm{d}t} + \frac{\tau}{\eta\left(p,T,\dot{\gamma}\right)}. \tag{2.22}$$

This version of the MAXWELL equation is however seldom used in EHL and the shear modulus is often assumed to be time independent throughout the contact.

If the DEBORAH number is less than one, $D < 1$, elastic properties may be neglected in a first approximation. Due to the fact that some EHL contacts exhibit values below unity the elastic portion of the lubricant behaviour is often omitted (e. g., MAYER, 2013). However, especially applications with low SRR, e. g., bearings, may necessitate the consideration of the elastic portion of the lubricant behaviour for a precise traction model. To correctly model the elastic part of visco-elastic fluid properties the knowledge of the shear modulus G is needed (see Sec. 2.5.1).

For the MAXWELL equation several alternative formulations have been proposed. These include the formulation by (BAIR and WINER, 1979a):

$$\dot{\gamma} = \frac{1}{G}\frac{d\tau}{dt} - \frac{\tau_{\text{lim}}}{\eta_0} \cdot \ln\left(\left(1 - \frac{\tau}{\tau_{\text{lim}}}\right)^{-1}\right) , \qquad (2.23)$$

which is the result of fitting laboratory data and contains the limiting shear stress. Similarly GECIM and WINER (1980) use:

$$\dot{\gamma} = \frac{1}{G}\frac{d\tau}{dt} + \frac{\tau_{\text{lim}}}{\eta_0} \cdot \tanh^{-1}\left(\frac{\tau}{\tau_{\text{lim}}}\right) . \qquad (2.24)$$

A commonly used equation is the use of a REE-EYRING fluid model for the viscous flow (e. g., JOHNSON and TEVAARWERK, 1977):

$$\dot{\gamma} = \frac{1}{G}\frac{d\tau}{dt} + \frac{\tau_{\text{E}}}{\eta_0} \cdot \sinh\left(\frac{\tau}{\tau_{\text{E}}}\right) . \qquad (2.25)$$

This model does not incorporate a limiting shear stress and would yield increasing shear stresses with increasing shear rate. The combination of this model with a low shear viscosity which constitutes an underestimation of viscosity the calculated stresses can show a behaviour similar to that of a limiting shear stress.

2.3 MODELING PHYSICAL LUBRICANT PROPERTIES

Due to the high pressures, high shear rates, and resulting temperature rises the physical properties of the lubricants in EHL contacts change significantly while passing through the contact. As discussed in Sec. 1.2, the lubricant viscosity changes several orders of magnitude, which is called *piezoviscosity*. A further significant change of fluid properties is the *glass transition*. This is a state where the lubricant stops acting as a liquid and rather shows the characteristics of a solid. The glass transition can be observed by a change of the gradient of the change of specific volume with pressure (ALSAAD, 1976; ALSAAD et al., 1978; BAIR, 1990; BAIR, 2007). Above the glass transition super-ARRHENIUS piezoviscous behaviour is dominant for glass forming liquids at high pressure.(VERGNE and BAIR, 2014; BAIR, MARTINIE and VERGNE, 2016).

The glass transition also influences the visco-elastic behaviour. It is an amorphous liquid state which is characterised by very high viscosity usually described as higher than 10^{12} Pas (JOHNSON, 1978). The response of the glassy state is predominantly elastic. The glass transition can either occur due to low temperature, high pressure, or high strain rate.

A form of the DEBORAH[9] Number $De = f \cdot \eta / G_\infty$, which is the ratio of relaxation time η / G_∞ to the time of one shear cycle $1/f$, can be used to determine if elastic behaviour dominates. For $De > 1$ the fluid exhibits visco-elastic behaviour. Rewritten for EHL contacts (JOHNSON, 1978) the DEBORAH number becomes:

$$De = \frac{\eta}{G} \Big/ \frac{a}{U} \tag{2.26}$$

with a the contact half width and U the velocity. JOHNSON states that $a/U \approx 10^{-4}$ s and $G \approx 10^9$ Pa meaning the DEBORAH Number D will be greater than one for viscosities exceeding 10^5 Pas. It needs to be pointed out that the DEBORAH number varies in the contact area due to the varying viscosity and the varying shear modulus.

Due to the fact that these conditions are present in the EHL contacts investigated (especially for the twin-disc contacts in Sec. 4.1.1) the lubricant behaviour always needs to be modeled as visco-elastic.

When considering whether the behaviour of a visco-elastic fluid is more elastic or more viscous both the WEISSENBERG and DEBORAH number are used. As was presented in Eq. 2.13 in Sec. 2.1.4 the WEISSENBERG number is given as product of relaxation time and shear rate $Wi = \lambda \cdot \dot{\gamma}$ –representing the ratio of elastic to viscous forces– while the DEBORAH number is the ratio of relaxation time to characteristic time T (or process/contact time) $De = \lambda / T$. The WEISSENBERG number incorporates the rate whilst the DEBORAH number incorporates the time. Thus in steady simple shear flows no change in behaviour is observed and the DEBORAH number reaches zero whilst the WEISSENBERG number can still be used to quantify elastic effects (DEALY, 2010). Both dimensionless numbers can reach identical values for non-steady flows where the time of interest and the shear rate are of same magnitude (POOLE, 2012). In EHL contacts they are identical if $1/T = \dot{\gamma}$ or following from $T = a/U$ and $\dot{\gamma} \approx \Delta U / h$ it can be derived that these numbers are nearly identical for low SRR cases, by substituting $U = v_1 + v_2$ and $\Delta U = v_1 - v_2$ identity is given for $SRR \approx h/a$ which can be considered to be in the region of $10^{-3} \ldots 10^{-4}$.

Models for the density, piezoviscosity, and temperature dependence of viscosity are presented and discussed in the following sections.

---

9 The DEBORAH number was coined by REINER during work with BINGHAM. The definition was $De = $ *time of relaxation/time of observation* (REINER, 1964). Common definitions today rather use *time scale of the process* or *fluid residence time* instead of the observation time (POOLE, 2012)

2.3.1 *Density*

Variation with temperature

The density of lubricants changes with temperature linearly like all bodies do (BAIR, 2007):

$$\frac{\varrho\,(p,T)}{\varrho\,(p,T_0)} = 1 - \alpha_\varrho\,(T - T_0)\,. \tag{2.27}$$

With α_ϱ denoting the density temperature coefficient

$$\alpha_\varrho = -\left(\frac{\partial \varrho}{\partial T}\right)_{p_0}$$

and T_0 denoting a reference temperature where the density has been determined. For mineral oils and similar lubricants a fixed parameter α_ϱ has been suggested in the standard DIN 51757:

$$\varrho = \varrho_0 \cdot 10^9 - \left(6,05 \cdot 10^{13} \cdot (\theta - \theta_0)\right)\,. \tag{2.28}$$

Variation with pressure

The density also varies with pressure. In practical applications the pressure-density relationship is often described using the model by DOWSON and HIGGINSON (1966):

$$\varrho(p) = \varrho_0 \frac{0,59 \cdot 10^9 + 1,34p}{0,59 \cdot 10^9 + p} \tag{2.29}$$

where ϱ_0 is density at ambient pressure sometimes written as:

$$\varrho(p) = \varrho_0 \cdot \left(1 + \left(\frac{C_a \cdot p}{1 + C_b \cdot p}\right)\right) \tag{2.30}$$

using $C_a = 0.6 \cdot 10^{-9}\,\mathrm{Pa}^{-1}$ and $C_b = 1.7 \cdot 10^{-9}\,\mathrm{Pa}^{-1}$. However, this model has been shown to be sufficiently accurate only up to $0.35\,\mathrm{GPa}$. To describe both pressure and temperature dependence of the lubricants equations of state have been proposed.

An isothermal equation of state found to describe density data under high pressures well was proposed by MURNAGHAN (1951):

$$\frac{V}{V_0} = \left(1 + \frac{K_0'}{K_0} \cdot p\right)^{\left(-\frac{1}{K_0'}\right)} \tag{2.31}$$

and K being defined as:

$$K = K_0 + K_0' \cdot p \tag{2.32}$$
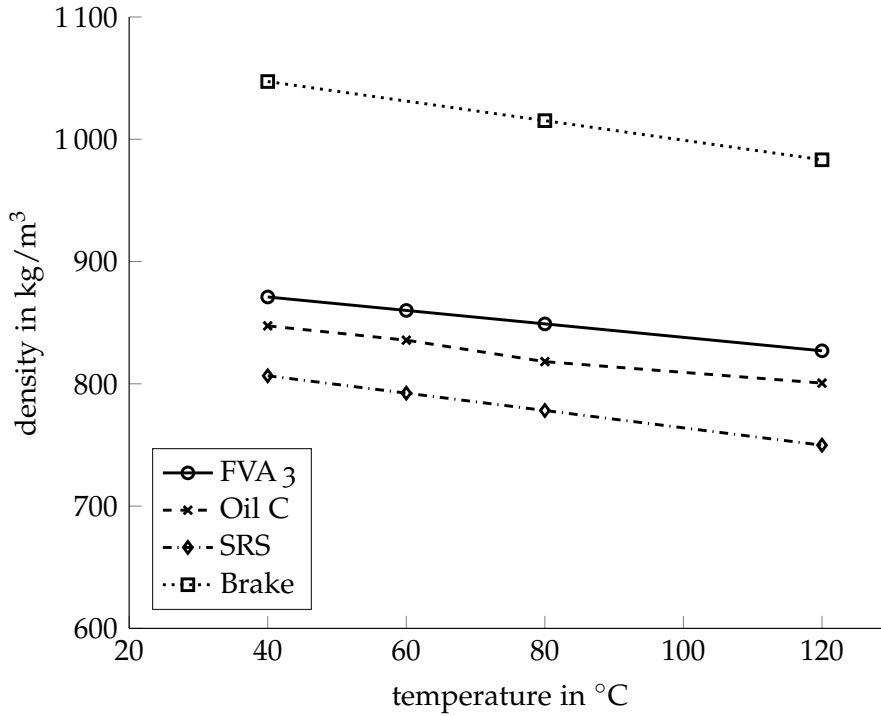
Figure 2.3.1: Temperature dependent density of several fluids, measured by ITR from (BROUWER, BADER and BEILICKE, 2016)

2.3.2 *Temperature dependence of viscosity*

The lubricant viscosity varies with temperature and pressure. Due to the high pressures and temperature increases in EHL contacts the correct modeling of the viscosity behaviour is essential to traction calculation. In the following section the temperature and pressure dependent behaviour of typical lubricants is discussed.

POISEUILLE (1840) proposes a variation of viscosity similar to the temperature dependence of density:

$$\mu = \frac{\mu_0}{1 + \alpha \cdot T + \beta \cdot T^2} \tag{2.33}$$

where α and β are constant coefficients, T is the temperature in degrees Celsius, and μ_0 is the absolute viscosity at $0\,°C$. SLOTTE (1881) uses three constants:

$$\mu = \frac{c}{(a + T)^n} \ . \tag{2.34}$$

While GRAETZ (1888) proposes similarly:

$$\mu = \frac{A\,(\theta - T)}{(T - T_1)} \ , \tag{2.35}$$

where θ is the critical temperature and T_1 a temperature in degree Celsius below the melting point where viscosity is infinite.
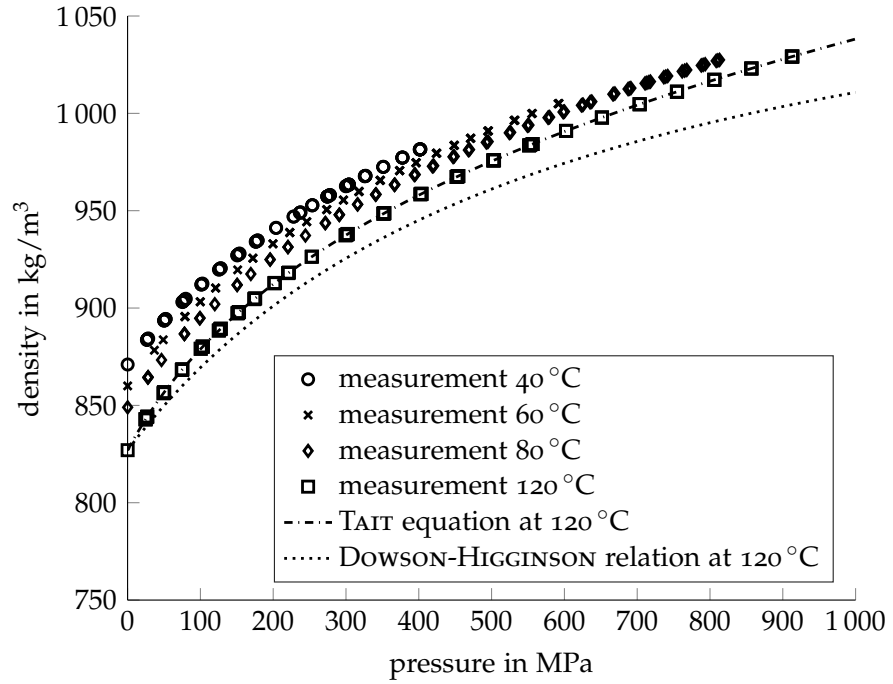
Figure 2.3.2: Pressure dependent density for FVA 3 measured by ITR from (BROUWER, BADER and BEILICKE, 2016) compared to TAIT and DOWSON-HIGGINSON relations

REYNOLDS (1886) proposes:

$$\mu_1 = \mu_2 \cdot e^{-\alpha^*(T_1 - T_2)} \tag{2.36}$$

sometimes given as (SEETON, 2006)

$$\mu = R \cdot e^{-\alpha t}$$

with μ the dynamic viscosity in mPas or cP and t as temperature in °C, α[10] and R are empirical constants determined from experimental data. REYNOLOLDS presented his work for olive oil and based his observations on data from 16 to 49 °C. This is followed by the model proposed by VOGEL (1921) which is still quite often used to describe the temperature influence on viscosity:

$$\eta_t = \eta_\infty^{\frac{t - t_1}{t - t_\infty}} \tag{2.37}$$

where η_t is the absolute viscosity in mPa s at the temperature t in °C. Thus η_∞ is the viscosity at $t \to \infty$, t_1 the temperature at which $\eta = 1$, and t_∞ the temperature at which $\eta \to \infty$. It was devised from data obtained for water, mercury, and petroleum oils. The equation

---

10 For olive oil and the famous experiment of BEAUCHAMP, REYNOLDS gives a value of $\alpha = 0.123$.

performs well for moderate temperatures. Due to the fact that t_1, t_∞, and η_∞ need to be known for the fluid it is not easy to generalise its application. However, an adapted version:

$$\eta_0(\vartheta) = A_1 \cdot e^{\left(\dfrac{B_1}{\vartheta - \vartheta_0}\right)} \tag{2.38}$$

according to TANNER (2000) is widely accepted. The coefficients A, B, and ϑ_0 need to be determined from laboratory data. TANNER points out that a great number of these models have been found using NEWTONian fluids and that some equations need to be improved for use with non-NEWTONian fluids. A different approach was chosen by FULCHER (1925) stating:

$$\log_{10}(\eta) = -A + \frac{B \cdot 10^3}{T - T_0} \tag{2.39}$$

for molten glasses, with A and B being empirical coefficients.

ARRHENIUS (1889) formulated:

$$k = k_0 \cdot e^{\left(-\dfrac{E_A}{R_g \cdot T}\right)} \tag{2.40}$$

for chemical reaction rates where k_0 is the rate constant, T the absolute temperature in K, E_A the activation energy, and R_g the universal gas constant. This was adopted by GUZMAN and ANDRADE (1930) and ANDRADE (1934) , whose work is more commonly known. They similarly proposed:

$$\eta = A \cdot e^{\left(-\frac{B}{T}\right)} . \tag{2.41}$$

RAMAN (1923) also proposed an ARRHENIUS law for viscosity by considering binary encounters between molecules and applying a BOLTZMANN distribution to the different aggregates of the molecules. He uses viscosity data from Benzene to verify his model.

WARD (1937) also worked on an Arrhenius law formulating:

$$\mu = A \cdot \frac{B}{R_g \cdot T} \tag{2.42}$$

and noting that the parameters A and B may be temperature dependent.

Considering the temperature dependence of the kinematic viscosity WALTHER (1928) proposed:

$$\log(\log(\nu)) = -M \cdot t + P \tag{2.43}$$

M and P are constants. UBBELOHDE introduced a similar relation, which led to this being called the WALTHER-UBBELOHDE relation. WALTHER (1931) published an improved version:

$$\log(\log(\nu + 0.95)) = -m \cdot \log\left(\frac{T}{T_0}\right) + \log(\log(\nu_0 + 0.95)) \tag{2.44}$$

and this was included in the standard DIN 51563. GENIESSE and DELBRIDGER (1932) presented a similar method included in ASTM 341-93:

$$\log\left(\log\left(\nu+0.8\right)\right)=a-b\cdot\log\left(T\right) \tag{2.45}$$

Numerous improved versions of different models have been proposed since then (BARLOW, LAMB and MATHESON, 1966; BARLOW, LAMB and MATHESON, 1966; CROUCH and CAMERON, 1961).

WRIGHT (1969) discussed the following equation on which the standard ASTM 341-93 is based:

$$\log_{10}\left(\log_{10}\left(\nu+\gamma+f(\nu)\right)\right)=A-B\cdot\log_{10}\left(T\right) \tag{2.46}$$

with

$$\gamma+f(\nu)=0.7+C-D+E-F+G-H$$

Where the coefficients are given as:

$$C=e^{(-1.14883-2.65868\nu)} \qquad G=e^{(37.4619-192.643\nu)}$$
$$D=e^{(-0.00381308-12.5645\nu)} \qquad H=e^{(80.4945-400.468\nu)}$$

MANNING (1974) proposed for the use in computational programs:

$$\log_{10}\left(\log_{10}\left(\nu+\gamma+f(\nu)\right)\right)=b_0-b_1\cdot\log_{10}\left(T\right) \tag{2.47}$$

with

$$\gamma+f(\nu)=0.7+e^{\left(-1.47-1.84\nu-0.51\nu^2\right)} \tag{2.48}$$

SEETON (2006) created a function for the viscosity based an extensive literature review, especially from WRIGHT:

$$\log_e\left(\nu+\lambda+f(\nu)\right)=A-B\cdot\log_e\left(T\right) \tag{2.49}$$

with a modified function of viscosity:

$$f(\nu)=e^{-\nu}\cdot K_0\left(\nu+\psi\right) \tag{2.50}$$

spelled out as:

$$\log_e\left(\nu+\lambda+e^{-\nu}\cdot K_0\left(\nu+\psi\right)\right)=A-B\cdot\log_e\left(T\right) \tag{2.51}$$

where ν is the absolute viscosity in cSt (mm^2/s), λ and ψ are generalised constants, A and B are coefficients fit for each fluid, and T is the absolute temperature in K. SEETON fit the parameters to historic fluid data (ASME RESEARCH COMITTEE ON LUBRICATION, 1953a) using the condition:

$$\lim_{\nu\to 0}\left(\nu+\lambda+e^{-\nu}\cdot K_0\left(\nu+\psi\right)\right)=1 \tag{2.52}$$

leading to:

$$\lambda = 0.7 \rightarrow \psi = 1.244066584703 \tag{2.53}$$

Of the described models the ones incorporated in standards for determining the temperature dependent kinematic viscosity are widely used. These are most often given in the literature concerned with bearing design. Especially the VOGEL equation is widely used. These equations need various input data; some relations are widely applied (e. g., Eq. 2.44) because, usually not all data are available. However, the validity of these relations is limited . They fit certain types of fluids with acceptable accuracy within a restricted range of parameters. Thus, the models need to be carefully chosen to fit the fluid they are supposed to describe as well as the limits of applicability.

2.3.3   *Pressure dependence of viscosity*

As shown in Sec. 1.2.1, the lubrication of concentrated contacts relies on the piezoviscosity of the lubricant. The pressure viscosity coefficient forms a central part of the EHL film thickness formula (Eq. 1.34).

BARUS (1893) studied marine glue and proposed a linear pressure-viscosity relationship. However, he also mentioned an exponential version in his paper. The latter is still one of the commonly used pressure-viscosity relations in EHL, also forming the basis of the HAMROCK-DOWSON formulae. It is called the BARUS equation:

$$\eta = \eta_0 \cdot e^{\alpha \cdot p} \tag{2.54}$$

where α refers to the pressure viscosity coefficient often also abbreviated with α_p.

For EHL conjunctions, BARUS's viscosity formulation is sometimes modified to make the pressure viscosity coefficient temperature and pressure dependent (JOHNSON, 1978; BROUWER, BADER and BEILICKE, 2016)

$$\eta = \eta(p = 1) * e^{((\alpha_0 + \alpha_1 \cdot p) \cdot p)} \tag{2.55}$$

with

$$\alpha_0 = \alpha_{00} \cdot e^{(\alpha_{01} \cdot T)} \quad \text{and} \quad \alpha_1 = \alpha_{10} \cdot e^{(\alpha_{11} \cdot T)}.$$

The coefficients are preferably determined by linear regression of data from viscometer measurements.

Pressure-viscosity coefficient

Due to the fact that the pressure-viscosity coefficient α is the main influence on viscosity, and thus should be known precisely, a lot of work has been conducted to establish methods to find optimal ways to

determine the pressure viscosity coefficient. Several definitions have been stated.

Determination always relies on the availability of viscosity measurements under pressure. HAMROCK (1991) defined it making use of all data available:

$$\frac{1}{\alpha^*} = \int_0^\infty \frac{\mu(p=0)}{\mu(p)} \mathrm{d}p \tag{2.56}$$

BAIR, LIU and WANG (2006) presented a number of definitions found in literature. These are:

$$\alpha(p) = \frac{1}{\mu} \frac{\mathrm{d}\mu}{\mathrm{d}p} \tag{2.57}$$

$$\alpha_0 = \left[\frac{\mathrm{d}\ln(\mu)}{\mathrm{d}p} \right]_{p=0} \tag{2.58}$$

which utilises only the tangent to the viscosity at ambient pressure. Another definition:

$$\alpha_\mathrm{B}(p) = \frac{\ln\left[\mu(p)/\mu(p=0)\right]}{p} \tag{2.59}$$

where p must be specified and determines the gradient from the data in the range $0 \ldots p$. Widely used is $p = 2000\,\mathrm{bar}$ (KUSS, 1982; WALBECK, 2004) from pressure viscosity data up to $2000\,\mathrm{bar}$. To mark the pressure viscosity coefficient obtained this way it will be denoted $\alpha_{p,2000\,\mathrm{bar}}$.

$$\alpha_{p,2000\,\mathrm{bar}} = \frac{\ln\left[\eta_0(2000\,\mathrm{bar})\right] - \ln\left[\eta_0(0\,\mathrm{bar})\right]}{p} \tag{2.60}$$

So and KLAUS (1980) developed a simple method to predict NEWTONian pressure-viscosity coefficients for mineral oils, resin and polymer blends, pure hydrocarbons, and non-hydrocarbons in a temperature range of $0 - 135\,°\mathrm{C}$. The empirical model requires only atmospheric viscosity and density data as well as the viscosity-temperature behaviour.

$$\alpha = 1.216 + 4.143 \cdot (\log \nu_0)^{3.0627} + 2.848 \cdot 10^{-4} \cdot m_0^{5.1903} \cdot (\log \nu_0)^{1.5976} \cdots$$
$$\cdots - 3.999 \, (\log \nu_0)^{3.0975} \cdot \varrho^{0.1162} \tag{2.61}$$

with ν_0 the atmospheric kinematic viscosity in cSt at temperature, m_0 viscosity-temperature property, i.e., the ASTM viscosity-temperature slope divided by 0.2, ϱ atmospheric density in g/mL at temperature of interest. However, the authors themselves note that at some points

the equation predicts physically not reasonable values, e. g., decrease of α with increasing viscosity.

Several authors also presented ways to determine the pressure viscosity coefficient from interferometric film thickness measurements (for experimental setup see Sec. 4.1.3) (e. g., YOKOYAMA and SPIKES, 2000; LEEUWEN, 2009) but this has been shown to be prone to errors especially if the the lubricant exhibits non-NEWTONIAN behaviour already in the inlet of the contact (BAIR, 2000; BAIR, 2014). Therefore, it should only be regarded as an "effective" pressure viscosity coefficient.

Several variations or slightly different pressure dependent viscosity formulations have been used to fit viscosity data (e., g. IRVING and BARLOW, 1971).

ROELANDS (1966) presented work on viscosity relationships in 1966 by using own investigations and fitting data available in the ASME pressure-viscosity report (ASME RESEARCH COMITTEE ON LUBRICATION, 1953a; ASME RESEARCH COMITTEE ON LUBRICATION, 1953b). The relations presented are still one of the most widely used viscosity models in EHL (see e. g., LUGT and MORALES-ESPEJEL, 2011; SPIKES and JIE, 2014):

$$\log\left(\log\left(\eta_0 + 4.2\right)\right) = -S_0 \cdot \log\left(1 + \frac{T}{135}\right) + \log\left(G_0\right) \qquad (2.62)$$

or

$$\log \eta + 1.2 = \frac{G}{\left(1 + \frac{\vartheta}{135}\right)^s} \cdot \left(1 + \frac{p}{2000}\right)^{C\cdot\log\left(1 + \frac{\vartheta}{135}\right) + D} \qquad (2.63)$$

where $C, D, G,$ and S are fluid specific constants. It should, however, be noted that the ROELANDS equation underestimates the viscosity at higher pressures. BAIR (2004b) pointed out that the correctness of the developed equation is debatable due to the data used during its development, i. .e., omission of some available data at higher pressures.

BODE (1989) proposed, based on measurements using a self-designed oscillatory quartz viscometer (BODE, 1984) and free volume considerations, the following equation of state for the density:

$$\varrho(p, \vartheta) = \frac{\varrho(\vartheta)}{1 - a_1 \cdot \ln\left(\frac{a_2 + a_3 \cdot \vartheta + a_4 \cdot \vartheta^2 + a_5 \cdot \vartheta^3 + p}{a_2 + a_3 \cdot \vartheta + a_4 \cdot \vartheta^2 + a_5 \cdot \vartheta^3}\right)} \qquad (2.64)$$

with

$$\varrho\vartheta) = \varrho_s \cdot \left(1 - \alpha_s \cdot \vartheta\right)$$

Viscosity is then merely a function of density ϱ:

$$\eta(p, \vartheta) = A_1 \cdot \exp^{\left(\frac{A_2 \cdot \varrho(p,\vartheta)}{\varrho_g(\vartheta) - \varrho(p,\vartheta)}\right)}$$

with

$$\varrho_g(\vartheta) = A_3 \cdot (1 + A_4 \cdot \vartheta)$$

The coefficients $a_1 \ldots a_5$, $A_1 \ldots A_4$, α_s, and ϱ_s are material specific constants obtained by fitting pressure density measurements.

GOLD et al. (2001) presented a so called modulus equation based on the BARUS equation, which can be expressed as one of ROELANDS viscosity models:

$$\eta = K \cdot e^{\left[\dfrac{B}{\vartheta + C}\right]} \cdot e^{\left[\dfrac{p}{a_1 + a_2 \cdot \vartheta + (b_1 + b_2 \cdot \vartheta) \cdot p}\right]}. \qquad (2.65)$$

The parameters $K, B, C, a_1, a_2, b_1, b_2$ are lubricant specific parameters found by fitting viscosity data.

A commonly used equation of state, based on free volume theory, is the TAIT-DOOLITTLE relation (DOOLITTLE, 1951a; DOOLITTLE, 1951b; DOOLITTLE, 1952), consisting of the TAIT equation of state

$$\frac{v}{v_0} = 1 - \frac{1}{K_0' + 1} \cdot \ln\left[1 + \frac{p}{K_0} \cdot (1 + K_0')\right] \qquad (2.66)$$

combined with the DOOLITTLE equation:

$$\mu(p) = \mu_0 \cdot e^{\left[B \cdot \dfrac{v_{\text{occ}}}{v_0} \cdot \left(\dfrac{1}{\left(\dfrac{v}{v_0} - \dfrac{v_{\text{occ}}}{v_0}\right)} - \dfrac{1}{\left(1 - \dfrac{v_{\text{occ}}}{v_0}\right)}\right)\right]} \qquad (2.67)$$

The DOOLITTLE parameter B, the occupied volume fraction at ambient pressure v_{occ}/v_0, the bulk modulus K_0 at ambient pressure, and the rate of change bulk modulus K_0' at ambient pressure can be found from measured data.

WILLIAMS, LANDEL and FERRY (1955) proposed an equation for amorphous polymers also found useful for glass-forming lubricants:

$$\log\left(\frac{\eta}{\eta_g}\right) = \frac{-C_1 \cdot (T - T_g)}{C_2 + (T - T_g)} \qquad (2.68)$$

They linked the viscosity to the viscosity at glass transition η_g. T_g describes the glass transition temperature. This equation was modified by YASUTOMI, BAIR and WINER (1984a) and YASUTOMI, BAIR and WINER (1984b) to read:

$$\log(\eta(T, p)) = \log(\eta_g) - \frac{C_1 \cdot (T - T_g(p)) \cdot F(p)}{C_2 + (T - T_g(p)) \cdot F(p)} \qquad (2.69)$$

with

$$T_g(p) = T_g(0) + A_1 \cdot \ln(1 + A_2 \cdot p)$$

and

$$F(p) = 1 - B_1 \cdot \ln\left(1 + B_2 \cdot p\right).$$

This equation is commonly known as the YASUTOMI equation. A further model which is good for temperature extrapolation is the improved YASUTOMI model (BAIR et al., 2013)

$$\mu = \mu_g \cdot e^{\left[\dfrac{-2.303 \cdot C_1 \cdot \left(T - T_g\right) \cdot F}{C_2 + \left(T - T_g\right) \cdot F}\right]} \tag{2.70}$$

with

$$T_g = T_{g0} + A_1 \cdot \ln\left(1 + a_2 \cdot p\right) \quad \text{and} \quad F = \left(1 + b_1 \cdot p\right)^{b_2}.$$

Where $T_g(p)$ is the glass transition temperature and $F(p)$ the relative free volume, which is determined according to PAREDES et al. (2012). These are used in a WILLIAMS-LANDEL-FERRY equation. The parameters are found through a fit to viscosity data. However, this model only yields a good agreement for the viscosity after the inflection point if a sufficient amount of data points above inflection are considered (BAIR et al., 2013). The inflection point being the pressure from which the viscosity increases in a greater than exponential manner. In Fig. 2.3.3 the inflection point can be seen for a pressure of around 800 MPa for the data measured at 80 °C.

For a better extrapolation of the pressure dependence especially after the inflection point BAIR (2015) proposes the hybrid model, incorporating temperature, consisting of the McEWEN (BAIR, 2015) model:

$$\mu = \mu_0 \cdot \left(1 + \frac{\alpha_0}{q}\right)^q \tag{2.71}$$

and the PALUCH model (BAIR, 2015)

$$\mu = \mu_0 \cdot e^{\left(\dfrac{C_F \cdot p}{p_\infty - p}\right)}. \tag{2.72}$$

The hybrid model according to BAIR (2015) can thus be written as:

$$\mu = \mu_0 \cdot \left(1 + \frac{\hat{\alpha}_0}{q} \cdot p\right)^q \tag{2.73}$$

with

$$\mu_0 = \mu_{0\infty} \cdot e^{\left(\dfrac{D_F \cdot T_\infty}{T - T_\infty}\right)}$$

and

$$\hat{\alpha}_0 = a_2 \cdot \left(\frac{1}{T}\right)^2 - a_1 \cdot \left(\frac{1}{T}\right) + a_0$$

as well as

$$q = b_1 \cdot \left(\frac{1}{T}\right) + b_0 \quad , \quad p_\infty = c_1 \cdot \left(\frac{1}{T}\right) + c_0.$$

The fragility parameters may be set equal, thus $D_F = C_F$, and the model yields good results even if only data before the inflection point is available (SCHMIDT, BAIR and TRUSLER, 2016). Special care must be taken to avoid singularities in the relation when implementing this model in numerical calculations.

Figure 2.3.3 shows the results of several models for mineral oil in comparison to a set of measured data. It is clearly visible that, while the predictions are sufficient at lower pressures the viscosity models diverge significantly at higher pressures. The differences of the viscosity can differ by several orders of magnitude. This is especially important since EHL contacts exhibit these high pressures (Sec. 1.2.1) and is especially of interest if the traction in the contact is investigated (Eq. 2.11).

The choice of viscosity model will greatly affect the resulting traction calculation (see Sec. 7.4). Due to the number of models in existence for the description of the pressure (and to a certain extent the temperature) dependence of the viscosity the chosen viscosity model is often a point of dispute. Whilst some models have clear limits concerning pressure ranges or fluids, other models are seen as universal. A reliable description of the pressure dependence remains to this day often problematic, due to the fact that the viscosity model combined with the available data change the predicted behaviour at EHL pressures. The correct description of the physical properties is then highly dependent on available viscometer data.

It will further be pointed out that some models may in combination yield results which satisfactorily describe the traction of the contact, however are not physically sound in themselves.

In this work care was taken to choose viscosity models which allow for sound physical behaviour and are based on viscometry up to high pressures. Due to the physical basis and the link to the free volume the TAIT-DOOLITTLE equation was used to calculate the pressure dependent density and viscosity in this thesis. In a further step the YASUTOMI and Hybrid model were integrated in the computation as well for purposes of comparison.
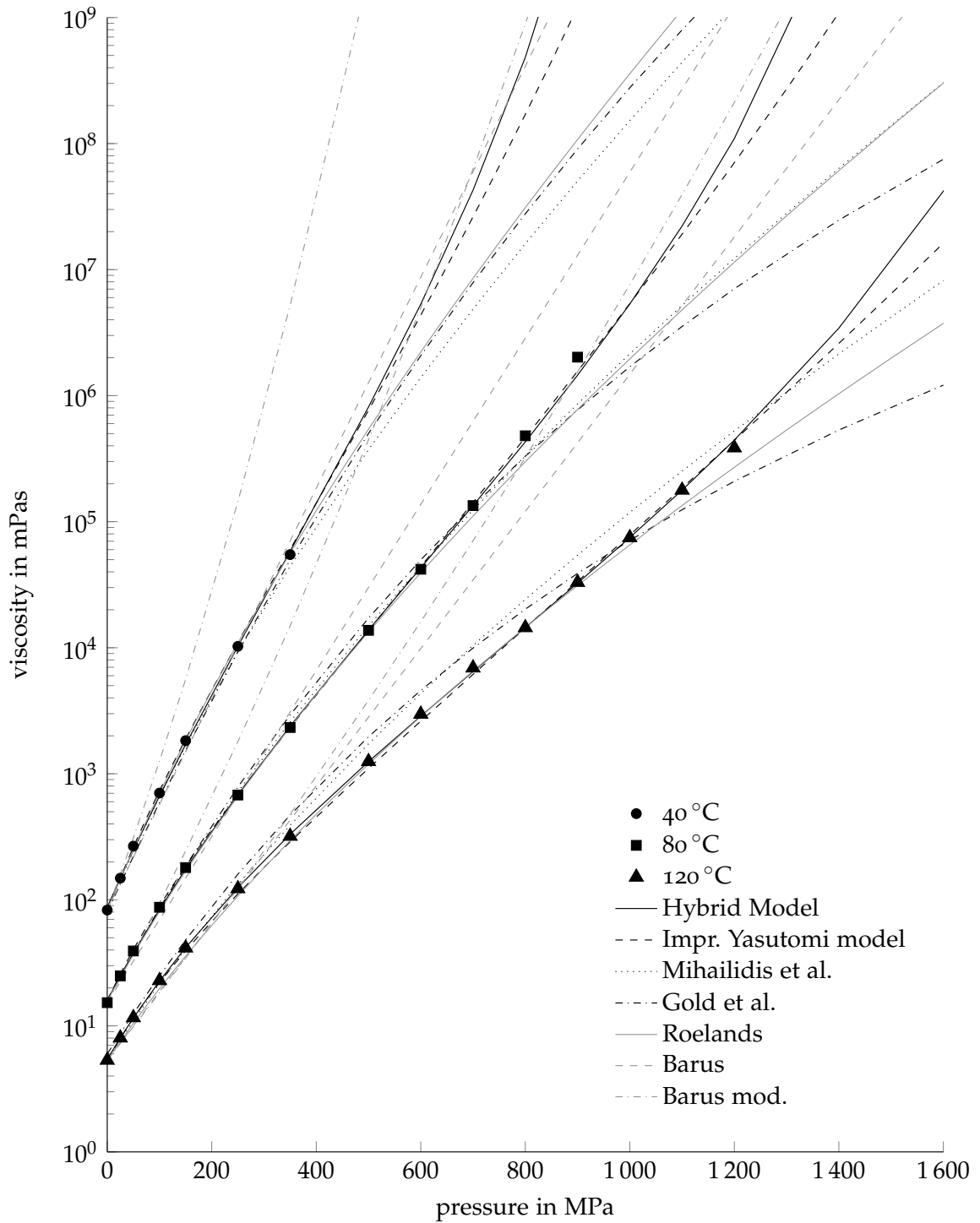
Figure 2.3.3: Measured pressure dependent viscosity and viscosity models for FVA 3 mineral oil. Measurements from ITR and GTech.

2.4   LUBRICANT BEHAVIOUR UNDER SHEAR AND PRESSURE

2.4.1   *Viscosity*

As discussed in Sec. 2.1.4, the shear rate shear-stress dependence has been shown not to be strictly linear. Several models of such a non-NEWTONian viscosity behaviour have been proposed. The viscosity in focus is called *high shear* viscosity and denoted as η in contrast to the *low shear* viscosity η_0[11].

EYRING (1936) developed and refined (REE and EYRING, 1955) a model to describe shear rate dependent fluid behaviour. It has been frequently applied to represent non-NEWTONian viscosity in EHL (BELL, 1962; BELL, KANNEL and ALLEN, 1964; JOHNSON, 1970; JOHNSON, 1978; SPIKES and JIE, 2014). It has been pointed out by BAIR, MARTINIE and VERGNE (2016) and BAIR (2017) that EYRING did not model the shear thinning behaviour considered here but rather a thixotropic fluid. However, in combination with certain viscosity models (especially with the viscosity model of ROELANDS (e. g. SPIKES and JIE, 2014)) the EYRING model is still widely used in EHL traction calculation due to the fact that this combination seems to represent real traction behaviour. Furthermore, GUEGAN et al. (2017) pointed out that the model developed by EYRING can well be applied to lubricant type molecules. However, the shortcomings of the ROELANDS pressure viscosity relation have been pointed out in Sec. 2.3 and therefore the results of the combination are questionable.

When considering viscosity relations for EHL application these problems and discussions need to be kept in mind. Furthermore, it should be observed that numerous models exist but not all are based on physically sound observations whilst many have only limited ranges of validity. It is interesting to note that TANNER (1965) as early as 1965 pointed out the exact same problem, that the choice of equation of state for non-NEWTONian behaviour is always based on a compromise between realism and complexity. In the following section an overview of common models is presented.

Considering the work of EYRING (1936) and REE and EYRING (1955) the viscosity can be written as:

$$\eta(\dot{\gamma}) = \frac{\tau_E}{\dot{\gamma}} \cdot \sinh^{-1}\left(\frac{\dot{\gamma} \cdot \eta_0}{\tau_E}\right) \ . \tag{2.74}$$

Or written as shear stress dependent shear rate:

$$\dot{\gamma} = \frac{\tau_E}{\mu} \sinh\left(\frac{\tau}{\tau_E}\right) \tag{2.75}$$

where the EYRING, or critical, stress is found as (JOHNSON, 1970):

$$\tau_c = \frac{\mathrm{d}\ln\bar{\tau}}{\mathrm{d}\dot{\gamma}} \ , \tag{2.76}$$

---

11 Or μ in English literature.

where $\bar{\tau}$ is the integral shear stress from traction experiments and $\dot{\gamma}$ the shear rate of the experiment. The critical shear stress τ_c is the shear stress describing the onset of shear thinning. To determine the critical shear stress, a viscometer measurement covering a range of shear stresses (shear rates) can be used. When intending to apply the results to EHL contacts, measurements in pressurised viscometers become a necessity.

EVANS and JOHNSON (1986) pointed out that the EYRING equation can not be applied when the work by the shear stress for promoting the flow exceeds the activation energy. The lubricant then exhibits a limiting shear stress.

Based on molecular network theory, CARREAU (1972) developed the following viscosity-shear relation:

$$\eta(\dot{\gamma}) = \mu_2 + \frac{\mu - \mu_2}{\left[1 + (\lambda\dot{\gamma})^2\right]^{\frac{1-n}{2}}} \tag{2.77}$$

where λ is the longest relaxation timeand μ_2 the second NEWTONian viscosity. For fluids with only one NEWTONian viscosity and by using the EINSTEIN-DEBYE relation the CARREAU equation can be rewritten as:

$$\eta(\dot{\gamma}) = \frac{\eta_0}{\left[1 + \left(\frac{\eta_0 \cdot \dot{\gamma}}{\tau_c}\right)^2\right]^{\frac{1-n}{2}}} \tag{2.78}$$

Due to the fact that most lubricants are normally not mono molecular they often exhibit a broad transition from NEWTONian behaviour to power-law response. Therefore the CARREAU-YASUDA model was proposed (YASUDA, ARMSTRONG and COHEN, 1981):

$$\eta = \mu \cdot \left[1 + \left(\frac{\mu \cdot \dot{\gamma}}{\tau_c}\right)^a\right]^{\frac{n-1}{a}} \tag{2.79}$$

for $a = 2$ this equation is identical to the CARREAU equation. When a decreases the transition range broadens. This model has been shown to be usable for a great number of lubricants (BAIR, 2004b). However, CUSSEAU et al. (2017) point out that for lubricants with viscosity index improvers this model may not be the best choice.

ZHANG (2015) proposes from the analysis of the response of a MAXWELL model:

$$\eta = \frac{\eta_0}{1 + \left(\frac{\eta_0\dot{\gamma}}{2G}\right)^2} \tag{2.80}$$

with

$$G = G_0 + \beta\eta_0|\dot{\gamma}| \tag{2.81}$$
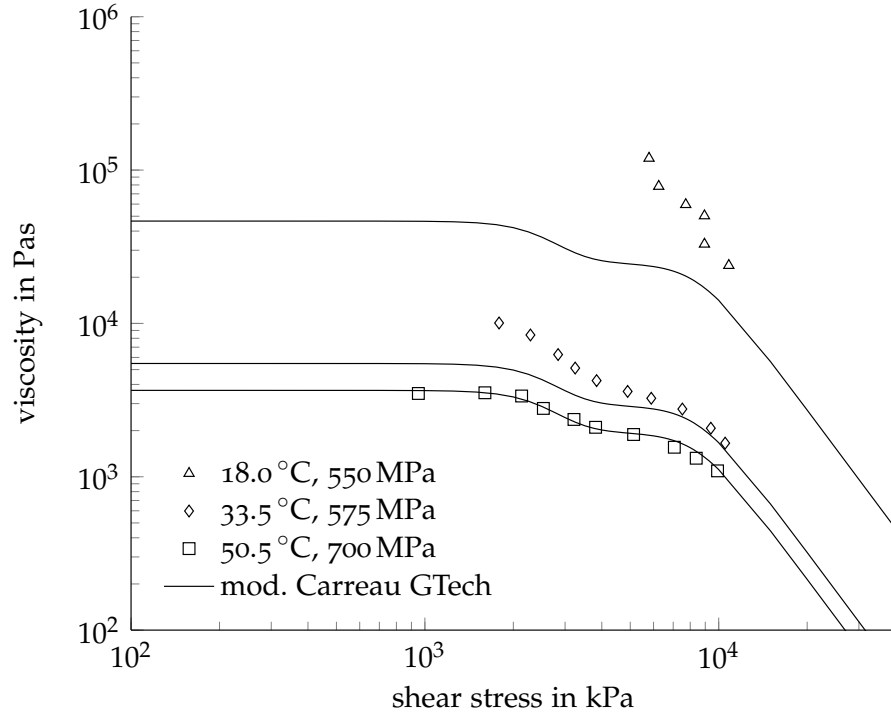
Figure 2.4.1: The shear stress dependent viscosity measured at GTech compared to the modified CARREAU model (Eq. 2.82)

with β a dimensionless constant. CUSSEAU et al. (2017) found that this relation fits investigated lubricants with viscosity index improvers well.

A double modified CARREAU equation was proposed by BAIR (2018) for liquids exhibiting a double NEWTONian plateau:

$$\frac{\eta}{\mu} = \left\{ \frac{\mu_1}{\mu} + \left(1 - \frac{\mu_1}{\mu}\right) \left[1 + \left(\frac{\tau}{G}\right)^2\right]^{\frac{\left(1 - \frac{1}{n_1}\right)}{2}} \right\} \left[1 + \left(\frac{\tau}{G_2}\right)^2\right]^{\frac{\left(1 - \frac{1}{n_2}\right)}{2}}$$

(2.82)

Measured data together with this model is given in Fig. 2.4.1 for FVA 3 mineral oil. The mineral reference oil shows signs of thixotropic behaviour or wax precipitation making it unclear whether the second NEWTONian really exists or whether it is result of wax forming in the liquid. For the data at 18 °C and 550 MPa this is assumed to be the case. Thus just the data at 50 °C and 700 MPa seem usable to obtain sound the parameters for the model.

The application of different fitting parameters for the data at 50.5 °C and 700 MPa is shown in Fig. 2.4.2. The parameters used for the fit are given in Tab. 2.4.1. It needs to be noted, that two fits of the data are

presented. The second fit being proposed by Brouwer with identical accuracy, i.e., the same goodness of fit meaning the paramter sets represent the measured data equally well.. Thus even with the same measurement a different implementation of the least squares curve fit can yield slightly differing models.

Table 2.4.1: Parameters for the double modified Carreau equation (Eq. 2.82) and FVA 3

Parameter	Fit GTech		Fit ITR	
i	1	2	1	2
n_i	0.1	0.28	0.1	0.4
G_i/kPa	3000	8500	3000	6500
a_i	5	6	5	6
μ_1/μ		0.53		
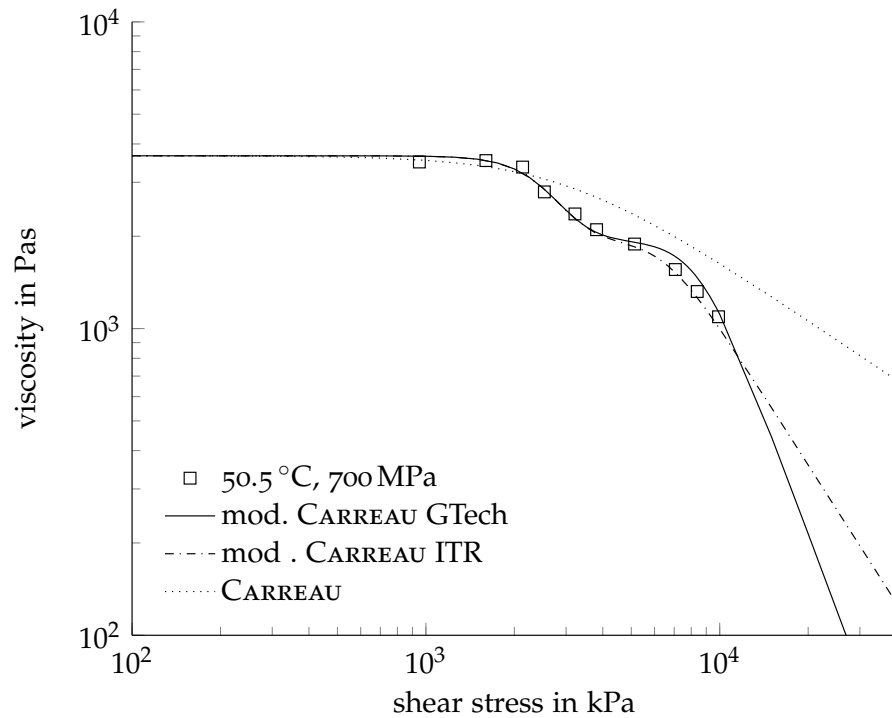
Figure 2.4.2: Comparison of different modified CARREAU (Eq. 2.82) fits for FVA 3. Even though identical data are used and the fits are of equal accuracy they yield slightly different extrapolations. The resulting viscosities for high shear stresses would diverge significantly. Furthermore the single CARREAU equation is shown. What needs to be pointed out is that this lubricants exhibits wax precipitation which could not be detected in a falling body viscometer for the pressure and temeperature. However, wax can lead to behaviour which looks similar to a second NEWTONian.

2.5   PARAMETERS FOR SHEAR STRAIN MODELS

In the following section the parameters used in the shear strain models introduced are discussed. In the following sections models for the shear modulus G, the critical shear stress τ_c, and limiting shear stress τ_{lim} are presented.

2.5.1   *Shear modulus*

Determination of the shear modulus G is still a challenge. When performing small-strain oscillatory shear measurements it can be shown that the component of the dynamic shear modulus in phase with the

shear strain G''[12] at the limiting high-frequency value is equal to the shear modulus G (BAIR, 2007):

$$G_\infty = \lim_{\omega \to \infty} G''(\omega) = G \ . \tag{2.83}$$

Thus an established way to determine the shear modulus is by measurement in rheometers using oscillating plates. This however, is only possible if the liquid can be kept in the gap. This problem often cannot be easily solved using oils. Some specialised experiments exist that can be used to measure G under pressure (BAIR, 1990). Another method is the use of transverse ultra-sound waves (HUTTON, 1984), which is also developed by SCHIRRU and DWYER-JOYCE (2016).

Numerous models for the shear modulus have been presented. An empirical model was proposed by DYSON (1970):

$$G_\infty = \frac{3 \cdot p}{2.52 + 0.024 \cdot T} \ . \tag{2.84}$$

Another empirical formula was developed by HUTTON and PHILLIPS (1972) for di(2-ethylhexyl)phthalate:

$$G_\infty = \frac{1.20 \cdot 10^7}{(T - 92.8\,\mathrm{K})^2} + \frac{1.74 \cdot 10^5 \cdot p}{(T + 16.7\,\mathrm{K})} \tag{2.85}$$

based on high-frequency transverse sound measurements in the temperature range $-30\,°\mathrm{C} \leq T \leq 30\,°\mathrm{C}$ and pressures up to $0.815\,\mathrm{GPa}$. T is the temperature in $°\mathrm{C}$ and p the pressure in MPa. This formula agrees with the proposed model by BARLOW et al. (1967) and BARLOW, ERGINSAVAND and LAMB (1967)

$$G_\infty = 0.5\,\mathrm{GPa} + 2.45 \cdot p \tag{2.86}$$

which was obtained at $30\,°\mathrm{C}$ for pressures up to $1.4\,\mathrm{GPa}$. BAIR (2007) states that both formulations agree well with measurements for mineral oil LVI260. However, a comparison of di(2-ethylhexyl)phtalate flow curves by BAIR (2007) showed that the equation would yield a G_∞ value that is two orders of magnitude too large.

JOHNSON (1978) states two equations for pressure and temperature dependency of G_∞. The pressure dependence is a generalised version of BARLOW's equation (EVANS and JOHNSON, 1986):

$$G_\infty = A + B \cdot p \tag{2.87}$$

with A stated as lying between 10^8 and $10^9\,\mathrm{Pa}$, whilst B is between 1 and 5, which are in agreement with the values from Eq. 2.86. Temperature dependence is given as:

$$G_\infty = \frac{C}{1 + K \cdot \Theta} \tag{2.88}$$

---

12 The component of the dynamic shear modulus in phase with the shear strain is called G'' in english literature. Some rheological communities however call this G' and use G'' as loss modulus, describing the viscous component of the shear strain.

where Θ is the temperature in °C and K around 0.01 and C a constant.

HOUPERT (1980) proposes a formula similar to the viscosity equations:

$$G_\infty = G_0 \cdot e^{\left(\alpha_G \cdot P + \left(\frac{1}{T} - \frac{1}{T_0}\right)\right)} \tag{2.89}$$

Whilst BAIR and WINER (1992) propose:

$$G_\infty = (a - b \cdot T) \cdot P \tag{2.90}$$

from measurements with a stress-strain-device (BAIR, 1990). For 5P4E the parameters a and b are 4.1 and 0.027 respectively. The temperature T is to be inserted in °C and p in GPa. The authors caution the use of this relation near pressures of zero as a shear modulus of zero at $p = 0$ does not seem reasonable. The same authors also state that for LVI260 and 5P4E, $G = 3p$ can be used as a good approximation.

The shear modulus is observed to be linked to the shear strength of the material. This is discussed in detail in Sec. 2.5.3.

2.5.2 *Critical shear stress*

To describe or determine the onset of shear thinning, i. e., the critical shear stress τ_{crit}, several models have been proposed over the years. Viscosity measurements at different shear rates, or better shear stresses, are necessary. Through the use of master curves measurements at different pressures and temperatures can be superimposed so that the critical shear stress of a fluid can be determined.

One problem of the use of viscometers is that at the high shear rates thermal softening can occur if the experiment is not well controlled. Thus only few specialised experiments exist which can be trusted to deliver the real viscosity at high shear rates under pressure (see e. g., BAIR, 2007).

However, a number of models have been proposed to obtain the critical shear stress from other parameters, e. g., pressure. In the following section some models are presented and discussed.

The REE-EYRING stress according to HOUPERT (1980):

$$\tau_{\text{RE}} = \tau_{\text{RE0}} \cdot e^{\left(\alpha_{\text{RE}} \cdot P + \beta_{\text{RE}} \cdot \left(\frac{1}{T} - \frac{1}{T_0}\right)\right)} \tag{2.91}$$

is similar to his proposed shear modulus and limiting shear stress formulation. It is linearised to:

$$\tau_{\text{RE}} = \tau_{\text{RE0}} + \alpha_{\text{RE}} \cdot P \,. \tag{2.92}$$

BAIR (2007) tries to model the critical shear stress based on molecular properties. He states that the rotational relaxation time, which is

responsible for the onset of shear thinning if the model of molecular alignment as mechanism is correct, can be formulated using the EINSTEIN-DEBYE relation:

$$\lambda_{\text{rel}} \approx \frac{\eta_0 \cdot M}{\varrho \cdot R_g \cdot \theta} \tag{2.93}$$

At a WEISSENBERG number of one the critical shear stress, i. e., onset of shear thinning occurs. Therefore:

$$\dot{\gamma} = \frac{1}{\lambda_{\text{rel}}} \tag{2.94}$$

and

$$\tau_C = \eta_0 \cdot \dot{\gamma}_C \tag{2.95}$$

and

$$Wi = \lambda_{\text{rel}} \cdot \dot{\gamma}_C = 1 \; . \tag{2.96}$$

Thus BAIR (2007) deduces for the critical shear stress:

$$\tau_C = \frac{\eta_0}{\lambda_{\text{rel}}} \approx \frac{\varrho \cdot R_g \cdot \theta}{M_{\text{mol}}} \tag{2.97}$$

which leads to a dependence of the critical shear stress on molecular mass and temperature.

HAMROCK (1991) states from a comparison of the EYRING formula with other models that the relationship between τ_c (termed as τ_E or EYRING stress) and the limiting shear stress τ_{lim} is:

$$\tau_c = \frac{\tau_{\text{lim}}}{3} \; . \tag{2.98}$$

The model using the EINSTEIN-DEBYE relation incorporates a physically sound mechanism. Whilst the other models may well be useful they are often based on the fitting of data with arbitrary functions. The use of Eq. 2.97 however has the shortcoming, that the molecular weight needs to be known. This is problematic if the formulation of lubricant is unknown or if the lubricant consists of mixtures. Thus the use of this relation often makes it necessary to estimate the molecular weight from models or assumptions.

2.5.3 Limiting shear stress

As described in Sec. 2.4 in most lubricants in EHL a maximum shear stress cannot be exceeded. The lubricant then behaves similar to a plastic flow when the yield limit is reached and the shear stress becomes shear rate independent. This shear stress was named limiting shear stress τ_{lim} by SMITH (1960) and is a material specific fraction of the pressure averaged over the contact (BAIR, 2007).

Mechanisms

Whilst the limiting shear stress has been observed in various experiments, several mechanisms for this behaviour have been proposed. PLINT (1967) hypothesised that slip planes should occur in the lubricant meaning that localised bands, wherein the slip of the lubricant occurs, should be present. Shear bands were shown by QURESHI (1992), BAIR, QURESHI and WINER (1993) and BAIR, WINER and DISTIN (1993) for pressures up to 0.3 GPa and by BAIR and McCABE (2004) for higher pressures using an optical cell. BAIR and McCABE (2004) demonstrated that in the lubricant shear bands occurred at an angle of $\approx 20°$. The behaviour of these slip bands has been compared to the yield behaviour of polymers (BAIR, 2007).

Other explanations are slip of the lubricant at the boundaries, i. e., the lubricant flows like a fluid, whilst the shearing is localised at one of the walls of the contact (STÅHL and JACOBSON, 2003). KANETA, NISHIKAWA and KAMEISHI (1990) and KANETA et al. (1992) presented experimental results pointing to a possible wall slip. GUO and WONG (2005) showed that this phenomenon could be influenced by the surface properties. The mechanism of wall-slip is sometimes applied in numerical simulations to model the limiting shear stress (STÅHL and JACOBSON, 2003; KUMAR and ANURADHA, 2014). ŠPERKA, KŘUPKA and HARTL (2014) show the flow of the lubricant as a plug with the shear localised in small regions close to or at the boundaries based on experiments and numerical calculations. TANNER (2000), however states that slip does not occur if the roughness scale of the wall exceeds the molecular size of the liquid and that elevated pressure should reduce the tendency for slip.

Thus several mechanisms have so far been proposed and partly demonstrated in measurements. CHANG (2005) summarises that different mechanisms may be responsible for the limiting behaviour, i. e., shear bands indicating lubricant rupture and slip at or close to boundaries due to temperature increase close to the interfaces when thermal conductivities are different.

A lowering of traction due to thermal influence of the interfaces was also found by HABCHI (2014) and HABCHI (2015) and reported by BOBACH et al. (2015). Both groups stated that lower friction, i. e., a lower maximum shear stress, can be attained in traction experiments when the partners or one of the partners are coated, e. g., by a diamond like carbon coating. The reported effect is that the heat transfer through the coating is reduced leading both to a temperature rise in the lubricating gap without affecting the inlet significantly. Although not solely linked to the limiting shear stress as this effect may be explained by purely viscous effects as well, an increase in temperature can, if a temperature dependence of the limiting shear stress exists, be in part also caused by thermal influence on the shear stress. Similarly JOHNSON and GREENWOOD (1980) investigated an EYRING fluid and

state that the maximum traction coefficient is solely governed by heating of the lubricant film. However, this contradicts before mentioned observations of a limiting shear stress in experiments in rheometers.

First steps to understand the physical behaviour of liquid lubricants under high pressure have been undertaken making use of molecular dynamic simulations (e. g., Gattinoni et al., 2013). These show promising steps, however still need to overcome several challenges. Examples are determining the correct lubricant wall interactions. A wrong choice of boundary conditions can easily lead to a behaviour which could be interpreted as the limiting shear stress but may be the result of surface force definitions. Martinie and Vergne (2016) compare results from molecular dynamics simulations to literature regarding the limiting shear stress. They come to the conclusion that the liming shear stress is driven by shear localisation, which in turn may manifest itself as wall slip, plug flow or shear banding.

It might be that through the insight of molecular dynamics a better understanding of the effects may be gained on the long term, however at present the mechanism responsible for the limiting shear stress still does not seem to be understood well. Moreover, several mechanisms leading to a limiting shear stress behaviour may be present in lubricated contacts depending on molecular structure as well as properties of the surfaces of the solids.

Measurement

The experimental determination of the limiting shear stress has been subject of several studies and different methods have been employed. The use of traction experiments (Smith, 1960; Johnson, 1970; Johnson and Tevaarwerk, 1977; Meyer, 2010b; Mayer, 2013; Wang, 2015) are widespread, whilst some researchers have used special experiments with homogeneous conditions making use of a modified Couette viscometer (Qureshi, 1992; Bair, 1990; Bair, 2007). Other homogeneous condition laboratory experiments include a high pressure chamber (HPC) (Höglund and Jacobson, 1986; Jacobson, 1991; Jacobson, 2006) detailed in Sec. 5.2. Other measurements include the use of EHD model contacts in a bouncing ball apparatus (Wikström and Höglund, 1994). A comparison of results of different methods is discussed in Sec. 5.2 especially Fig. 5.2.8.

The limiting shear stress not only governs the maximum traction transferable through the EHL film but also influences the lubricant film thickness profile. This has been demonstrated through experiments by Guo and Wong (2005) and numerically by Shieh and Hamrock (1991), Zhang and Wen (2002a) and Zhang and Wen (2002b).

Models

In the following section models to describe the limiting shear stress
are presented. Figure 2.5.1 shows the limiting shear stress for different
pressures measured in laboratory apparatus for two lubricants. The
apparatus is a high strain device derived from a modified pressur-
ised Couette viscometer. The cylinder is turned only one revolution
to avoid thermal softening and the shear force is measured (Bair,
1990). A pressure dependence can be easily identified. However, a
strict temperature dependence is not easily visible.
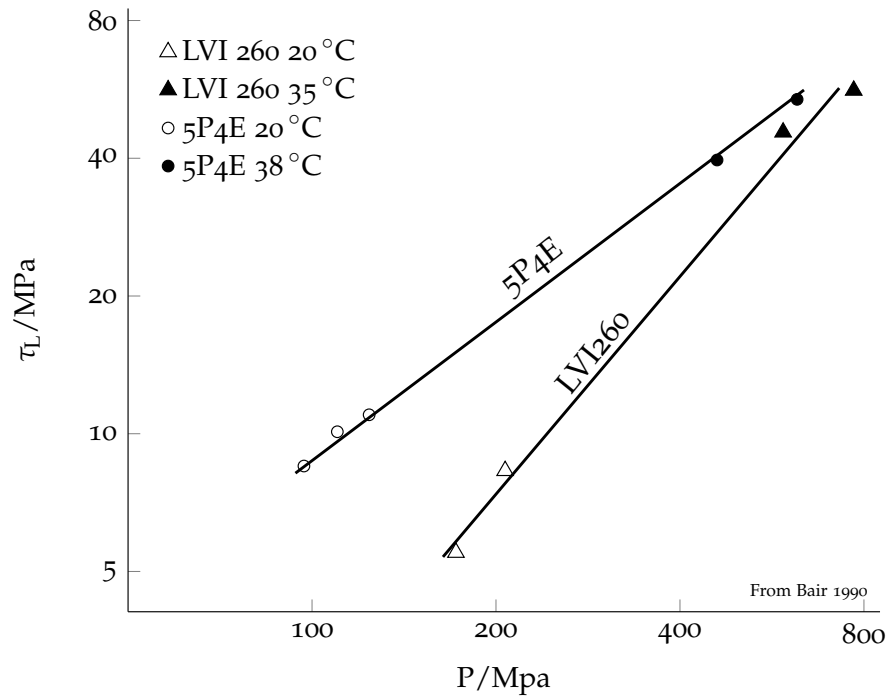
Figure 2.5.1: Limiting shear stress for LVI 260 and 5P4E measured by Bair
(1990) under laboratory conditions.

Several models for mathematical description of the limiting shear
stress have been proposed over time. Johnson and Tevaarwerk (1977)
are the first to propose a linear relationship between pressure and lim-
iting shear stress:

$$\tau_L = \tau_{L0} + \gamma \cdot P \tag{2.99}$$

with τ_{L0} representing an offset of the shear stress at ambient pres-
sure and γ the pressure gradient of the limiting shear stress.

Bair and Winer (1992) introduce a model with temperature de-
pendence and a linear pressure dependence:

$$\tau_L = (a - b \cdot T) \cdot P \tag{2.100}$$

setting $a \approx 0.95$ and $b \approx 3.5 \cdot 10^{-4}$. The temperature dependence is
not pressure independent in this case.

WIKSTRÖM and HÖGLUND (1994) propose a model based on the JOHNSON-TEVAARWERK model (Eq. 2.99) but incorporated a temperature influence by modifying the parameter γ in Eq. 2.99 in the form:

$$\gamma = a + b \cdot P + c \cdot T + d \cdot P \cdot T \,. \tag{2.101}$$

The proposed values for a are between 0.086 and 0.14, b between -0.0117 and $-27 \cdot 10^{-5}$, c between $-27 \cdot 10^{-5}$ and $+48 \cdot 10^{-5}$, and d in the range of $-5 \cdot 10^{-5}$ and $+11 \cdot 10^{-5}$. This in turn leads to values for γ from 0,08 to 0.09 for the conditions investigated.

HOUPERT (1980) proposes a model, used also by HOUPERT, FLAMAND and BERTHE (1981) and SOTTOMAYOR (2002), incorporating temperature which is similar to his model of the REE-EYRING-Stress and the shear modulus and which closely resembles pressure viscosity relationships:

$$\tau_{\mathrm{L}} = \tau_{\mathrm{L0}} \cdot \mathrm{e}^{\left(\alpha_\tau \cdot p + \beta_\tau \left(\frac{1}{T} - \frac{1}{T_0}\right)\right)} \,. \tag{2.102}$$

Where α_τ describes the pressure dependence and β_τ the temperature influence. Values proposed for a diester are $\tau_{\mathrm{L0}} \approx 3\,\mathrm{MPa}$, $\alpha_\tau = 11.47 \cdot 10^{-9}$ /Pa and $\beta_\tau = 585\,\mathrm{K}$. The reference temperature T_0 is chosen as 313 K.

HOUPERT, FLAMAND and BERTHE (1981) linearise the term to a form which is in agreement with the model by Johnson and Tevaarwerk.

$$\tau_{\mathrm{L}} = (A \cdot p - B) \cdot \mathrm{e}^{\left(\beta_\tau \left(\frac{1}{T} - \frac{1}{T_0}\right)\right)} \tag{2.103}$$

The temperature influence is described as minimal by all authors. BRANDÃO et al. (2011) and CAMPOS, SOTTOMAYOR and SEABRA (2006) even set the value for β_τ to zero, thus eliminating any temperature dependence.

In similar fashion RESHTOV and GRYAZIN (1990) propose:

$$\tau_{\mathrm{L}} = (\tau_0 + \gamma_R \cdot P) \cdot (1 - \varepsilon \cdot (T - T_R)) \tag{2.104}$$

HSIAO and HAMROCK (1992) use an equation with similarities to the work by HOUPERT, FLAMAND and BERTHE (1981):

$$\tau_L = \tau_{L0} \cdot \left(1 + \alpha_{\tau_{L0}} \cdot \frac{p}{\tau_{L0}}\right) \cdot \mathrm{e}^{\left[\beta_{\tau_L} \cdot \left(\frac{1}{T - T_R} - \frac{1}{T_0 - T_R}\right)\right]} \,. \tag{2.105}$$

With T_R the reference temperature $-273\,^{\circ}\mathrm{C}$, $\alpha_{\tau_{L0}}$ the dimensionless pressure-limiting-shear-strength proportionality constant, and β_{τ_L} the temperature-limiting-shear-strength coefficient in K.

MEYER (2010b) uses a twin-disc test rig to establish a formulation for the limiting shear stress. He proposes:

$$\tau_{\mathrm{lim}}(\bar{p}, v_{\mathrm{w}}) = (A_1 \cdot \bar{p} + A_2) \cdot \ln(v_{\mathrm{w}}) + (B_1 \cdot \bar{p} + B_2) \tag{2.106}$$

with $\bar{p}$ and v_{w} the mean contact pressure in N/mm^2 and the entrainment velocity in m/s respectively. Parameters for Santotrac 50 at 60 °C are given as $A_1 = 0, A_2 = -6.15, B_1 = 0.1051$, and $B_2 = 1.33$. The data were fitted from measurements in the fully lubricated as well as the mixed lubrication regime and are only valid for one temperature. Furthermore, it must be noted that this model is derived from twindisc data meaning not lubricant behaviour but integral EHL contact behaviour is described.

WANG (2015) proposes a bilinear approximation of the assumed pressure dependence –forming the basis of the calculation model used later– which allows for easy numerical handling:

$$
\tau_{\mathrm{max}} =
\begin{cases}
\tau_{\mathrm{crit}} & \text{for } p < p_0 + \frac{\tau_{\mathrm{crit}}}{\xi} \\
(p - p_0) \cdot \xi & \text{for } p \geq p_0 + \frac{\tau_{\mathrm{crit}}}{\xi}
\end{cases}
\tag{2.107}
$$

Here, the critical shear stress τ_{crit} represents the onset of shear thinning, p_0 is the pressure offset of the linear approximation, and ξ is the gradient of the pressure dependence. This model assumes that the lubricant needs to exhibit shear thinning before a limiting shear stress is reached. In absence of measured data the maximum shear stress endurable in the low pressure regime is set to τ_{crit}, sometimes also called EYRING stress, determining the onset of shear thinning. To exceed this value, the necessary shear rates in the low pressure regime would generate so much heat that no substantial further increase of τ is to be expected. The parameters are gained by fitting twin-disc traction experiments.

MAYER (2013) and LOHNER, MICHAELIS and STAHL (2016) derive a formulation for the limiting shear stress τ_{lim} from twin disc traction experiments similar to Eq. 2.106 but incorporate temperature. They separate the formulation into two parts, an experimental or contact integral part, i.e., traction data fit to $\tau_{\mathrm{lim|exp}}$, and a contact local limiting shear stress used for TEHL simulations $\tau_{\mathrm{lim|sim}}$. They formulate (LOHNER, MICHAELIS and STAHL, 2016):

$$
\tau_{\mathrm{lim|exp}} \left(p_{\mathrm{m}}, v_{\Sigma}, T_{\mathrm{ref}} \right) = E_{\dot{\gamma}1} \cdot p_{\mathrm{m}} + \left[E_{\dot{\gamma}2} + E_{\dot{\gamma}3} \cdot \ln \left(v_{\Sigma} \cdot 1 \frac{\mathrm{s}}{\mathrm{m}} \right) \right] + E_{\dot{\gamma}4} \cdot T_{\mathrm{ref}}
\tag{2.108}
$$

With $E_{\dot{\gamma}i}$ denoting lubricant specific parameters and $p_{\mathrm{m}}, v_{\Sigma}, T_{\mathrm{ref}}$ the mean pressure, sum velocity ($v_1 + v_2$), and the reference temperature in K respectively. The reference temperature used to fit the data is the bulk temperature of the discs measured during the experiment.

From the fit the authors deduce the contact local limiting shear stress $\tau_{\text{lim}|\text{sim}}$:

$$\tau_{\text{lim}|\text{sim}}\left(p, v_{\Sigma}, T_{\text{ref}}, T\right) = \dots$$

$$\dots \begin{cases} \tau_{\text{lim,m}} & \text{for} \quad \tau_{\text{lim}|\text{sim}} \leq \tau_{\text{lim,m}} \\ \frac{4}{\pi} \cdot \tau_{\text{lim}|\text{exp}}\left(p_{\text{m}} = p, v_{\Sigma}, T_{\text{ref}}\right) \cdot \sinh\left(\frac{T_{\text{ref}}}{T}\right) & \text{for} \quad \tau_{\text{lim}|\text{sim}} > \tau_{\text{lim,m}} \end{cases}$$

$$(2.109)$$

with $\tau_{\text{lim,m}}$, T denoting the minimum limiting shear stress and the temperature respectively. The value for the minimum limiting shear stress $\tau_{\text{lim,m}}$ is set to $5\,\text{N/mm}^2$. This is done to not run into a physically unsound negative limiting shear stress, however the value seems to be chosen arbitrarily. When considering other models it can however be noted, that WANG (2015) sets this value at the shear stress for the onset of shear thinning τ_C which is around the same magnitude whilst the minimum limiting shear stress given by HOUPERT (1980) is around 3 MPa also of similar magnitude. The value of τ_0 given by JACOBSON (1991) is around 15 MPa.

Through a study employing traction experiments conducted isothermally NDIAYE et al. (2017) develop a temperature dependence of the limiting shear stress.

$$\bar{\tau}_{\text{L}} = \Lambda \bar{P} - \beta T + \tau_{\text{L}0} \tag{2.110}$$

where Λ and β are the limiting shear stress pressure and temperature coefficients respectively. This is the only formulation with a pressure independent temperature effect other than Eq. 2.108. For benzyl benzoate the coefficients $\Lambda = 0.0811$, $\beta = 0.503\,\text{MPa/K}$ and $\tau_{\text{L}0} = 137.1\,\text{MPa}$ are given.

Furthermore, NDIAYE (2017) links the limiting shear stress to the onset of glass transition in the lubricant through RAMAN spectroscopy. While this has been hypothesised already for a long time, previous data from laboratory measurements could not show a direct link of limiting shear stress and glass transition (BAIR, 1990; BAIR, 2007). More precisely BAIR (1990) states that curiously the limiting shear stress pressure relationship seems untouched by the glass transition.

Equations 2.108 and 2.109 –included in Tab. 6.1.1– yield values that are quite similar to the results from MEYER (2010b), WANG (2015), or other authors. The added temperature dependency is given as about $-0.5\,\text{MPa/K}$ for a mineral reference oil FVA 3.

BROUWER and SCHWARZE (2013) present a model for the limiting shear stress based on the energy barrier of the LENNARD-JONES potential. They compare the resulting limiting shear stress with traction experiments and state acceptable agreement. However, this method yields lower than expected values for higher pressures ($p > 800\,\text{MPa}$).

Thus discussions are still ongoing to broaden the range of validity of this model (e. g. BROUWER, BADER and BEILICKE, 2016).

Shear modulus dependence of limiting shear stress

As mentioned in Sec. 2.5.1 it is assumed that $G \propto \tau_{\text{lim}}$. Whilst most proposed models base on traction experiments with only few laboratory experiments proposals have been made to link the limiting shear stress to mechanical fluid properties. From oscillatory measurements DYSON (1970) proposes the following relation between limiting shear stress and shear modulus:

$$\tau_{\text{L}}(G) \approx 0.25 \cdot G_{\infty} \tag{2.111}$$

This relation has also been used to estimate the shear modulus (WANG, 2015).

EVANS and JOHNSON (1986) and TABOR state the relation

$$\tau_{\text{lim}} \approx \frac{G}{30} \tag{2.112}$$

which is the expected value for the ultimate shear strength of a solid where the intermolecular VAN DER WAALS bonds are broken.

3

AIMS AND SCOPE

The computation of traction in EHL contacts being of great importance when striving to reduce losses, has been an ongoing challenge for several decades. The accurate prediction of traction is strongly dependent on the rheological models of the applied lubricants. Several models incorporating non-NEWTONian behaviour, as well as limiting shear stress, have been proposed (e. g., JACOBSON, 1991; BAIR, 2007). The fluid behaviour itself is dependent on the shear rate, pressure, and temperature found in the contact. Since the introduction of EHL theory discussions between researchers have been ongoing, one fraction advocating traction experiments –which have the disadvantage that non homogeneous conditions are the basis of the obtained fluid parameters– and the other fraction preferring laboratory measurements to gain accurate models and model input data for computational models of the losses in the contact.

One of the effects governing the traction transferred through an EHL contact is the limiting shear stress. This work investigates the maximum shear stress transmitted in an EHL contact using a twin-disc machine, mini traction machine (MTM), high pressure chamber measurements (HPC), and computations. Due to the fact that the twin-disc machine (and MTM) only yields integral data from the whole contact area and can thus not be used to determine true fluid properties the experiment is coupled with local temperature measurements within the contact during traction experiments, in order to consider the differing conditions present in the contact.

An existing computational model is adapted to include shear thinning, different pressure viscosity relations, and different limiting shear stress functions to investigate the influence of temperature on the viscosity and the limiting/maximum shear stress in the contact. Thus a study of the influence different limiting shear stress models, temperature effects on viscosity, and pressure-viscosity relations on the total traction of the contact is achieved. Thus contributing to answering the question whether the traction transferred through the lubricant film is limited due to a temperature dependence of the limiting shear stress or whether the dominant effect is the temperature influence on viscosity.

This work aims to generate a better understanding of the lubricant behaviour in EHL conditions by based on high pressure viscometer data, high pressure chamber results, data gained from traction experiments, and the measurement of local temperatures within the EHL contacts in these traction experiments, thus allowing a better under-

standing and modeling of the shear stresses occurring in the lubricant film.

4

EXPERIMENT

If it disagrees with experiment
it is wrong.
— Richard P. Feynman

The experiments shown were conducted using a number of lubricants. The properties are listed in Table 4.0.1.

Table 4.0.1: Physical properties of lubricants measured by ITR from (Brouwer, Bader and Beilicke, 2016)

Lubricant	Type	$\eta_{40\,°C}$ in mPas	$\eta_{100\,°C}$ in mPas	$\varrho_{15\,°C}$ in kg/m^3
FVA 3	Mineral reference oil	80.98	9.1	884.8
Brake	Polyglycol base	7.08	2.2	1067.2
SRS	Calibration fluid	2.6	1.8	827.6
Oil A	Engine Oil	24.8	5.2	854.7
Oil B	Engine Oil	39.6	6.9	853.4
Oil C		137	20	862
Oil D	Hydraulic oil	29.2	4.9	873.9
Santotrac 50*	Traction fluid	30.5	23.7	845.3

* not measured at ITR

4.1 TRACTION EXPERIMENTS

Traction experiments have for a long time been used to investigate the lubricant behaviour in concentrated contacts (Crook, 1963; Smith, 1960; Bell, Kannel and Allen, 1964; Johnson and Cameron, 1967). The use of tribometers or traction experiments has the positive effect that the conditions of the real application can be duplicated. Methods have been been proposed to extract viscosity data from traction curves (e. g., Evans and Johnson, 1986), these have also been criticised (Bair, 2000). However, the disadvantage is that the the conditions in the contact are inhomogeneous and thus only a mean value but not the direct lubricant behaviour can be observed.

Figure 4.1.1 shows the typical characteristics of traction curves measured with twin-disc machines. Depicted is the traction coefficient

versus the slide to roll ratio. Furthermore, different regimes are indicated. The behaviour of the traction curves is similar to the behaviour of a flow curve measured in a rheometer (Fig.2.1.4), however it represents the integration across a rolling contact.

Furthermore, the curves in the right can be used to identify the lubricant behaviour, i.e., for regimes with behaviour C and D a DEBORAH number $D >> 1$ is found and visco-elastic lubricant behaviour is expected.
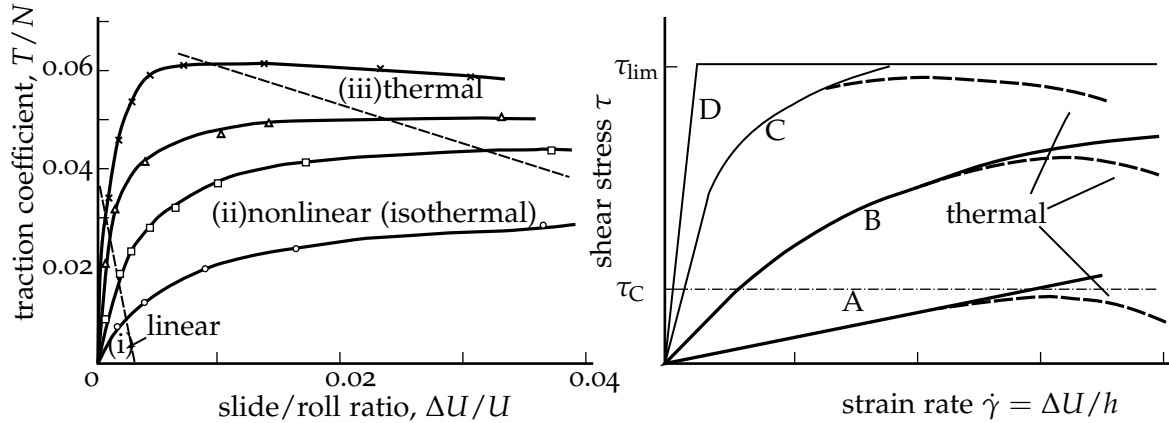
Figure 4.1.1: Left: Friction regimes according to JOHNSON and TEVAARWERK (1977). Note: The axis have been mislabelled in the original publication see also (JOHNSON and CAMERON, 1967). Right: The effect of viscous and elastic behaviour as well as shear thinning and limiting shear stress taken from EVANS and JOHNSON (1986). A B C D

Figure 4.1.2 shows the principle behaviour of traction curves with increasing pressure, decreasing temperature and rolling speed. An increase in pressure yields higher traction coefficients with a more clearly marked maximum of the traction curve. The same effect appears with decreasing temperature and entrainment velocity. The effects acting here are the increase in viscosity, i.e., shearing losses, and an increase in mixed friction respectively.

4.1.1 *Twin Disc Experiments*

Traction measurements were conducted using a twin disc test rig, shown in Fig. 4.1.3. A crowned disc, with a crowning radius of 50 mm, is run against a cylindrical disc. Both discs are made of hardened 100Cr6 (AISI 52 100) steel, super finished to a surface roughness of $Ra \approx 32$ nm. Thus, an isotropic surface pattern is achieved. The normal force is applied by a hydraulic cylinder to the shaft supporting the cylindrical disc, which in turn is mounted on a linear bearing. This allows for free movement perpendicular to the shaft's axis. The experiments were conducted at mean contact pressures up to 2.7 GPa. The discs are driven directly by electric motors with defined rotational speeds. One of the electric drives is supported by an aerostatic
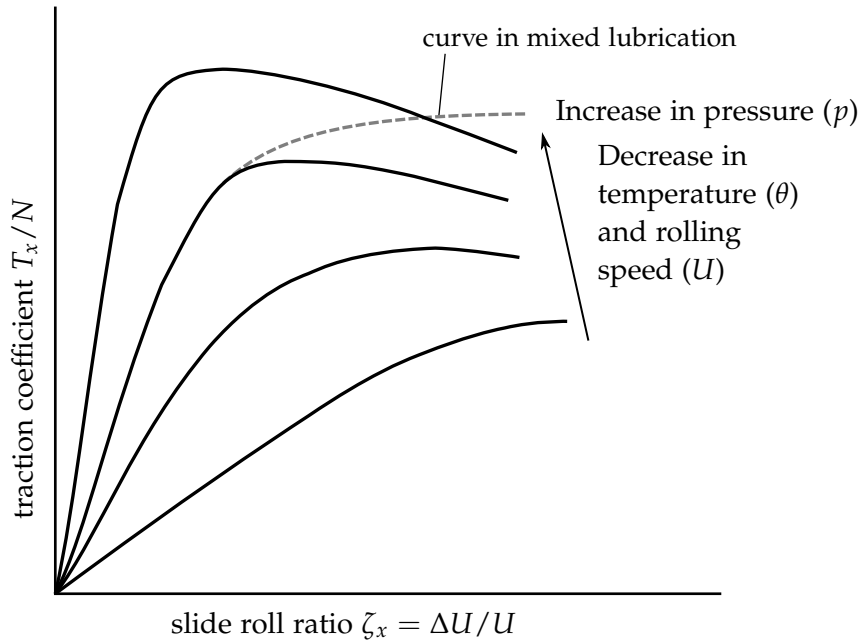
Figure 4.1.2: Behaviour of traction curves dependent on speed, temperature, and pressure from (JOHNSON, 1978). Although the behaviour is labelled for decreasing entrainment velocity in the original puplication these characteristic curves are only valid for a decreasing entrainment velocity whilst maintaining full film lubrication. For decreasing rolling speed with the resulting curve reaching a mixed lubrication regime, the grey curve has been added.

bearing allowing for the measurement of the reaction torque. Thus, the force transmitted through the EHL contact can be determined. To achieve this, the friction of the supporting bearings is first subtracted. The fluid is supplied to the contact from the top in direction of entrainment. The fluid is heated to a temperature which is measured directly before the contact inlet. The experiment is performed by varying the slide to roll ratio (SRR) from minus 10 % to plus 10 %. The hydrodynamic velocity is kept constant during the whole experiment, i. e., one disc is accelerated while slowing down the other one to reach a defined SRR.

The magnitude of the elastic slip was determined and subtracted from the measured data as shown in Sec. 2.1.5. All shown data is thus assumed to purely represent the lubricant behaviour.

4.1.2 *MTM Experiments*

For regimes of lower pressures (0.4 GPa up to 0.8 GPa) traction experiments were performed using a Mini Traction Machine (MTM) from
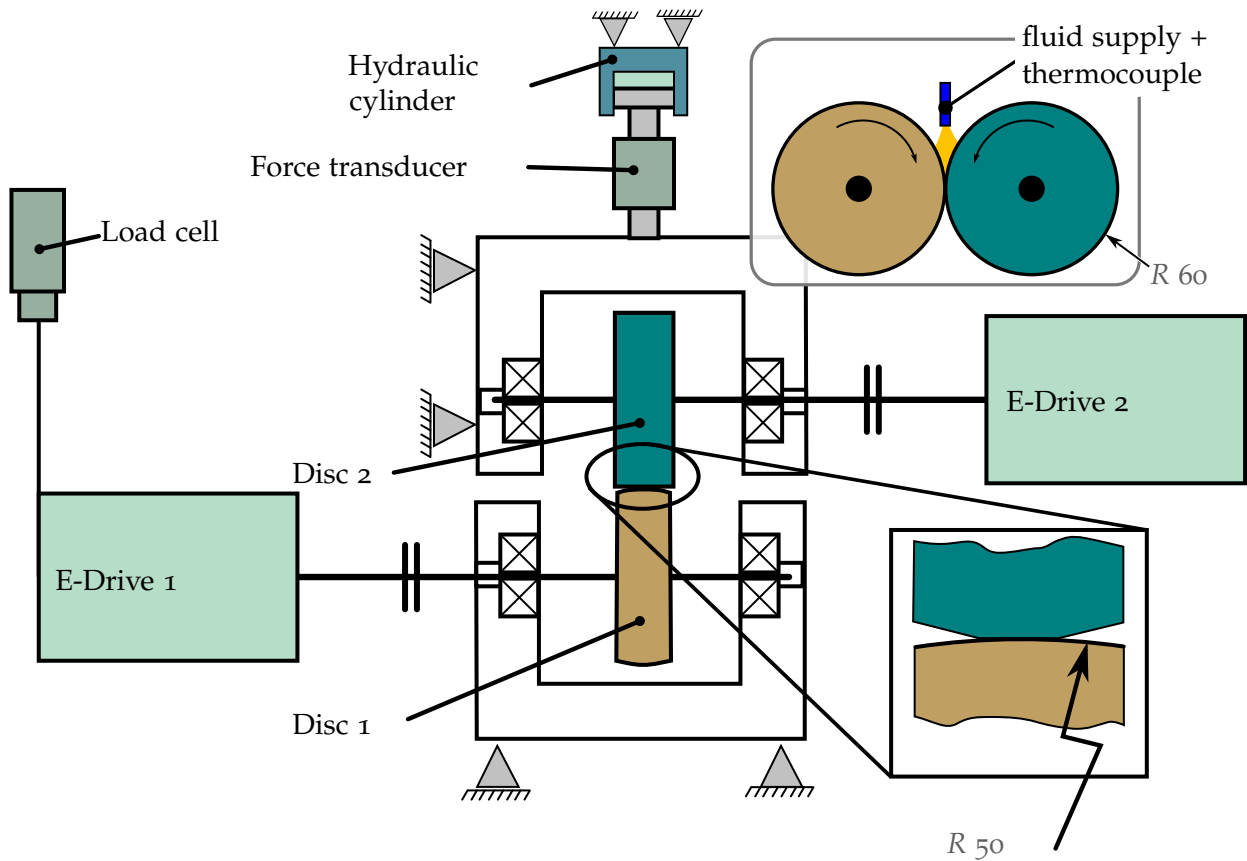
Figure 4.1.3: Twin disc traction experiment also used by WANG, 2015; MEYER, 2010b

PCS Instruments. The design of the test rig is depicted in Fig. 4.1.4. Here, a hardened steel ball with 3/4" diameter is run against a flat disc on a radius of 46 mm. The disc runs in an oil bath which is temperature controlled.

The experiment is started after a stationary temperature distribution is reached. During this period disc and ball are run in alternating directions to reach homogeneous conditions in the oil bath.

The experiment is conducted by measuring the resulting traction in forward and reverse rotation, i. e., positive and negative *SRR* respectively, at a defined absolute *SRR* value. The measured values are then averaged, i. e., each resulting data point is the average of negative and positive *SRR*.

The resulting traction curves were analysed in the same manner as the twin disc results.

4.1.3   *EHL Film Thickness Measurements*

The film thickness was measured using a PCS INSTRUMENTS EHL 1 test rig. The test rig was kindly made available by the VW central laboratory in Wolfsburg. The set-up is depicted in Fig. 4.1.5. The film thickness measurements are based on interferometry. A Steel ball is
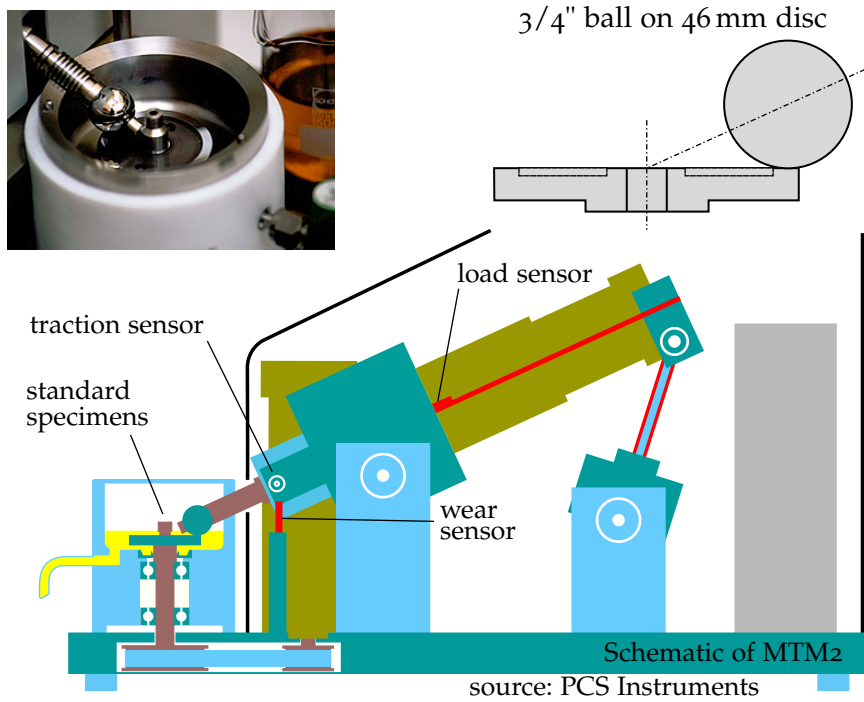
Figure 4.1.4: Mini Traction Machine (PCS Instruments)

run against a glass disc with a semi reflective layer. The layer itself is coated by a silica layer. The interference of the light from the semi reflective layer and the steel ball is evaluated and thus the film thickness can be determined. The ball is supported on three bearings leading to low spin slip in the contact which could otherwise influence film formation. The parameters for the experiments are given in Tab. 4.1.1.

The measurement of the film thickness was conducted at a single point on the track and the thickness of the silica layer at that point was measured using the dry contact. All experiments were conducted with rising velocity. The temperature was measured in the oil bath about 1 mm in front of the ball. The temperature was kept stable for at least 30 minutes prior to each measurement.

Figure 4.1.6 shows the obtained results for FVA 3 oil. The dashed lines indicate film thickness as calculated by film thickness equations (Eq. 1.33). The agreement is satisfactory. Based on this, the film thickness values calculated by the formula are used as basis for gap height calculation in Sec.7.

4.2 EXPERIMENTS TO DETERMINE TEMPERATURES

4.2.1 *Local Temperature in EHL Contact*

The local temperature and its distribution have been of interest for researchers for a long time with the reason being that this temperature
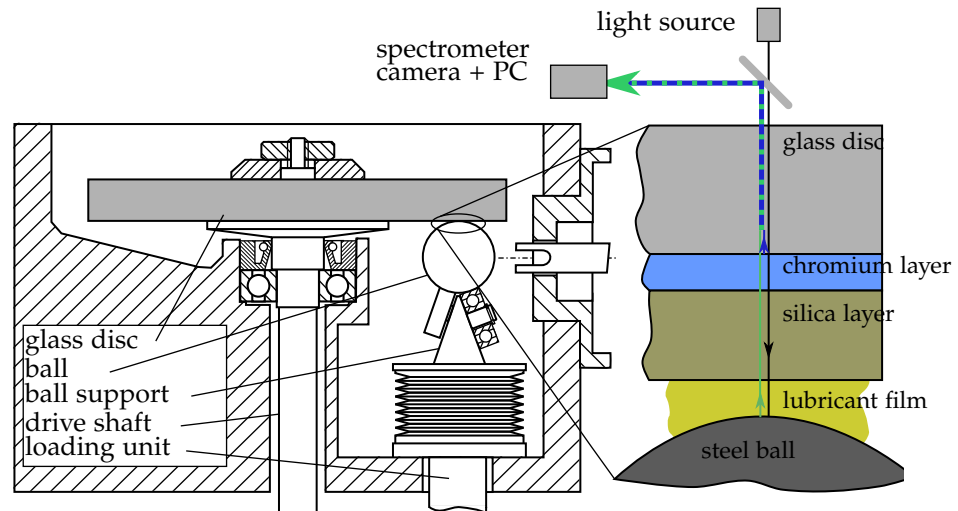
Figure 4.1.5: EHL machine (PCS Instruments)

influences the viscosity and thus traction as well as the film thickness (e. g. CROOK, 1958; CROOK, 1961a; CROOK, 1961b; CROOK, 1963). Responsible for the temperature rise is the friction in the contact. Two mechanism lead to heating: Compression and shearing. The compression can be the result of pressure build up or due to the rolling friction. When running at zero slip the compression is expected to be solely due to the pressure profile (GOHAR, 1988).

REDDYHOFF, SPIKES and OLVER (2009a) studied the temperature with infra-red measurements finding that an increase due to pressure rise occurs. At the outlet a drop in temperature, even cooling below the inlet temperature, occurs due to rapid pressure drop in the lubricant. This even caused phase changes to be suspected to occur for one lubricant (5P4E).

The shear heating of the lubricant is caused by the rolling friction as well as the sliding component of friction. The contribution of the rolling friction is mostly insignificant compared to that of the sliding friction, provided sliding friction is present (GOHAR, 1988).

CROOK (1963) states that even with the surfaces showing considerable temperature rises (i. e., flash temperatures) the temperature rise within the lubricant is low (GOHAR, 1988).

Numerous numerical investigations based on the solution of the energy equation have been conducted to gain insight into the temperature within an EHL contact (KIM and SADEGHI, 1992; KIM and SADEGHI, 1993; CHANG and FARNUM, 1992).

The PÉCLET number represents the ratio of convected heat by fluid motion to the diffused heat into the solids. The energy equation used for the bounding surfaces is normally only valid at high PÉCLET numbers. Based on the of work by JAEGER (1942) and CARSLAW and JAE-

Table 4.1.1: Parameters of film thickness measurements

Steel ball	100Cr6 (AISI 52100)
Ball radius	19.05 mm
Elastic modulus	207 GPa
Poisson's ratio	0.3
Disc	Quartz glass
Curvature	∞
Track radius	34...44 mm
Elastic modulus	75 GPa
Poisson's ratio	0.22
Load	20 N
$P_{\mathrm{Hertz}}/p_{\mathrm{mean}}$	527 MPa/351 MPa
Velocity	0.2...4.5 m/s
Temperature	20...80 °C
Measurement uncertainty (acc. PCS)	±1 nm

GER (1959) the solution of the problem has been possible for arbitrary PÉCLET numbers (e. g. Bos, 1995; KIM et al., 2001).

$$Pe = \frac{a \cot u_{\mathrm{s}}}{2 \cdot \kappa} \tag{4.1}$$

according to (KIM et al., 2001) with κ diffusivity, a radius of the HERTZian contact circle in m or half the maximum length of the heat source in the direction of the velocity, and u_{s} the mean speed of surfaces in m/s.

Whilst the use of thermocouples is widespread the challenge is to gain an insight into the temperature distribution in the contact, that means obtain a temperature map. Several methods to measure contact temperature exist. In this work, infra-red thermography is applied. Early measurements using infra-red thermography date back to the eighties (AUSHERMAN et al., 1976; NAGARAJ, SANBORN and WINER, 1979). Recent developments in the field of infra-red thermographic cameras have led to investigations resulting in measurements of two dimensional temperature distributions even considering asperity contacts (REDDYHOFF, SPIKES and OLVER, 2009b; REDDYHOFF, SPIKES and OLVER, 2009a; LE ROUZIC and REDDYHOFF, 2013; YAGI, KYOGOKU and NAKAHARA, 2006). Nearly all experiments measuring local temperature –i. e., considering temperature distribution perpendicular to the entrainment direction– thus far have been performed using ball on disc apparatus. However, a number of experiments have been carried out measuring the temperature within EHL contacts in
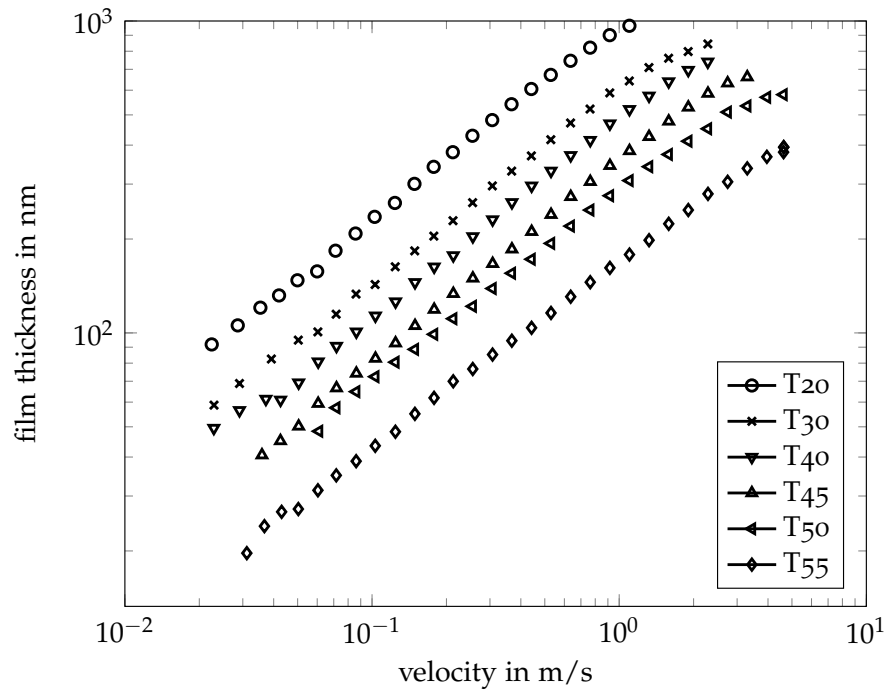
Figure 4.1.6: Film thicknesses measured for FVA 3

twin disc machines, cam followers, and gear test rigs using thin film sensors (LEEUWEN, MEIJER and SCHOUTEN, 1987; SCHMIDT, 1985; BAUMANN, 1987; PEEKEN et al., 1990; DAUBNER, 2001).

To determine the temperature in the contact and gain an insight into the real temperature dependent lubricant behaviour, two experiments were set up.

4.2.2   *Body Temperature*

In the first experiment, the twin disc traction test was modified by integrating a thermocouple was introduced into the discs about 1.2 mm below the contact. The measured temperature thus mainly represents the temperature of the disc body, due to the slow reaction time of the measuring system. Non the less, the temperature influence can be closer investigated with this knowledge. Furthermore, such temperatures may be used as boundary conditions in simulations. The thermocouples were Ni-CrNi (type K) with the amplifier situated on the shaft end. From there the signal was transmitted via a slip ring system (HBM SK12) to the DAQ device. For calibration the disc was heated to known temperatures. To ensure homogenous temperature the disc was kept at least 30 minutes at the stabilised temperature. The use of thermocouples has the disadvantage that the measurement depends on the temperature at the amplifier. Thus the housing of the amplifier was designed in such a way, that the air flow during

rotation keeps the housing at ambient temperature. A schematic of the set-up is depicted in Fig. 4.2.1.

When running an experiment during which the *SRR* is set to a fixed value and held for a certain time the temperature behaviour in Fig. 4.2.2 is observable. It is visible that the bodies start heating up from heat generated in the contact. At least 100 s are needed to reach stationary body temperatures. Furthermore, the temperature gradient is dependent on the *SRR* –with greater *SRR* leading to steeper gradient due to higher temperatures from the contact. It is visible that a stable body temperature is not attained for less than 100 s. This in turn means, that during the traction experiments transient conditions, that is changing body temperatures, are present. The influence of this effect on the maximum shear stress is shown and discussed in Fig. 6.1.3 in Sec. 6.1.2.
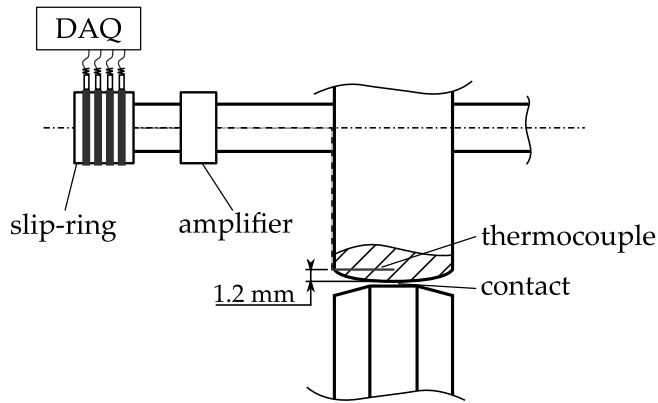
Figure 4.2.1: Set up to determine the body temperature
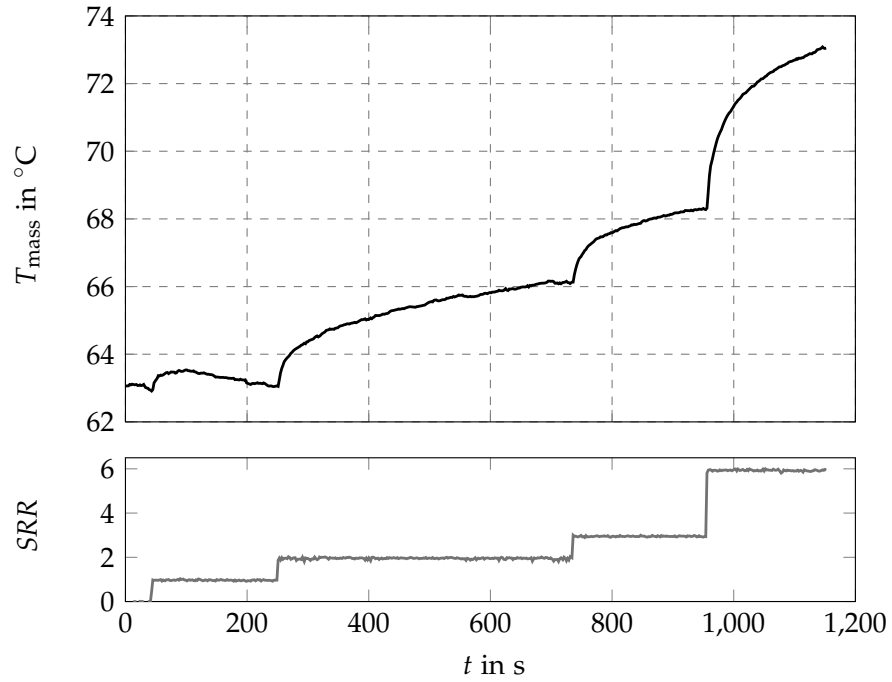
Figure 4.2.2: Behaviour of mass temperature during a traction experiment. It can be understood, that a rise in *SRR* will lead to a warm up of the body with a stabilisation time greater than 100 s.

4.2.3 *Measurement of Local Temperature in EHL Contact*

For the second experiment, an infra-red camera was used and the twin-disc experiment modified to observe the EHL contact and gain temperature maps from within the rolling sliding contact.

Infrared thermography

According to PLANCK the total radiant power into the hemisphere of a black body of a given Temperature T in the wavelength interval $\lambda, \lambda + \mathrm{d}\lambda$ can be expressed as (VOLLMER and MÖLLMANN, 2011):

$$M_\lambda \left(T\right) \mathrm{d}\lambda = \frac{2\pi hc^2}{\lambda^5} \cdot \left(e^{\frac{hc}{\lambda kT}} - 1\right)^{-1} \mathrm{d}\lambda \qquad (4.2)$$

$h = 6.626 \cdot 10^{-34}\,Js$
$c = 2.998 \cdot 10^8\,m/s$

Here, h is PLANCK's constant, c is the speed of light in vacuum, λ is the wavelength of the radiation, and T is the absolute Temperature. Figure 4.2.3 shows the resulting radiant power for different temperatures and the band visible for infrared cameras.

The excitance of black body sources is calculated as:

$$M \left(T\right) = \int_0^\infty M_\lambda \left(T\right) \mathrm{d}\lambda = \int_0^\infty M_\nu \left(T\right) \mathrm{d}\nu = \varsigma T^4 \qquad (4.3)$$
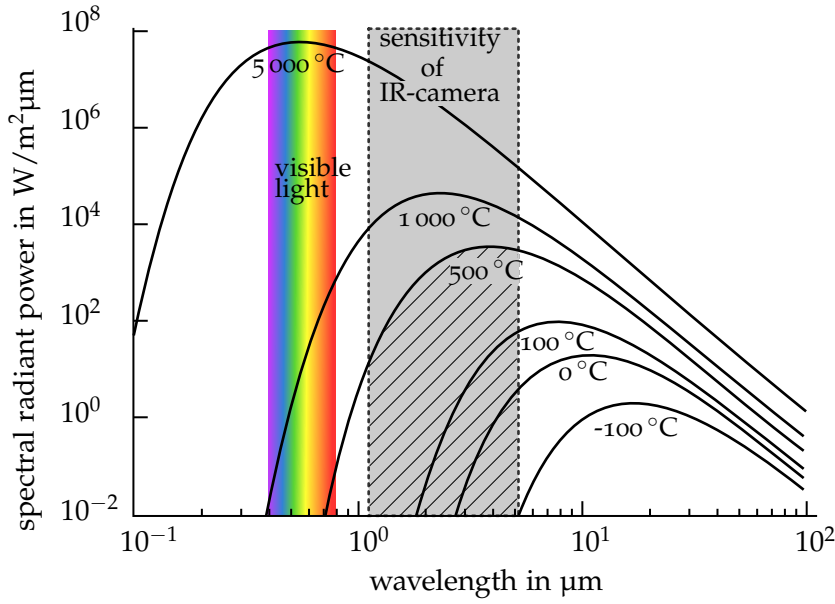
Figure 4.2.3: PLANCK's law and the wavelength measured. Hatched is the spectral range measured by the used infra-red camera.

With ς denoting the STEFAN-BOLTZMANN constant. As IR imaging only detects a predefined spectral range of $0 \rightarrow \lambda$ the black body radiation is compared to the total emission.

$\varsigma = 5.67 \cdot 10^{-12} \, W/m^2 K^4$

$$F_{(0 \rightarrow \lambda)} = \frac{\int_0^\lambda M_\lambda d\lambda}{\int_0^\infty M_\lambda d\lambda} \tag{4.4}$$

Figure 4.2.3 also depicts the band described by above equation, shown hatched for a temperature of 500 °C. This can be used to obtain the portion of black body radiation and excitation for the limited band detected by the IR sensor.

Due to the fact that technical surfaces do not represent ideal black-bodies the emissivity ε is defined as the ratio of actually emitted radiation and the radiation a black body would emit. In a similar manner a transmissivity τ and a absorptivity α can be defined. From KIRCHHOFF's law it follows that the radiation absorbed is equal to the radiation emitted.

$$\varepsilon = \alpha \tag{4.5}$$

Real systems are mostly either grey bodies emitting less radiation than a black body due to their surface or selective emitters. Possible radiating bodies are depicted in Fig. 4.2.4. Figure 4.2.5 shows the infra-red spectrum of FVA 3 mineral oil. The radiation is confined to a band around 3 µm. The lubricant thus acts as a selective emitter, whilst the contacting disc can be described as a grey body.
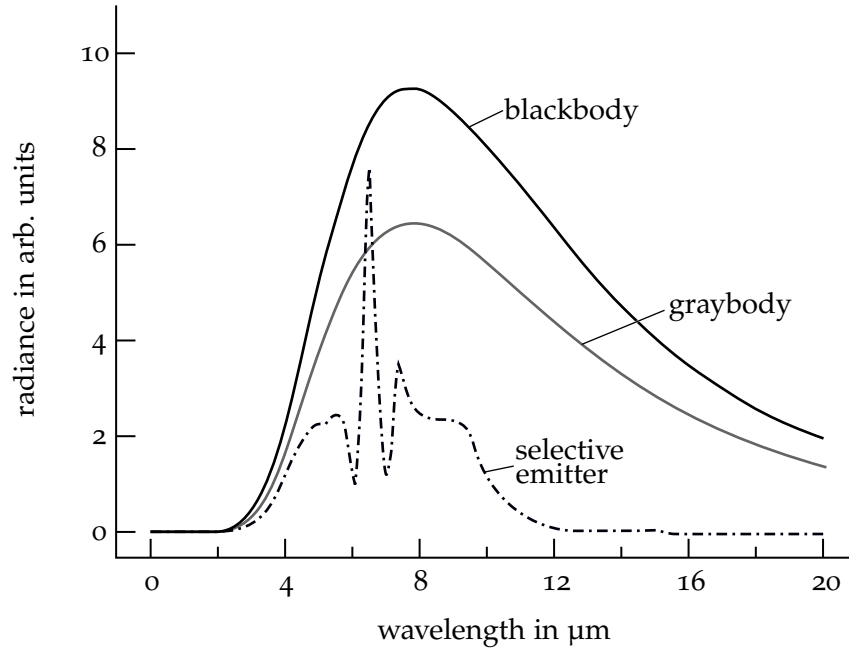
Figure 4.2.4: Exemplary spectral emissivities and corresponding radiation for black bodies, grey bodies, and selective emitters from VOLLMER and MÖLLMANN (2011)

Any radiation ϕ_0 is either reflected (ϕ_R), transmitted (ϕ_T), or absorbed (ϕ_A).

$$\phi_0 = \phi_R + \phi_T + \phi_A \tag{4.6}$$

In contrast, metals with high reflectivities above 90% will have emissivities below 0.1. Very well polished metal surfaces can have the lowest possible emissivities of the order 0.01, which practically render IR imaging impossible.

Thus the following temperature and wavelength dependent coefficients can be defined

$$\alpha\left(\lambda, T\right) = \frac{\phi_{\lambda,\alpha}}{\phi_{\lambda,0}}, \quad \tau\left(\lambda, T\right) = \frac{\phi_{\lambda,\tau}}{\phi_{\lambda,0}}, \quad \rho\left(\lambda, T\right) = \frac{\phi_{\lambda,\rho}}{\phi_{\lambda,0}}. \tag{4.7}$$

It can be deduced from Eq. 4.6 that

$$1 = R + t + \alpha \tag{4.8}$$

which combines the reflected radiation R with transmitted radiation t and absorbed radiation α. For IR intransparent bodies $t = 0$ and the emissivity can be estimated as

$$\varepsilon = 1 - R \tag{4.9}$$

It is important that the emissivity is directly connected to the reflectivity. The emissivity depends on material, surface structure, geometry,
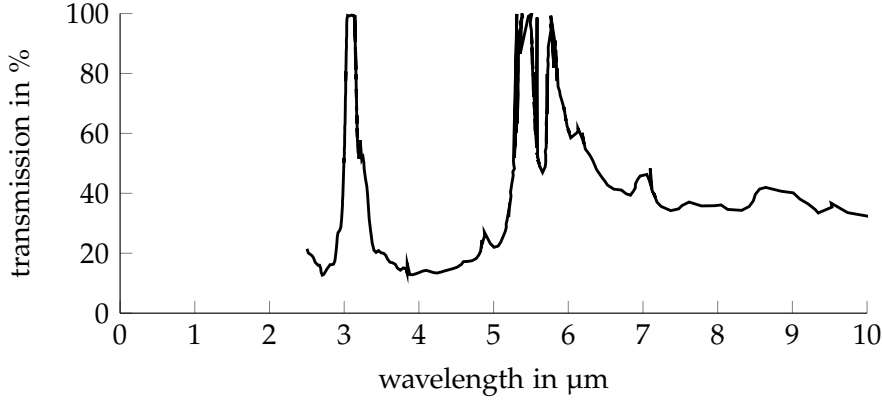
Figure 4.2.5: Infra-red spectrum of FVA 3 mineral reference oil. The band of lubricant emission around 3 μm is visible. Thus it is obvious that the lubricant acts as a selective emitter.

viewing angle, wavelength, and temperature. The emissivity is essential to determine a temperature from the radiation detected by the IR sensor. Thus a knowledge of the emissivity determines the quality of the measurement results.

To quantify the temperature from the measured radiation, the radiometric chain needs to be observed. As depicted in Fig. 4.2.6, the chain consists of the object of interest with a temperature T_{MO} emitting the radiation ϕ_{MO}, reflecting $\phi_{U,æ}$, and transmitting $\phi_{H,T}$. The detected radiant power is further influenced by the radiation from the measuring range ϕ_{MS}. The detected radiant power ϕ_{det} can thus be written as:

$$\phi_{det} = \tau_{atm}\varepsilon\phi_{object}^{BB}\left(T_{object}\right) + \tau_{amb}\left(1 - \varepsilon\right)\phi_{amb}\left(T_{amb}\right) + \dots$$
$$\dots\left(1 - \tau_{atm}\right)\phi_{atm}\left(T_{atm}\right) \tag{4.10}$$

where

$\varepsilon\phi_{object}^{BB}\left(T_{object}\right)$ represents the radiant power of the object which is reduced by the transmittance τ_{atm} of the atmosphere,

$\tau_{amb}\left(1 - \varepsilon\right)\phi_{amb}\left(T_{amb}\right) = r\phi_{amb}\left(T_{amb}\right)$ the reflected radiation from the surroundings, and

$\left(1 - \tau_{atm}\right)\phi_{atm}\left(T_{atm}\right)$ the radiant power emitted by the atmosphere. The radiant power of the object can thus be determined as

$$\phi_{object}^{BB}\left(T_{object}\right) = \frac{\phi_{det}}{\tau_{atm}\varepsilon} - \frac{\left(1 - \varepsilon\right)}{\varepsilon}\phi_{amb}\left(T_{amb}\right) - \frac{\left(1 - \tau_{atm}\right)}{\tau_{atm}\varepsilon}\phi_{atm}\left(T_{atm}\right) \tag{4.11}$$

Using a camera specific calibration curve ϕ_K instead of the black body radiant power the temperature of the object T_{object} can be obtained

$$T_{object} = \phi_K^{-1}\varepsilon^{-1}\left(\frac{\phi_{det} - \left(1 - \tau_{atm}\right)\phi_{atm}\left(T_{atm}\right)}{\tau_{atm}} - \left(1 - \varepsilon\right)\phi_{amb}\left(T_{amb}\right)\right)$$
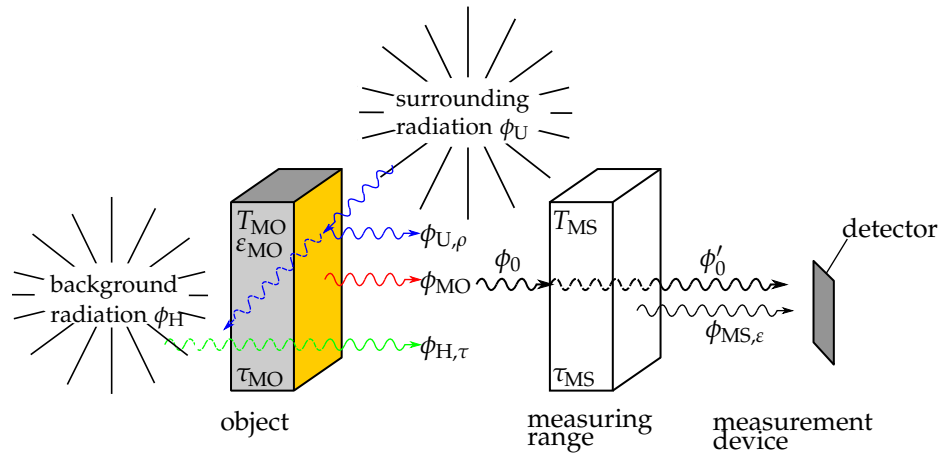
Figure 4.2.6: The radiometric chain with the influences of measuring range, surrounding, background. From FOUAD and RICHTER (2012)

$$\tag{4.12}$$

However, the knowledge of

ε the emissivity of the object,

T_{amb} the surrounding temperature,

T_{atm} the atmospheric/ambient temperature, and

τ_{atm} the atmospheric transmittance

are essential to determine the object temperature accurately.

The atmospheric transmittance τ_{atm} is calculated in the camera software using the LOWTRAN (KNEIZYS et al., 1988) model based on the atmospheric temperature T_{atm}, the relative humidity, and the measurement distance. These values are input into the software and need to be determined or at least valid assumptions for these values need to be made.

It must be noted that the the measurement is sensitive to reflections (e. g. by the camera itself which is called NARCISSUS effect) and radiation from surrounding bodies. To avoid reflections from the surroundings the optical path was shielded from the surrounding by IR-opaque material. Furthermore, parts of the path were encased in an active cooling system, thus keeping emissions by the shielding on a constant low level. Furthermore, due to the temperature dependence of these factors, a temperature dependent calibration is necessary. The temperature is measured constantly in the camera itself for application of the correction factors.

Figure 4.2.7 shows the radiation from an EHL contact. It consists of the radiation of the surroundings N_{o} which is reflected at all interfaces. Furthermore, the radiation by the IR-transparent window N_{s}, the radiation by the lubricant film N_{f}, and the radiation of the surface

of the solid body N_b. All radiation components are picked up with some losses; reflections away from the sensor occur as well as detection of additional reflections from outside. For example, the radiation from the fluid film is reflected by the solid surface and is then picked up on top of the radiation directly entering the detector.

To be able to account for the different radiation parts, filters can used due to the fact that the emitted wavelengths differ. For example, the lubricant acts as a selective emitter as was shown in Fig. 4.2.5. AUSHERMAN et al. (1976) already described methods utilising filters. REDDYHOFF, SPIKES and OLVER (2009a), REDDYHOFF, SPIKES and OLVER (2009b) and LU, REDDYHOFF and DINI (2017) presented a method utilising coatings with different emissivities to distinguish between the radiation sources. This methodology is depicted in Fig. 4.2.8.
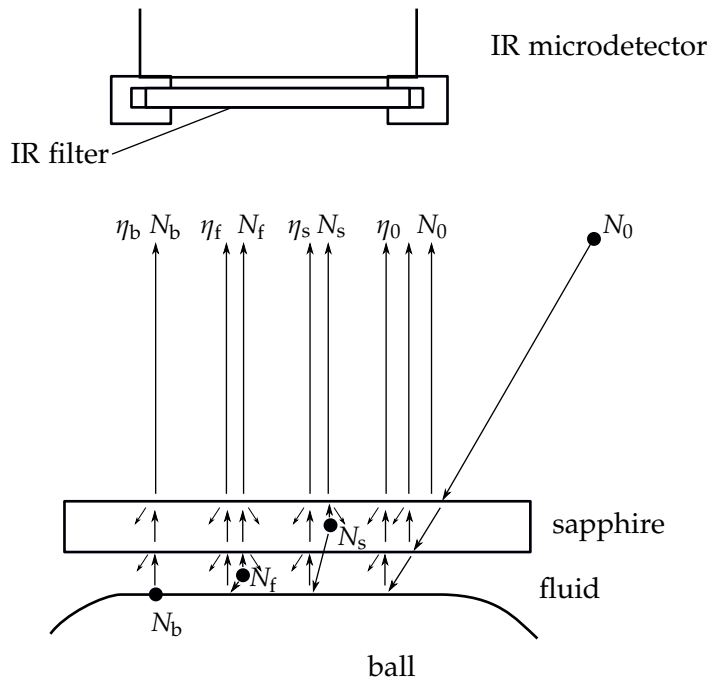
Figure 4.2.7: Radiation components in an EHL contact. Graphic reproduced from AUSHERMAN et al. (1976)

It is not applied in the current work, however, the system has been prepared to make use of the same technique to determine the temperature of the system elements separately.

Experiment

For the second experiment, the same twin disc test rig as in the traction experiments (Sec. 4.1.1) was used. One of the steel discs was replaced by a sapphire shaft as shown in Fig. 4.2.9. The crowning radius of the 100Cr6 counter disc was increased to 100 mm to lower contact pressure. The properties necessary to obtain the contact details
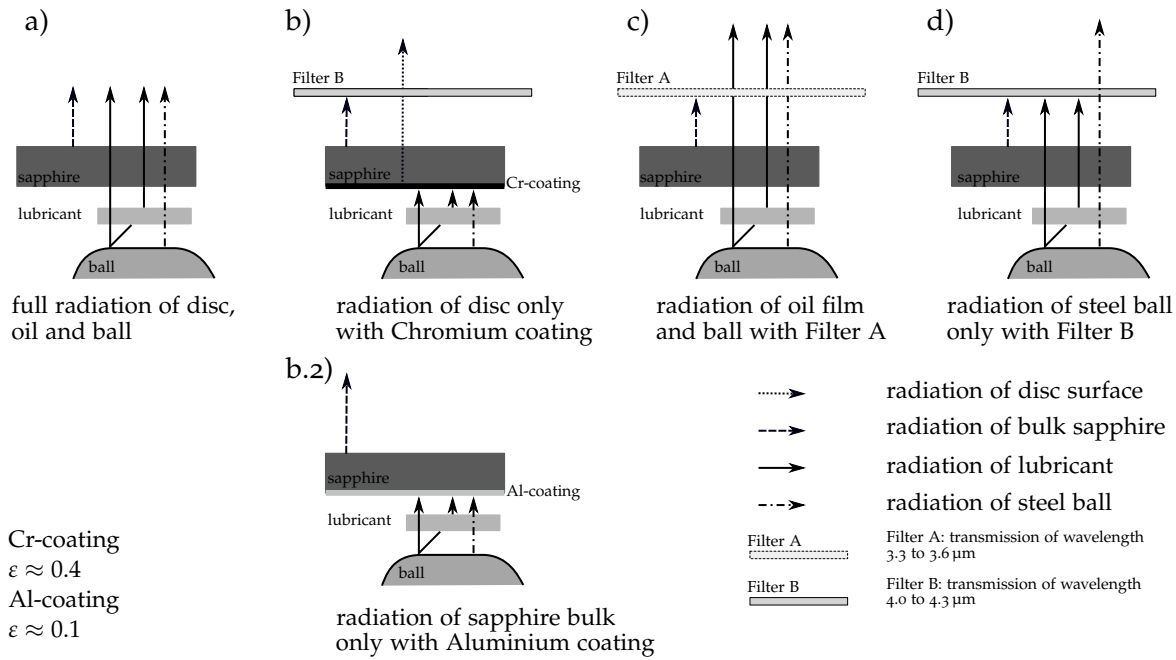
Figure 4.2.8: Division of the radiation parts from REDDYHOFF, SPIKES and OLVER (2009b) and LU, REDDYHOFF and DINI (2017). Schematic representation of the radiation components of the system: in a the radiation received by infrared camera is emitted by disc, oil and ball; in b the radiation from the oil and ball surface is reflected by the chromium coating (150 nm) so that only the radiation of the disc surface (chromium surface) can be received by infrared camera; in b.2 the radiation from the bulk sapphrie is received only; in c the radiation of steel ball and oil can pass through filter A; in d only the radiation from steel ball can pass through filter B

are given in Tab. 4.2.1. It should be noted that the elastic modulus of sapphire differs significantly from steel, leading to different contact pressures and deformations in comparison to the so far investigated steel-steel contacts. The thermal conductivities of sapphire and steel however are similar in the temperature ranges of interest, so that the thermal behaviour of the contact should not be influenced.

The contact was observed using an infra red camera (DCG Systems InSb 640 SM see Tab. 4.2.2) with a macro lens in combination with macro rings enabling a lateral resolution of 6 μm. For the determination of temperature from radiation, the software MPS 5/ETC is used. It uses Eq. 4.12 to calculate a temperature value for each pixel of the sensor. Thus, a two dimensional temperature map of the contact was obtained.

From the test design follows that the influence of the radiation from the EHL contact the reflectivity and transmittances play a vital role. For the losses by the mirror Fig. 4.2.10 shows that for the wavelengths of interest a reflectivity of 0.98 is attained. The sapphire shaft has a transmittance of 0.88 and functions as a low pass filter with a cut-off wave length of about 5.5 μm (see Fig. 4.2.11). These losses were taken

Table 4.2.1: Properties of contact partners

	Steel 100Cr6 (AISI 52 100)		Sapphire Al$_2$O$_3$	
Thermal conductivity in Wm^{-1}K^{-1}	33	(20 °C)	40	(25 °C)
	32.2	(350 °C)	12	(400 °C)
	31.4	(700 °C)	4	(1200 °C)
YOUNG's modulus in GPa	210		360-450	
Transmittance	–		200 nm-5.5 µm	

Table 4.2.2: Properties of the IR camera system

Camera:	DCG Systems InSb 640 SM
Detector material:	indium antimonide (InSb)
Spectral range:	1.1 − 5.3 µm
Detector size:	640 x 512 pixel (at full frame rate)
Pixel size:	15 x 15 µm
Detector cooling:	active using sterling cooler. $T_{\text{detector}} = 77\,\text{K}$
Full frame rate:	100 Hz
Objective:	MWIR Wechselobjektiv Makro
Depiction scale:	1:1
Aperture:	f/4.3 Use of macro rings

into account implicitly during the calibration as the whole chain was calibrated.

Calibration

To calibrate IR cameras, often technical black bodies are used. These are systems of a defined and known temperature which have surface properties yielding high emissivities (usually $\varepsilon \approx 0.96$). For the calibration the black body is placed in front of the camera so that the whole sensor is filled with the black body and a picture is taken. This is repeated for several temperatures of the black body. Because both the temperature of the black body and its emissivity are known, the radiation picked up by each pixel can be transformed into a temperature. This system was applied –using a DCG Systems' black body
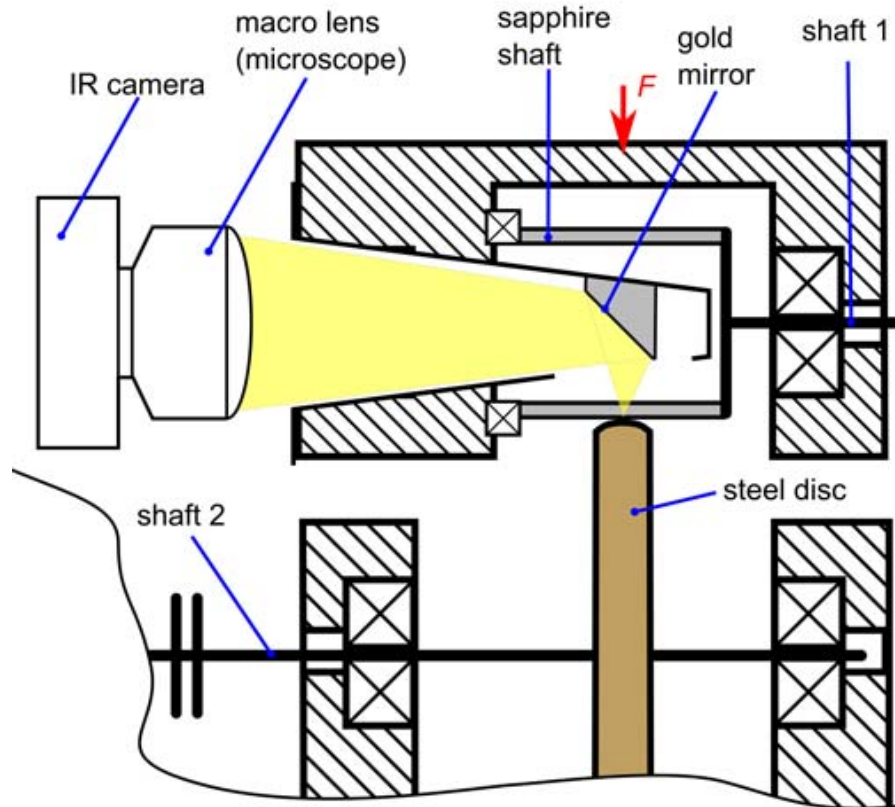
Figure 4.2.9: Experiment for measuring contact temperatures

BB04– taking into account the whole measurement chain, i. e., the black body was placed at the position of the steel disc. The resulting calibration curves have the shortcoming that the emissivity of the scene[1] is not known, i. e., it must be guessed or determined separately by a calibration of the temperature measurement, allowing for the emissivities of the respective components to be determined. Here the scene itself, i. e., the steel disc is used as calibration source. The scene is heated to a specific temperature and held there until stable temperatures are measured for at least 30 min. The resulting measured emission can be calibrated. Due to the fact that the local emissivities are variable the emissivity of each pixel is calibrated. This has the disadvantage, that a movement or adjustment of the camera is not possible without jeopardising the measurement. Furthermore, the emissivity of the scene can only be determined while the test rig is stationary. Thus two effects lead to problems during the test. On the one hand the moving parts may change the position of the areas of identical emissivity during the experiment. On the other hand the lub-

---

1 Scene in this context means the picture viewed by the camera sensor. It consists of the contact area as well as the metallic surface of the disc which is outside of the contact.
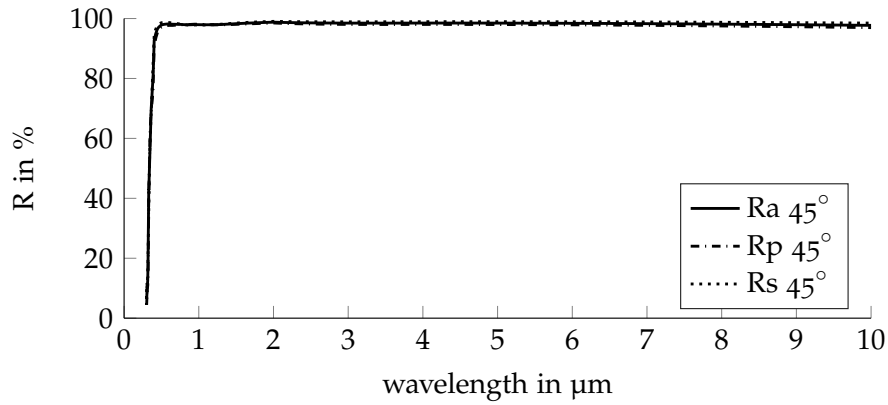
Figure 4.2.10: Reflectivity of gold coated mirror at 45°.
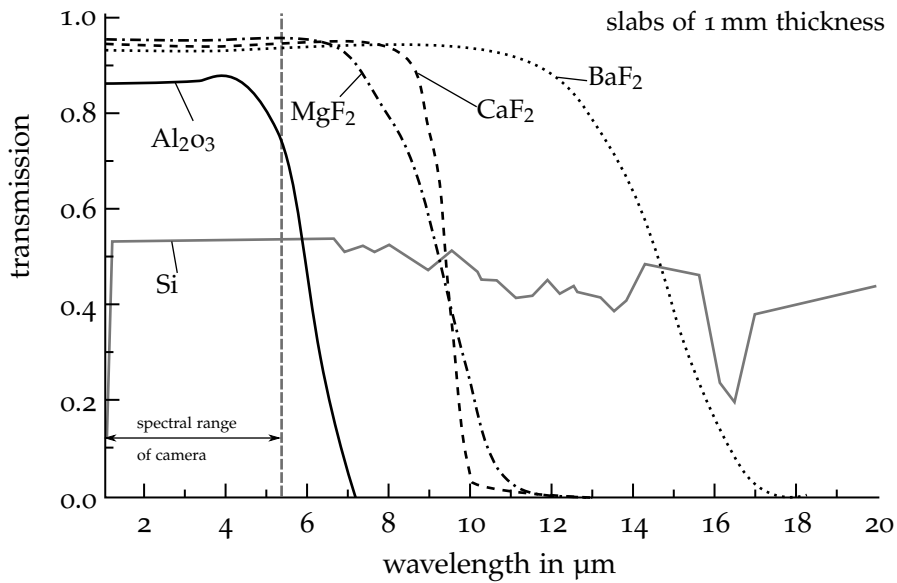
Figure 4.2.11: Typical transmission spectra for 1 mm thick slabs. Sapphire (AL_2O_3). From VOLLMER and MÖLLMANN (2011)

ricant film present during an experiment with rotating discs will lead to a different emissivity behaviour than the stationary disc which is present during calibration. LU, REDDYHOFF and DINI (2017) point out that the emissivity of the lubricant is not linear but is film thickness dependent as well.

The presented results used the calibration conducted using the black body. However, the second calibration method was chosen to understand the emissivity influence and changes. Where necessary a local correction of emissivities was applied.

EXPERIMENTAL RESULTS

5.1 DATA FROM TRACTION EXPERIMENTS

The traction curves, shown exemplary in Fig. 5.1.1 and Fig. 5.1.2 for different pressures, exhibit a nearly linear rise of the traction coefficient up to 0.8 % *SRR*. In the regions beyond, the traction coefficient increases non linearly to a maximum before decreasing again with rising *SRR*. This decrease is attributed to temperature effects, i.e., shear heating, resulting from the higher shear rates (as consequence of higher *SRR*). Furthermore, it can be observed that higher contact pressures lead to higher traction coefficients. The linear part of the traction curve (*SRR* between 0 % and 0.8 %) is attributed to elastic lubricant behaviour and varies only moderately for different contact pressures. As explained before, the elastic deformation of the solid bodies was subtracted in advance.
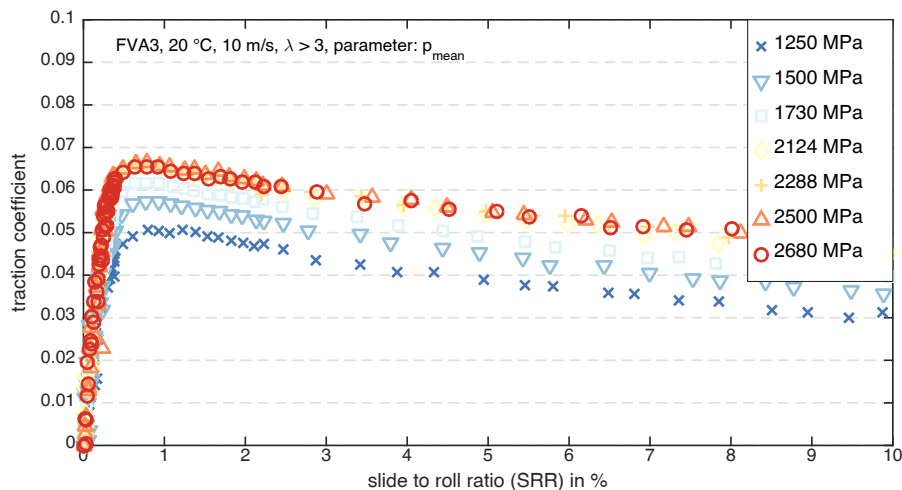
Figure 5.1.1: Traction curves of twin-disc experiment at different pressures. The inlet temperature was kept constant during the experiment, each data point represents the mean values of at least 5 experiments.

Typical traction curves for the MTM experiment are shown in Fig. 5.1.3 for rising entrainment velocities. These curves show that for low entrainment velocities the traction coefficient rises up to the end of the experimental *SRR* range. However, with a rising entrainment velocity, the curves start to exhibit a maximum wit a subsequent decrease. This is attributed to two effects: The possible presence of mixed friction at low speeds and a rise in shear heating influencing the traction at higher *SRR* and higher velocities, thus causing a decrease of viscos-
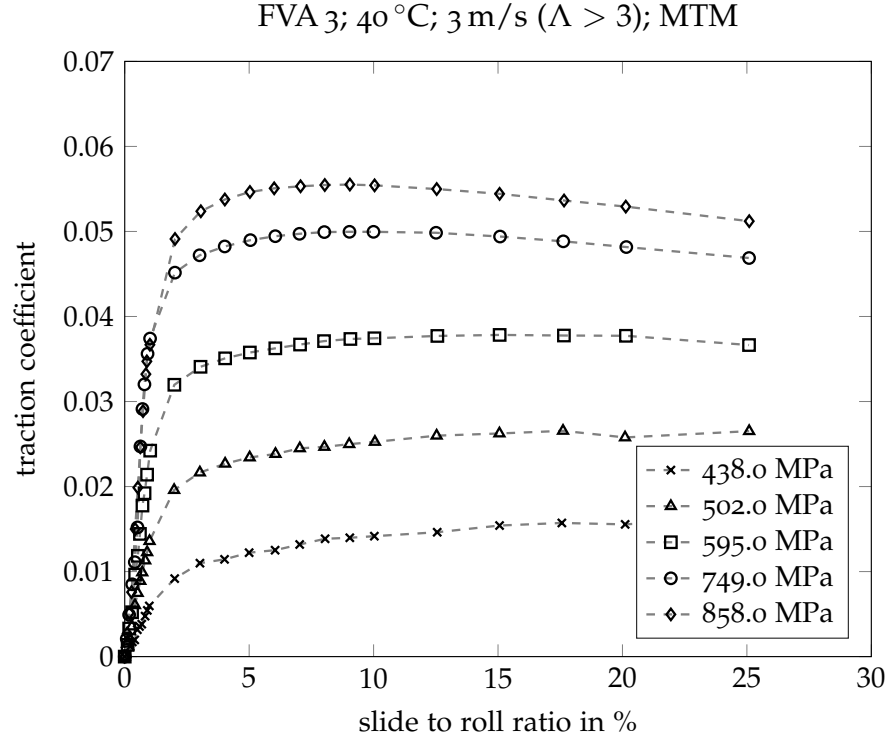
Figure 5.1.2: Traction curves of MTM experiment at different pressures. The oil bath temperature was constant and each data point represents the mean value of positive and negative *SRR*.

ity. The same principal behaviour can be observed for the twin-disc traction experiments.

From the coefficient of friction, the average shear stress $\bar{\tau}$ was calculated by multiplication with the mean contact pressure $\bar{p}$. The maximum average shear stress reached in each experiment was determined and from these results a pressure dependence of the maximum average shear stress $\bar{\tau}_{\mathrm{max}}$ was deduced (WANG, 2015). Thus it can be written:

$$\bar{\tau}_{\mathrm{max}} = \max{(\bar{\tau})} \quad \text{and} \quad SRR(\bar{\tau}_{\mathrm{max}}) < 0.1 \tag{5.1}$$

Figure 5.1.4 shows the principle of determining the maximum average shear stress. Thus, for the traction curves from Fig. 5.1.3 was only possible from 2.4 m/s onwards. $\bar{\tau}_{\mathrm{max}}$ represents the maximum average shear stress obtained from integration over a HERTzian contact area exhibiting inhomogeneous local conditions (e. g., pressures). Figure 5.1.5 shows the pressure dependent maximum average shear stress determined in this manner. At low pressures, it is possible that the limiting shear stress does not dominate the maximum of the traction curve. Thus only traction curves with pressures above 500 MPa were evaluated.

FVA 3; 60 °C; 50 N ($p_{\mathrm{mean}} = 749\,\mathrm{MPa}$); MTM
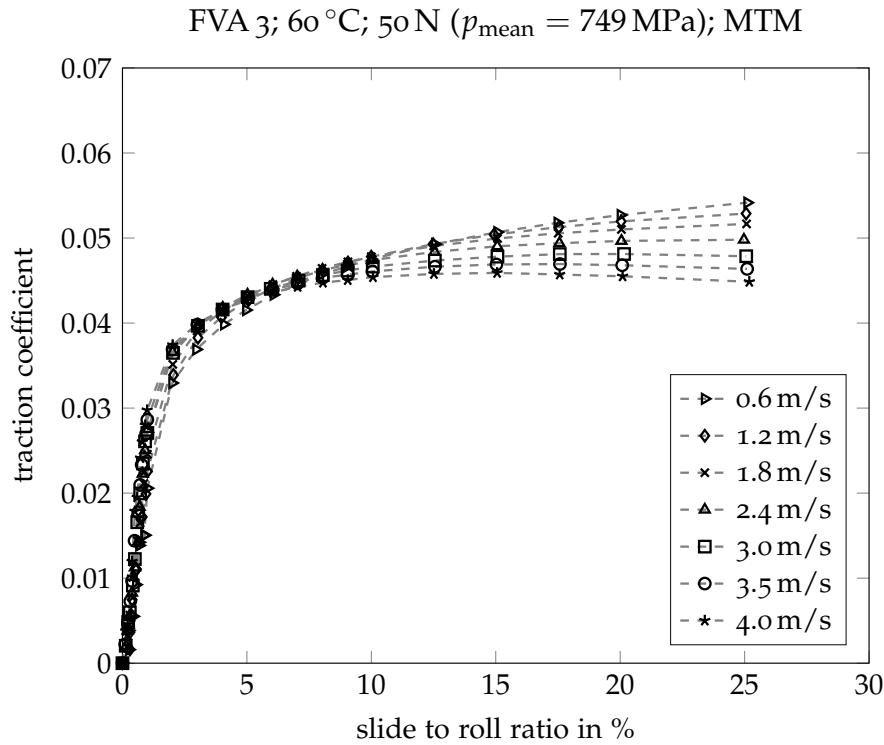
Figure 5.1.3: Traction curves from the MTM experiment speed varied.

Apparently, a linear relationship between mean pressure and maximum average shear stress exists in the graphs. This is in agreement with the observations presented in Sec. 2.5.3. Furthermore, the maximum average shear stresses reached in the experiment rise with decreasing hydrodynamic rolling speeds below 5 m/s. Above an entrainment speed of 5 m/s, the values for different rolling speeds are almost identical. This coincides with the film thickness parameter Λ –defined as ratio of central film thickness h_{c} and root mean squared roughness R_{q}– reaching values $>> 3$, thus showing a clear indication of full film lubrication. This agrees with observations by WANG (2015) who showed that the maximum shear stress $\bar{\tau}_{\mathrm{max}}$ is constant with increasing speed, when $\Lambda > 1$. It can be noted that the rise of the maximum shear stress at lower speeds is most probably due to intensified mixed lubrication in the contact. At full film lubrication, however, the maximum shear stress attained is apparently not sensitive to the entrainment speed.
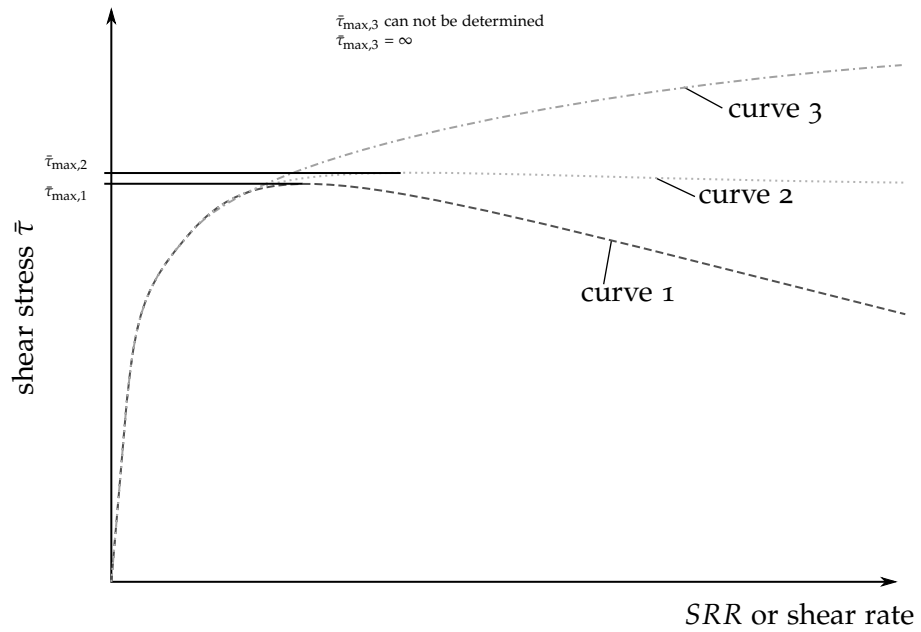
Figure 5.1.4: Determination of $\bar{\tau}_{max}$. Curve 1 and curve 2 a maximum average shear stress $\bar{\tau}_{max}$ is attainable, curve 3 does not yield a valid $\bar{\tau}_{max}$
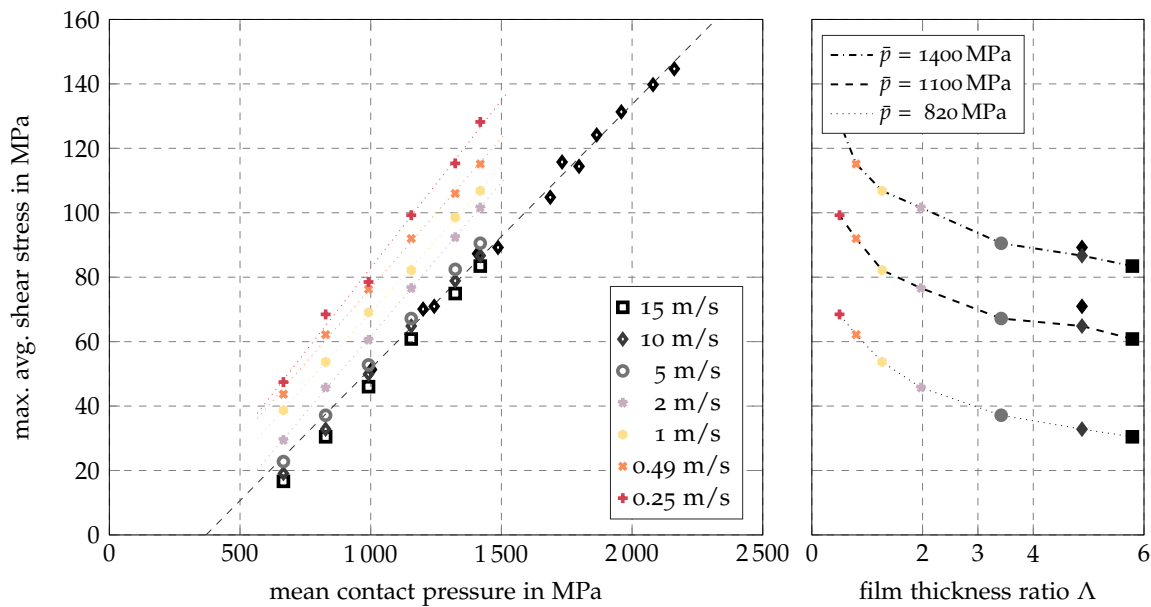
Figure 5.1.5: Pressure dependence of maximum shear stress at different entrainment velocities. The inlet temperature was kept constant during the experiment, each data point represents the mean values of at least 5 experiments. Right: Dependence of the maximum shear stress on the film thickness ratio, i. e., entrainment velocity.

5.2   MAXIMUM SHEAR STRESS UNDER HOMOGENEOUS EHL-LIKE LABORATORY CONDITIONS

The results gained from traction experiments represent integral values. Thus, it cannot be assumed that the limiting shear stress of the fluid was reached in every point of the contact. Due to this, an experiment was sought which places a fluid sample under homogeneous conditions similar to those in an EHL contact. A useful experiment was presented by BAIR (1990), however this was not available at the time the experiments were conducted.

Data from experiments performed at the Institute of Tribology and Energy Conversion Machinery at the Technical University of Clausthal by SCHWARZE and BROUWER, using a high pressure chamber designed by HÖGLUND (1984) and JACOBSON (1991) and JACOBSON (2006), was used for comparison. The results are published in BROUWER, BADER and BEILICKE (2016) and BADER et al. (2015). Figure 5.2.1 shows a schematic of the experiment.

In these experiments, a fluid sample is trapped between two plungers and then compressed to the given pressure. Subsequently, the wall of the container is moved past the fluid sample and the reaction forces are measured. These experiments were conducted in pressure ranges from 0.6 GPa to 1.4 GPa. The resulting shear stresses were calculated by division of the force F by the cylindrical area of the sample. All experiments were conducted at ambient temperature.
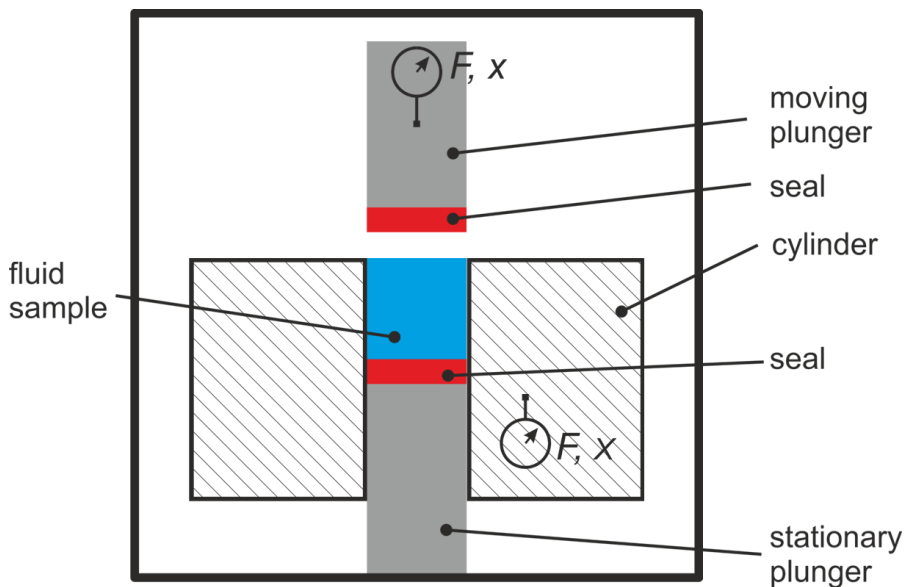
Figure 5.2.1: Schematic of HPC
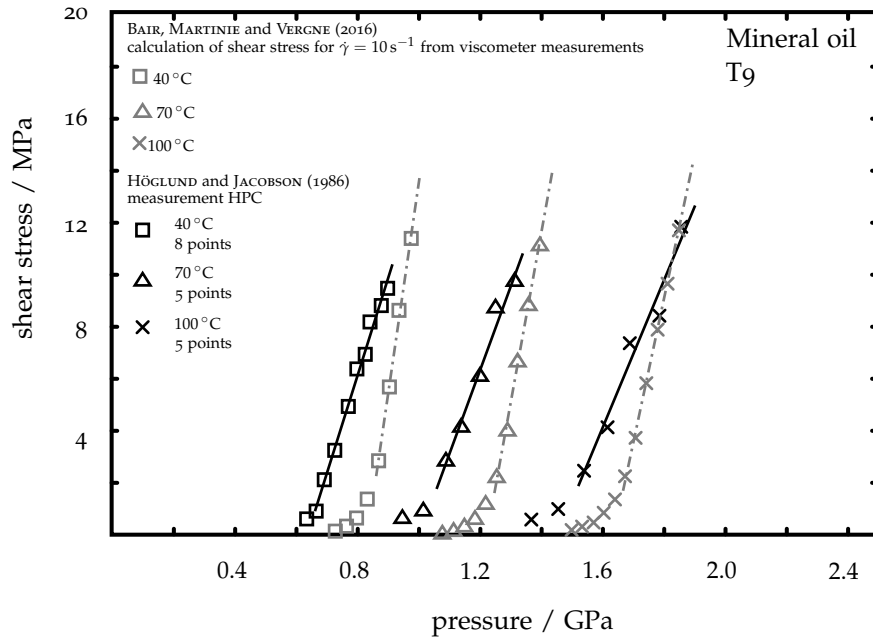
Figure 5.2.2: Comparison of HPC (1986) measurement from Höglund and Jacobson (1986) and calculations from Bair, Martinie and Vergne (2016)

The HPC experiments represent homogeneous conditions for the whole sample volume with regard to pressure. Thus, it can be speculated that the maximum shear stress reached may indeed be identical to the limiting shear stress of the fluid. However, it is not defined what the velocity profile in the sample volume is. Thus, a definition of a shear rate is not feasible. Furthermore, it may well be that the effect leading to the measured friction force is a pure plug flow. Non the less, the flow profile within a real EHL contact has also been subject to discussion(Šperka, Křupka and Hartl, 2014; Martinie and Vergne, 2016). It could thus be, that the same effects govern the limiting shear stress in traction experiments.

Bair (1990) and Bair, Martinie and Vergne (2016) showed for a similar experiment, that shear rates of around $10\,\mathrm{s}^{-1}$ are to be expected. The authors further note that the resulting shear stresses are in agreement for a calculation of the shear stress from standard viscometer measurements without consideration of the limiting shear stress. The results are shown in Fig. 5.2.2. Thus, it is not clear whether the results are actually depicting the limiting shear stress or are just the result of the pressure influence on viscosity at low shear rate.

A comparison of data gained from the HPC and traction experiments is presented in Fig. 5.2.3 for a mineral oil. Both the traction experiments and the HPC experiments yield a linear relation between shear stress and pressure. Furthermore, it is noticeable that all these shear stresses are of similar magnitude for a given pressure, with the

HPC measurements resulting in slightly lower shear stresses. This may be influenced by temperature differences in the experiments or possibly be due to the integrating nature of traction measurements. The conditions in the HPC experiment are homogeneous regarding the pressure, and temperature –when neglecting the heating in the film possibly present due to shearing– however the shear profiles may well be inhomogeneous.
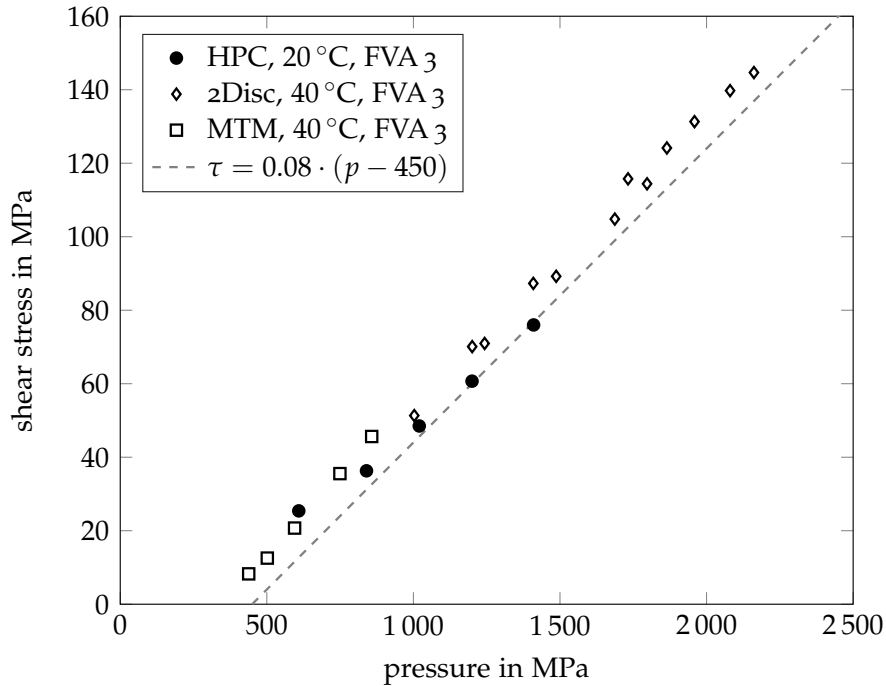
Figure 5.2.3: Comparison of maximum shear stress reached in MTM, twin-disc, and HPC experiments with FVA 3 mineral oil

Figure 5.2.4 shows the comparison for a polyglykol. It can be seen, that in both cases in the regions above $1\,$GPa a linear relationship between maximum shear stress and pressure is visible. However, in this case the gradient of the HPC measurements and the twin-disc are significantly different. The resulting shear stresses are identical for around $1.2\,$GPa. Analyses of the traction curves shown in Fig 5.2.6 and Fig. 5.2.7 show that the traction curves clearly reach a maximum. Thus the determination of $\bar{\tau}_{max}$ according to the criterion in Eq. 5.1 is possible.

It needs to be considered that the twin-disc experiments are depicted with the mean stress as parameter. Thus, within the contact area pressures in the range from $0\,$Pa up to 1.5 times the mean pressure are encountered. Figure 5.2.5 illustrates the pressure ranges. It appears that the HPC results coincide within the pressure range covered by the twin-disc measurements. However, if the HPC results do depict the true limiting shear stress the values derived from traction experiments should, provided they are dominated by the limiting shear
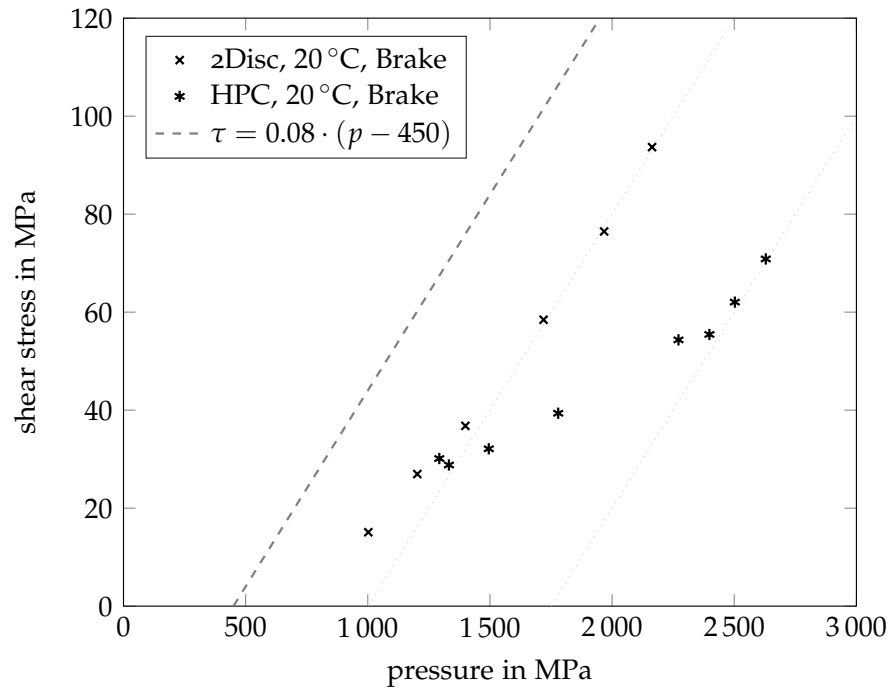
Figure 5.2.4: Comparison of maximum shear stress reached in twin-disc, and HPC experiments for Brake fluid (polyglycol base). The values for the twin-disc experiment are plotted against the mean contact pressure. Dotted lines with gradient 0.08.

stress and its pressure dependence reach values just below those of the HPC, due to the non-uniform pressure distribution in the EHL contact. This is as opposed to the uniform one in the HPC.

Even with the use of vastly different methods WORKEL et al. (2000) showed that the results gained are in good agreement for Santotrac 50, see Fig. 5.2.8.Resulting CoF values are governed by the limiting shear stress and show quite good agreement for nearly all types of experiment. BAIR and WINER (1979b) measured using a high pressure cell, i.e., a modified COUETTE type viscometer. JACOBSON (1985) used a bouncing ball apparatus (1). Similar but modified versions were used by WORKEL et al. (2000) (2, 3). HÖGLUND and JACOBSON (1986) used a device similar to the HPC. These are the only data not in line with the other measurements showing a significantly lower order of magnitude. RAMESH (1989) used a plate impact experiment based on the HOPKINSON bar. The data ANONYMOUS (1972), LOEWENTHAL and ROHN (1983), MEYER (2010b), EVANS and JOHNSON (1986), and own measurements are from twin-disc machines with only longitudinal sliding used in the values depicted.

It can however be noted that all the different experiments, conducted at several laboratories, yield very close values for the maximum coefficient of friction with the exception of the HPC experiment. It can be noted, that for experiments at pressures from 0.7 . . . 1.5 GPa the res-
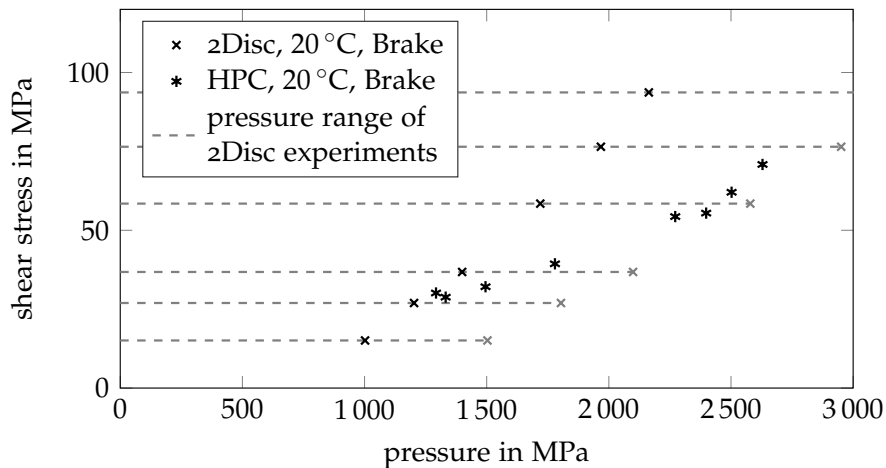
Figure 5.2.5: Comparison of twin-disc results with pressure range in contact indicated

ults of measurements with twin-disc experiments are slightly lower than the results from homogeneous conditions (BAIR and WINER, 1979b). This should be explicable due to the pressure distribution and the fact that certain areas of the contact within the EHL may not yet have reached the limiting shear stress. Furthermore, the depicted experiments were not conducted using the same fluid batch. Thus a change of formulation may have occurred.

It is furthermore noteworthy that the linear pressure relationship is not clearly visible in the results of this fluid. The traction results might be interpreted to have a linear relation with pressure, however the homogeneous experiments seem to exhibit a pressure independent shear stress-pressure (CoF-pressure) relation. This may be due to the fact, that Santotrac 50 is a designed traction fluid where this property is paramount to reliable operation and is achieved through the use of high molecular weight polymers. This might be a further explanation of the results of the HPC as possibly the experiment only measures the response of the base oil at low shear rates and thus does not represent the lubricant response in EHL contacts.

It can thus not be clearly stated that the results of the HPC are truly the resulting limiting shear stress. Non the less, it is interesting that the HPC values are very close to the results gained from traction experiments for a number of lubricants as shown in Fig. 5.2.9. The physical properties are given in Tab. 4.0.1. The different behaviour may be due to molecular differences and similar observations of models not fitting polyglycol have been pointed out by WAN and WONG (2010).
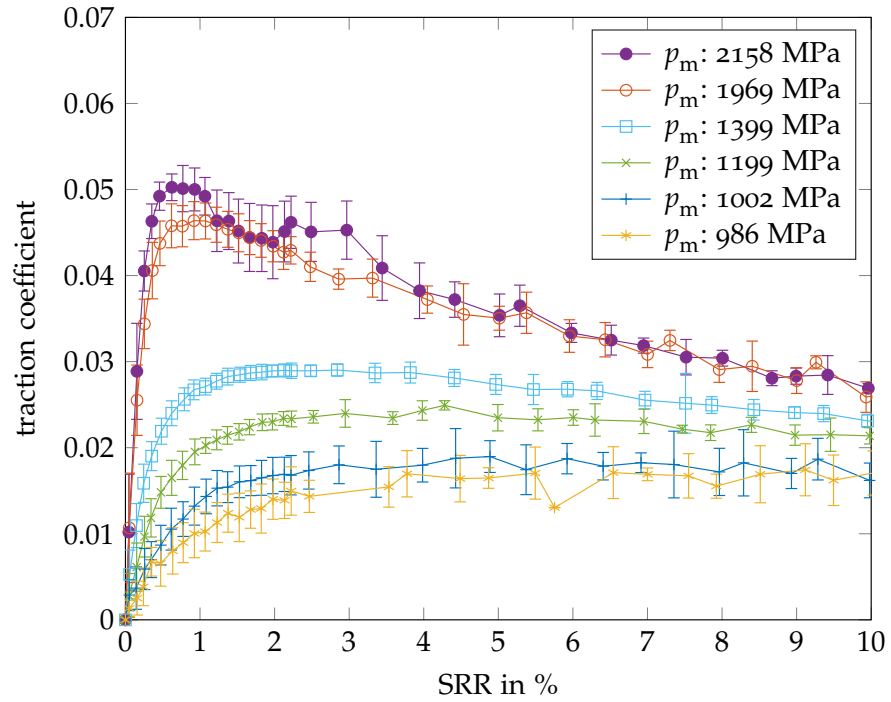
Figure 5.2.6: Traction curves of brake fluid at 10 m/s and 0 °C.
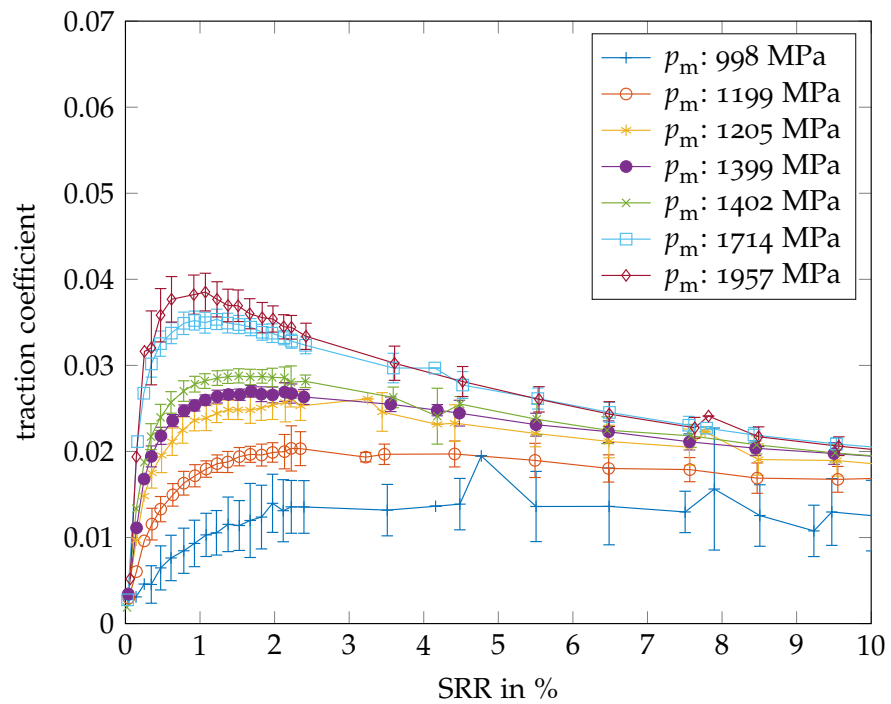
Figure 5.2.7: Traction curves of brake fluid at 15 m/s and 10 °C.
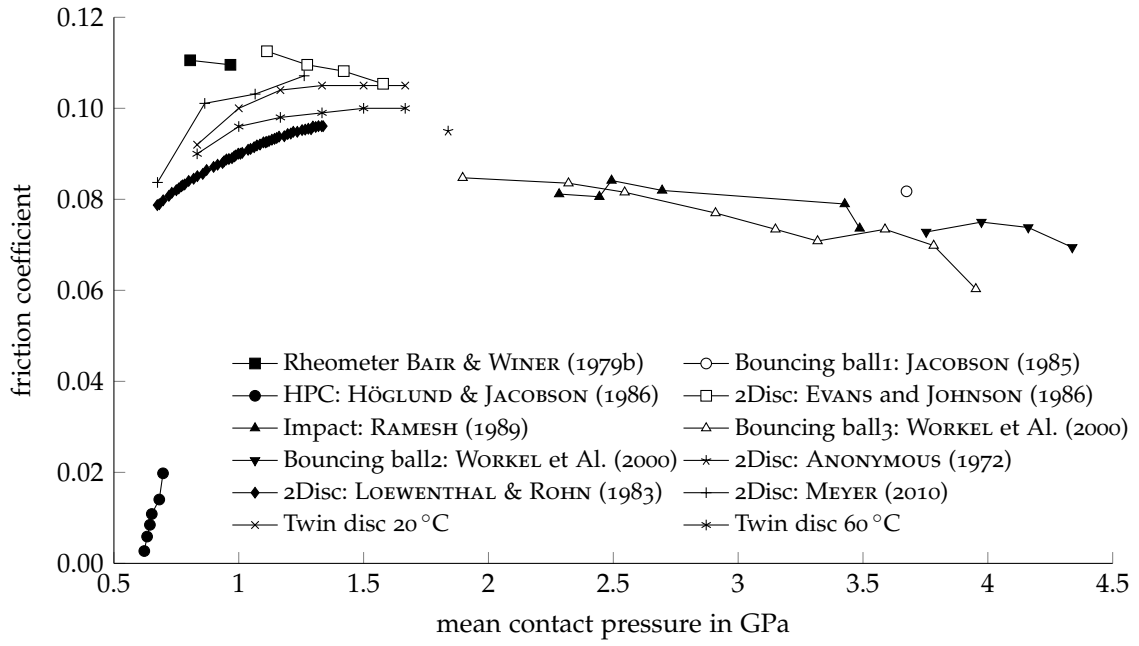
Figure 5.2.8: Comparison of maximum CoF reached in different experiments for Santotrac 50. From WORKEL et al. (2000) with data added.
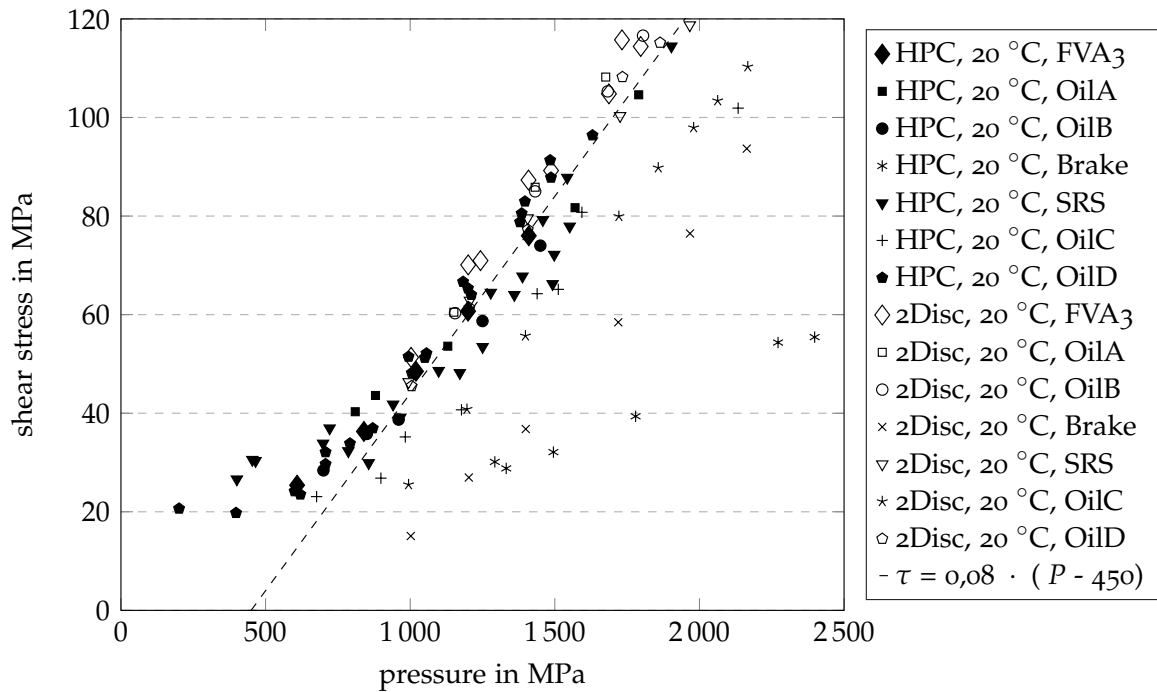
Figure 5.2.9: Comparison of twin-disc and HPC, all oils

MODEL OF LUBRICANT

6.1 PROPOSED MODEL FOR LIMITING SHEAR STRESS

Due to the observed good agreement of the results from integral traction measurements and the results from the HPC, it is assumed that the approximation of the limiting shear stress by the maximum shear stress gained from traction tests may yield satisfying results in despite of its integrating nature. At least, this holds true at pressures in the contact which are high enough to let the limiting shear stress dominate.

Therefore, the observed linear pressure dependence of the maximum shear stress forms the basis for the theoretical model for τ_{lim}.

Fit 1 in Figure 6.1.1 shows the model for the locally limiting shear stress used in the simulations, meaning that the integral maximum shear stress gained from the traction experiments is used as local limiting shear stress. This model was used in similar form by WANG (2015) and BEILICKE, BOBACH and BARTEL (2016). The latter authors incorporated this model in a TEHL simulation.

6.1.1 *Comparison with other models*

The previous section showed that the maximum shear stresses from twin disc, MTM, and HPC experiments all exhibit a linear pressure dependence. The following section compares the approximation presented in the last section with results from other authors.

When comparing the data from Fig. 5.2.3 with the proposed models, the fits presented in Fig. 6.1.1 are obtained. The parameters for the models are given in Table 6.1.1. The pressure range used was restricted to 500 MPa and beyond, due to the assumption that, in regions of lower pressure, the maximum shear stress resulting from the traction curves may rather reflect thermal effects than a maximum governed by the limiting shear stress. Fit 1 corresponds to the linear region of the bilinear model proposed by WANG (2015).

The model by BAIR and WINER (1992) Eq. 2.100 does not fit well with the observed relationship, due to the missing onset of the pressure dependence above a pressure threshold. It is depicted as Fit 3 in Tab. 6.1.1 with the assumption of $b = 0$. This is valid due to the fact that the shown fits were obtained for one temperature.

The model by JOHNSON and TEVAARWERK (1977) Eq. 2.99 in itself overestimates the real shear stress. Only the choice of –a physically not reasonable– negative value for τ_0 would make this model repres-

ent the measured data equally well as the model described above. It is depicted in Fit 1† of Tab. 6.1.1.

It can be concluded that all models fit the measured data reasonably well between 1 000 and 2 200 MPa. However, the model according to Eq. 2.107 provides the best correlation over the complete measured range for a single temperature (40 °C) and speeds where $\Lambda > 3$.
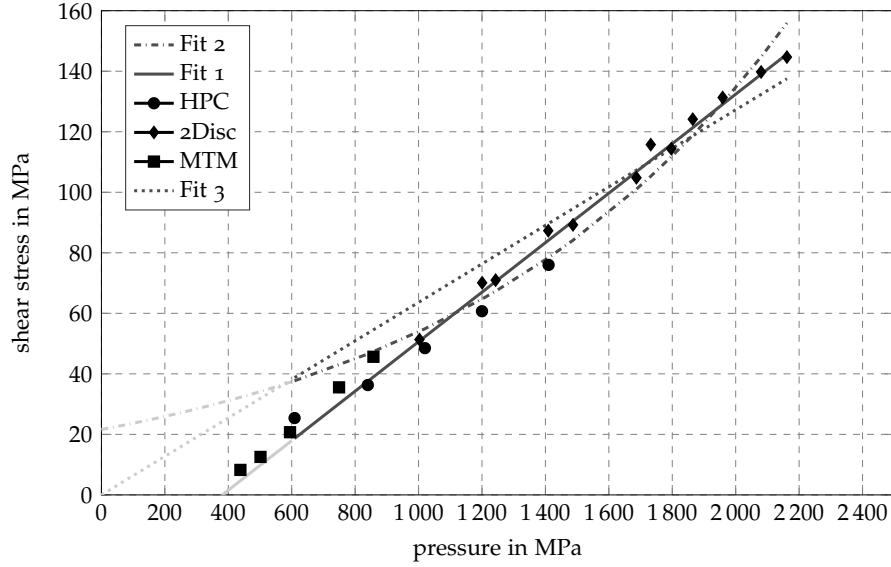
Figure 6.1.1: Comparison of data fit to models of limiting shear stress. Experimental data from Fig. 5.2.3

Table 6.1.1: Results for fitting the obtained max. shear stresses.

Fit	Model	Parameters	
Fit 1*	$\tau_{\mathrm{max}} = (p - p_0) \cdot \xi$	$p_0 = 330\,\mathrm{MPa}$, $\xi = 0.08$	Eq. 2.107
Fit 1†	$\tau_L = \tau_0 + \gamma \cdot p$	$\tau_0 = \text{-}27\,\mathrm{MPa}$, $\gamma = 0.08$	Eq. 2.99
Fit 2	$\tau_L = \tau_{L0} \cdot e^{\left(\alpha_\tau \cdot p + \beta_\tau \left(\frac{1}{T} - \frac{1}{T_0}\right)\right)}$	$\alpha_\tau = 0.001\,\mathrm{Mpa}^{-1}$, $\tau_{L0} = 21\,\mathrm{MPa}$, $\beta_\tau = 0^\ddagger$	Eq. 2.102
Fit 3	$\tau_L = (a - b \cdot T) \cdot P$	$a = 0.064$, $b = 0^\ddagger$	Eq. 2.100
Fit 4	$\tau_L = E_{\dot\gamma 1} p_\mathrm{m} + E_{\dot\gamma 2} + \ldots$	$E_{\dot\gamma 1} = 0.08$, $E_{\dot\gamma 2} = 15.67\,\mathrm{N/mm}$,	Eq. 2.108
	$\ldots E_{\dot\gamma 3} \ln\left(v_\Sigma \frac{\mathrm{s}}{\mathrm{m}}\right) + E_{\dot\gamma 4} T_\mathrm{ref}$	$E_{\dot\gamma 3} = \text{-}12.07\,\mathrm{N/mm}$, $E_{\dot\gamma 4} = \text{-}0.53\,\mathrm{N/K}$	

*$\lambda > 1$ if $\lambda < 1 \rightarrow \xi > 0.08$

† corresponds to Fit 1* but incorporates a –physically not sound– negative starting shear stress

‡ assumption

6.1.2 *Temperature influence – expereimental results*

In the previous section, a dominant influence of pressure on the maximum shear stress reached in the traction experiments was shown. This is in good agreement with findings presented by previous researchers. Some of the previously mentioned models (Sec. 2.5.3) also incorporated a temperature dependence (HOUPERT, FLAMAND and BERTHE, 1981; WIKSTRÖM and HÖGLUND, 1994; HOUPERT, 1980; BAIR and WINER, 1992). Therefore, it shall be checked in how far temperature influences the maximum shear stress and in how far this may be attributed to temperature dependency of the limiting shear stress.

6.1.2.1 *Thermocouple results*

First, the influence of the oil inlet temperature was investigated and results are shown in Fig. 6.1.2. It is noticeable that the entrainment speed does not influence the maximum shear stress reached. This is due to the fact that all experiments were conducted in the full film lubrication regime. However, a slight decrease of the maximum shear stress attained is present with increasing oil inlet temperature. It is in the range of -0.6 MPa/K and appears to be constant for the investigated pressures.
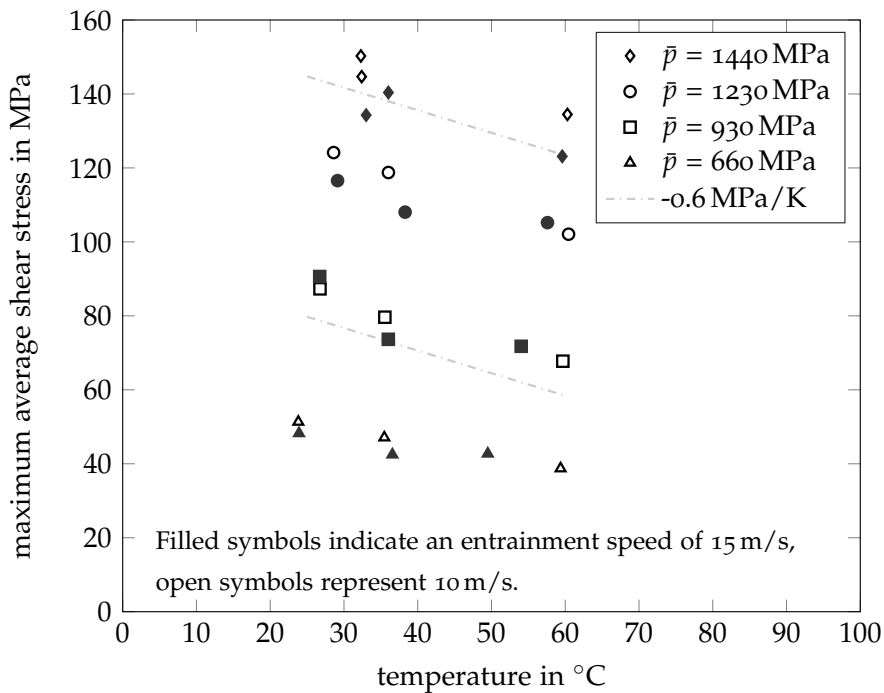
Figure 6.1.2: Observed influence of oil inlet temperature on maximum shear stress. Each data point represents the mean value of at least 5 experiments with constant inlet temperature.

Here, the effect discussed in Sec. 4.2.2, especially in Fig. 4.2.2 is visible. A heating up of the discs was in progress at each data point. Due

to the holding time of 10 s at each *SRR* value, no stationary temperature for that point was reached. If holding time would have been reduced or lengthened the amount of temperature increase would also differed. This transient experimental procedure was used to keep the temperature as close to the oil inlet temperature as possible while still reaching stable speeds and *SRR* values.

To gain a better understanding, results for the temperature measurements with the thermocouple are presented in Fig. 6.1.3. The upper plot shows the results of four traction curves, with the lower graph showing the temperature of the disc. The experiments were conducted following each other immediately with no cooling down time between the traction tests. The first traction experiment was started when the disc temperature had reached the value of the oil inlet temperature (with at least 30 min of heating up). The subsequent experiments were started when the *SRR* of the preceding experiment had reached 10 %. Thus, a rise of the temperature is visible, with each experiment starting at a slightly higher temperature. It can be concluded that during each traction experiment (i.e., upward variation of *SRR* from 0 to 10 %) the temperature increases about 40 K. The decrease of the traction coefficient from 0.06 to $\approx$ 0.04 in Fig. 6.1.3 corresponds to a decrease in shear stress of about 35 MPa. A similar decrease is to be expected when assuming the gradient of -0.6 MPa/K for the maximum shear stress derived from Fig. 6.1.2.
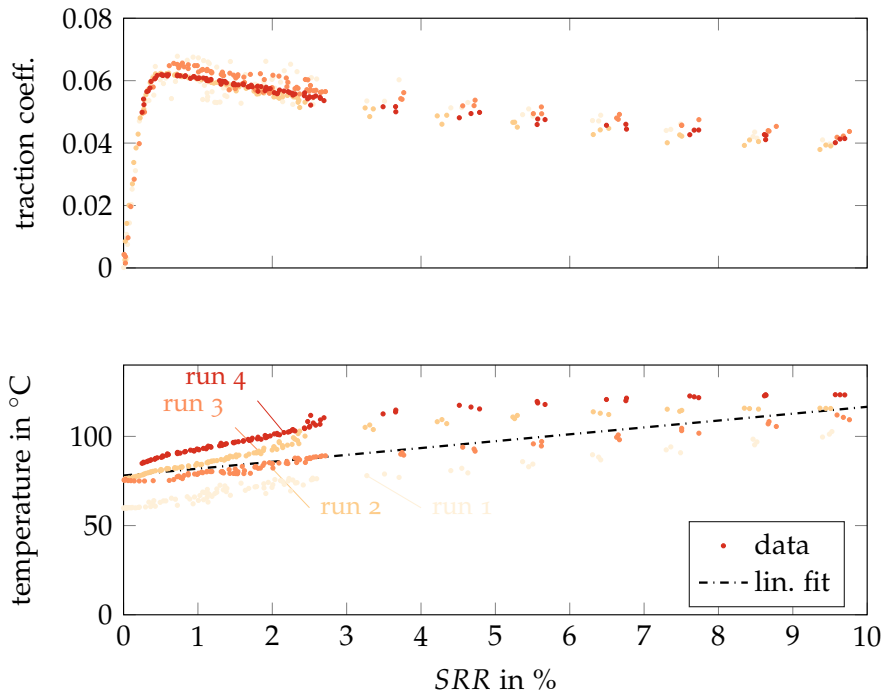
Figure 6.1.3: Temperature of contact bodies measured via thermocouple after repeated traction measurements. Each data point was held for 10 s, $\bar{p} = 1.8\,\text{GPa}$, $v = 15\,\text{m/s}$, $T_{\text{oil}} = 60\,^{\circ}\text{C}$. Measurements start at lowest temperature and lead to increase with each repetition.

6.1.2.2 *Thermography results*

In order to investigate temperature effects in detail, experiments with the thermographic camera were conducted as described in Sec. 4.2.3. In these experiments, the setup was heated for at least 60 min. Then the experiment was carried out by running the steel disc against the sapphire hollow shaft at a defined pressure, speed, and fixed *SRR* for a short period of time. The next experiment with different parameters was performed after a waiting time of at least 60 min. Thus, the starting conditions for each experiment may be assumed as identical, which is different from the experiments in Fig. 6.1.3. Figure 6.1.4 shows a temperature map of the contact. The highest temperature is observed close to the contact centre. Furthermore, it is noticeable that the temperature behind the contact is higher than the temperature in the entrainment region. However, at the outlet the temperature first decreases sharply and subsequently rises again. In the regions outside the contact the temperature increases only slightly. It must be noted that the steel disc had a circumferential scratch (defect) which leads to a slightly asymmetric temperature field in the contact area. Furthermore, it should be considered that the data present integral temperatures across the film and have not yet been differentiated in a manner proposed for example by REDDYHOFF, SPIKES and OLVER
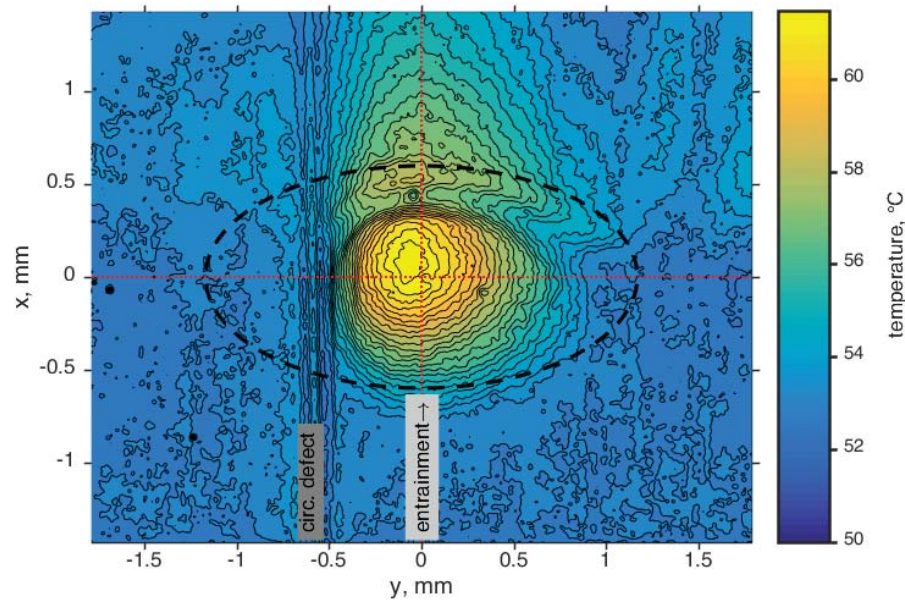
Figure 6.1.4: Temperature map. $v = 7\,\text{m/s}$, $\bar{p} = 900\,\text{MPa}$, $SRR = 11\,\%$. Data represent test with $T_{\text{oil}} = 50\,°\text{C}$. Measurements partly conducted by MARX (2015)

(2009a) and REDDYHOFF, SPIKES and OLVER (2009b); i. e., the temperatures obtained here are based on the combined emission originating from the sapphire body, the lubricant, and the steel surface.

A longitudinal temperature profile through the contact centre is shown in Fig. 6.1.5 for different SRRs. It can be observed that an increase of SRR, that means an increase as well of the heat flow into the contact, leads to higher temperatures in the contact. Furthermore, the rapid cooling mentioned before is observable in the outlet region, which may be attributed to decompression. Behind the contact, the temperature starts to increase again, leading to a temperature "tail" behind the contact. This is attributed to heat flowing from the discs into the lubricant behind the contact. The rise in temperature is roughly proportional to SRR. The observed trends are in agreement with literature, e. g. DAUBNER (2001), who observed local temperature variations in Hertzian contacts using thin film sensors. Comparisons with theoretical calculations regarding the expected temperature rises are still ongoing.
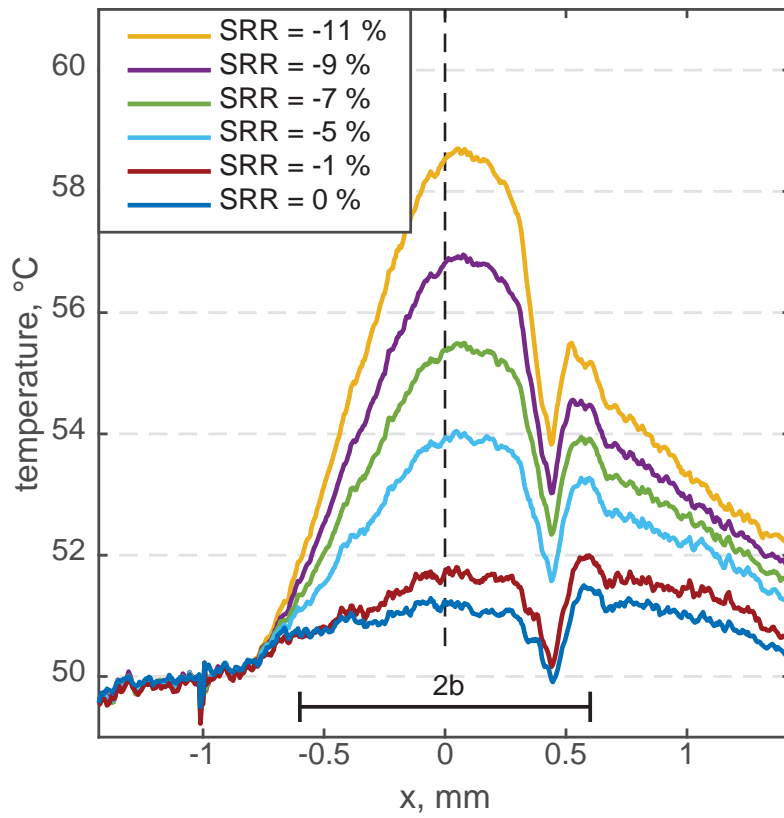
Figure 6.1.5: Temperature profiles at $y = 0$ for different *SRR*. $v = 7\,\text{m/s}$, $\bar{p} = 900\,\text{MPa}$, $T_{\text{oil}} = 50\,^{\circ}\text{C}$.

TRACTION CALCULATION

To improve the understanding of the lubricant behaviour in the contact a simple calculation was implemented in MATLAB. Although not an ideal environment for fast calculations, it was chosen for the ease of implementing different models quickly. In the following sections a description of the calculation routine is given with a subsequent discussion of results.

7.1 METHOD

It was attempted to simulate the measured traction curves using an approach based on the work presented by POLL and WANG (2012), WANG and POLL (2013) and WANG (2015). A finite difference approach was chosen to solve the shear stress distribution in the contact region.

For that purpose, the contact region is discretised and subsequently the equations are solved along parallel paths in the entrainment direction. The pressure distribution and gap form is calculated using a multi-grid solution (yielding a realistic EHL film profile) or a simplified HERTZian pressure distribution with a constant film thickness h_{cen}. The gained pressure and gap height are set as boundary conditions and the local shear rates are calculated for each element.

The fluid was represented by a MAXWELL model incorporating elastic, viscous, and limiting shear stress terms:

$$\dot{\gamma} = \frac{1}{G} \cdot \frac{\mathrm{d}\tau}{\mathrm{d}t} + \frac{\tau}{\eta\left(p, T, \dot{\gamma}\right)} \, . \tag{7.1}$$

Shear modulus and viscosity are calculated locally for each respective element. The elastic shear modulus was estimated locally as proposed by DYSON (1970):

$$G = 4 \cdot \tau_{\text{L}} \, . \tag{7.2}$$

For the equation of state the TAIT-DOOLITTLE (Eq. 2.67) model was used, combined with high pressure viscometry data. These data where measured using high pressure oscillating quartz viscometers at the Institute of Tribology and Energy Conversion Machinery of the Technical University of Clausthal. For some lubricants additional measurements with high pressure falling body viscometers from the Center for High Pressure Rheology Georgia Institute of Technology were used. Thus:

$$\eta(p, T) = \eta(p_0, T) \cdot e^{\left[B \cdot R_0 \cdot \left(\frac{1}{\frac{\rho(p_0, T)}{\rho(p, T) - R_0}} - \frac{1}{1 - R_0} \right) \right]} \, . \tag{7.3}$$

The shear rate dependent viscosity was calculated according to the CARREAU equation (Eq. 2.77), with coefficients from Tab. 7.3.1.

$$\eta = \eta_0(p, T) \cdot \left[1 + \left(\frac{\eta_0(p, T) \cdot \dot{\gamma}}{\tau_0} \right)^2 \right]^{\frac{n-1}{2}} \tag{7.4}$$

For FVA 3 the double modified CARREAU equation (Eq. 2.82 and Fig. 2.4.1) was used combined with data from high pressure COUETTE viscometer measurements also done at the Center for High Pressure Rheology Georgia Institute of Technology.

The critical shear stress τ_{crit} was determined by the EINSTEIN-DEBYE relationship Eq. 2.97.

$$\tau_{crit} = \frac{\rho \cdot R_g \cdot T}{M} \tag{7.5}$$

M is the molecular mass, R_g the universal gas constant, and ρ the density. The molecular mass is determined via an approximation proposed in the ASTM 2502-14 as was done byWANG (2015).

Using these values, a local shear stress $\tau_{loc}(x, y)$ can be calculated.

$$\tau_{loc}(i,j) = \frac{\frac{1}{2 \cdot u}\left(\dot{\gamma}_{i,j} + \dot{\gamma}_{i-1,j}\right) \cdot \Delta x + \frac{2 \cdot \tau_{i-1,j}}{G_{i,j} + G_{i-1,j}} - \frac{\tau_{i-1,j} \cdot \Delta x}{\left(\eta_{i,j} + \eta_{i-1,j}\right) \cdot u}}{\frac{2}{G_{i,j} + G_{i-1,j}} + \frac{\Delta x}{\left(\eta_{i,j} + \eta_{i-1,j}\right) \cdot u}} \tag{7.6}$$

With Δx denoting the grid resolution in entrainment direction and i, j the grid coordinates in x and y direction respectively. From these locally calculated values for the shear stress a mean shear stress resulted via integration, which was then compared with the data from the traction experiment.

The limiting shear stress in the fluid model was calculated according to Eq. 2.107 (WANG, 2015), using the data of Fit 1 in Table 6.1.1 to describe the pressure dependence. The values needed for the pressure dependence of τ_{max} were determined by fitting traction experiments (see Fit 1 Tab. 6.1.1 fit from Fig. 5.2.3). The fit was calculated for each temperature independently. Thus any temperature dependence present was included indirectly in the data.

In the calculation, the local shear stress is first assumed to result from the product of shear rate and viscosity and is truncated when exceeding the value τ_{max} (acc. Eq. 2.107). Thus, τ_{loc} is calculated as follows:

$$\tau_{loc}(i,j) = \begin{cases} \eta_{loc}(p_{loc}, T_{loc}, \dot{\gamma}_{loc}) \cdot \dot{\gamma}_{loc} & \text{if} \quad \tau_{loc,max}(i,j) \le \tau_{lim}(p, T, \lambda) \\ \tau_{lim,loc}(p_{loc}) & \text{if} \quad \tau_{loc,max}(i,j) > \tau_{lim}(p, T, \lambda) \end{cases} \tag{7.7}$$

The resulting shear stress of the contact is then gained by integration over all elements:

$$\tau_{\text{global}} = \frac{1}{A_{\text{Hertz}}} \int \int \tau_{\text{loc}}(i,j) \, \mathrm{d}j \mathrm{d}i = \frac{\sum_{i=1}^{n} \sum_{j=1}^{m} \tau_{\text{loc},i,j} \cdot \Delta x \cdot \Delta y}{\sum_{i=1}^{n} \sum_{j=1}^{m} \Delta x \cdot \Delta y} \quad (7.8)$$

with Δy being the grid resolution perpendicular to entrainment and m, n being the number of elements in x, y direction respectively. HAB-CHI et al. (2010) truncate the shear stress in a similar manner, albeit using a different calculation method and limiting shear stress model. Due to the numerical truncation a non differentiable shear stress distribution can lead to poor transitions of the traction from low to high *SRR*.

MORGADO et al. (2009) use a similar calculation incorporating the linear limiting shear stress relationship in combination with the CAR-REAU viscosity. However, they utilise a pressure-viscosity relationship according to BARUS.

The parameters used to describe the fluid and the models are given in Tab. 7.3.1.

7.2   ISOTHERMAL CALCULATION

In a first step, the calculations where performed assuming an iso-thermal contact. The oil supply temperature was taken as the temperature used for the calculation of the local viscosities, which corresponds to the data presented by WANG (2015) and BADER et al. (2015). The results are depicted in Fig. 7.2.1.
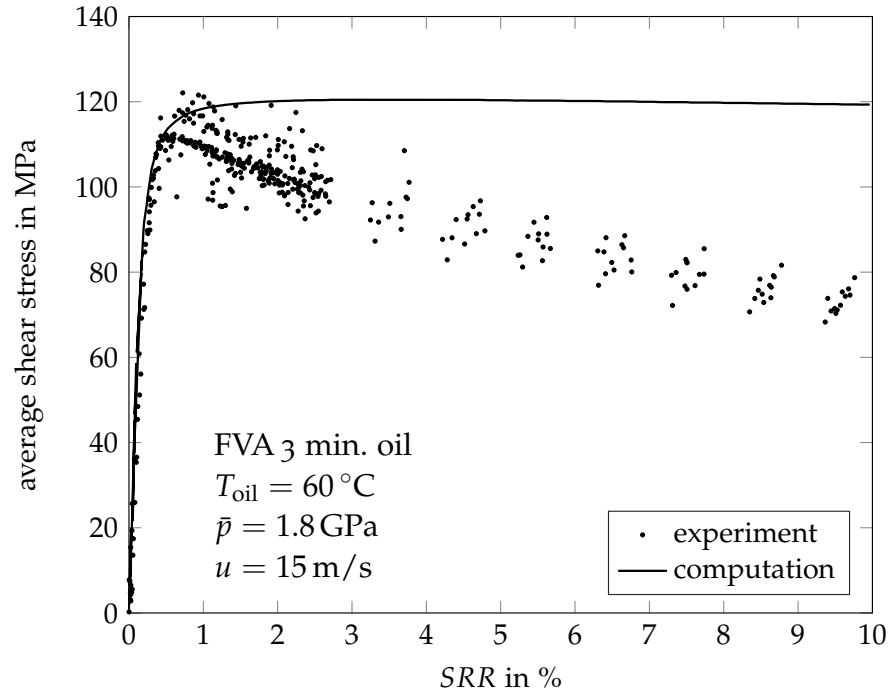
Figure 7.2.1: Comparison of isothermal calculations with experimental data. The experimental data are the ones presented in Fig. 6.1.3 . Calculated with the values presented in Tab. 6.1.1 as input.

It can be observed that the simulation corresponds well to the experimental data in the region of low *SRR*. However, in regions of higher *SRR* above $> 1.5\%$, the calculated shear stress is constant whilst the experiments show a declining shear stress. This is due to temperature effects which are not taken into account in the simulation. The calculated traction however, is dominated by the maximum shear stress τ_{max} in this region. This is visible by noting that the ratio of contact area reaching τ_{lim}, denoted A^*, to total contact area A is above 90 %, see Fig. 7.2.2.
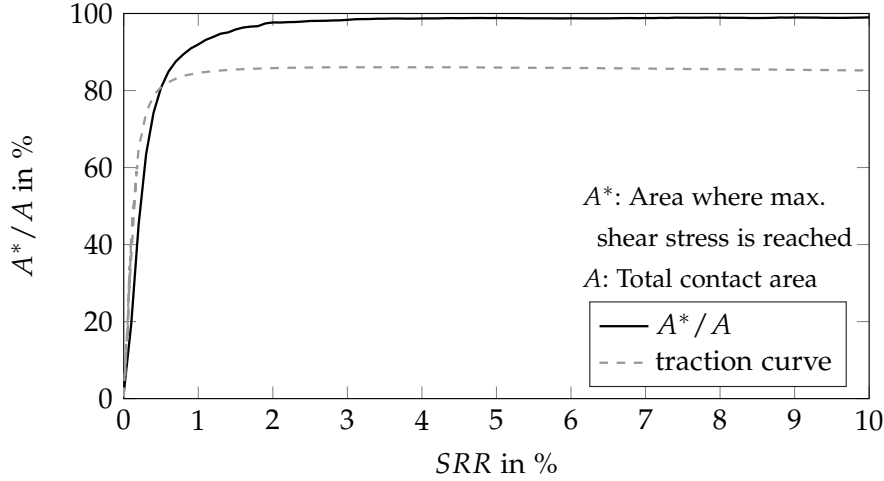
Figure 7.2.2: Ratio of area of contact area A to area A^* reaching maximum shear stress τ_{max} according to isothermal calculation presented in Fig. 7.2.1.

7.3 CALCULATION WITH THERMAL INFLUENCE

Subsequently a calculation based on the real local temperatures was performed. Here, the temperature was incorporated based on the experimentally gained maps of local temperatures (Fig. 6.1.5). The solution of the energy equation for the oil and the solids was not used as no full solution of the EHL problem (i.e., REYNOLDS equation, deformation) was implemented due to the wish for a low calculation time and that a measured temperature depicts the true temperature. This corresponds to the methodology used by (e.g., SHIRZADEGAN, 2015; SHIRZADEGAN et al., 2016) for a quick traction estimation rather than a complete contact solution.

GRIEVE and SPIKES (2002) and SPIKES and JIE (2014) make use of a temperature correction based on work by ARCHARD (1959) and also used by EVANS and JOHNSON (1986). They correct the traction curves by calculating a temperature rise in the contact in the form (SPIKES and JIE, 2014):

$$\Delta \bar{T} = \Delta \bar{T}_{\mathrm{surf}} + \Delta \bar{T}_{\mathrm{oil}} = \frac{1}{(2\pi K_{\mathrm{s}} \rho c)^{0.5}} \left(\frac{2b}{U} \right)^{0.5} \bar{\tau} \Delta u + \frac{h}{8 K_{\mathrm{oil}}} \bar{\tau} \Delta u \ .$$

$$(7.9)$$

With the first term describing the flash temperature of the solid and the second the temperature rise of the oil. Using b as half-width of the contact, K_{s}, ρ, and c being thermal conductivity, density, and specific heat of the solid bodies respectively. U, h, and K_{oil} the entrainment speed, the film thickness, and the thermal conductivity of the oil at the mean pressure of the contact, respectively. The time taken for the surfaces to pass through the contact is $2b/U$. The heat generated per unit area in the contact is $\bar{\tau} \Delta u$. The equation is valid for both solids of

the same material and travelling at equal velocities to the contact. The factor 8 is used for the assumption that the heat is generated in the total film while a value of 4 would mean the heat is only generated in the central plane (Spikes and Jie, 2014).

The flash temperature concept (Blok, 1955; Archard, 1959; Blok, 1963) was not used in the calculation due to the necessary introduction of yet another model with uncertain validity or parameters. Instead the measured temperatures, representing an integral contact temperature (i.e., result of oil temperature and solid temperature), were mapped onto the calculation domain. The resolution of the thermographical image was projected onto the finite difference grid, so that each element had a unique temperature value. For SRR values between measured data points, temperatures were interpolated linearly. The local viscosities were then calculated based on these local temperature values.

This method has the drawback that only operating conditions with a temperature measurement (i.e., a sapphire-steel contact, limited maximum pressure) can be directly calculated. However, the idea is to determine the influence of temperature on the maximum and the limiting shear stress as well as, in a later step validate a temperature calculation which can then be used to calculate steel-steel contacts. With the use of a temperature model this would not have been effective, due to the fact that insight gained into temperature behaviour would have meant always that this insight would be based on the temperature model.

Figure 7.3.1 shows results from these calculations. As opposed to Fig. 6.1.3 and Fig. 7.2.1, the decrease of shear stress at a given SRR is much less as the temperatures were approximately kept constant independently of SRR. This was achieved by conducting the measurement of a traction curve in the manner that each SRR value was acquired starting from the temperature stabilised pure rolling condition. During traction experiments with the steel-steel contact the SRR values were reached in consequetive order (see Sec. 6.1.2 especially Fig. 6.1.3).

In spite of the assumption of a temperature independent τ_{lim}, a temperature influence is visible now in the computed traction-SRR relationship, which is in decent agreement with the experiments. In the region of $SRR > 2\,\%$ the shear stress now decreases due to temperature influence, although τ_{lim} is kept constant in the calculation, i.e., is only dependent on the pressure in the element and temperature independent. Some discrepancy is still visible when comparing the simulation to the experimental data above $5\,\%$ SRR. Figure 7.3.2 shows the ratio of the contact area where the shear stress is already truncated to the limiting shear stress, as opposed to Fig. 7.2.1 this time under the influence of a temperature induced viscosity decrease. It can be noted that in regions of SRR around $3\,\%$ nearly $90\,\%$ of the

The figure contains the following labels and annotations:

axes: average shear stress in MPa (vertical, 0 to 80); SRR in % (horizontal, 0 to 10)

FVA 3 min. oil
steel against sapphire
$T_{\mathrm{oil}} = 40\,°\mathrm{C}$
$\bar{p} = 960\,\mathrm{MPa}$
$u = 7.5\,\mathrm{m/s}$
no temp. dependence of $\tau_{\max}$
press. dependence of $\tau_{\max}$

· experiment
— computation
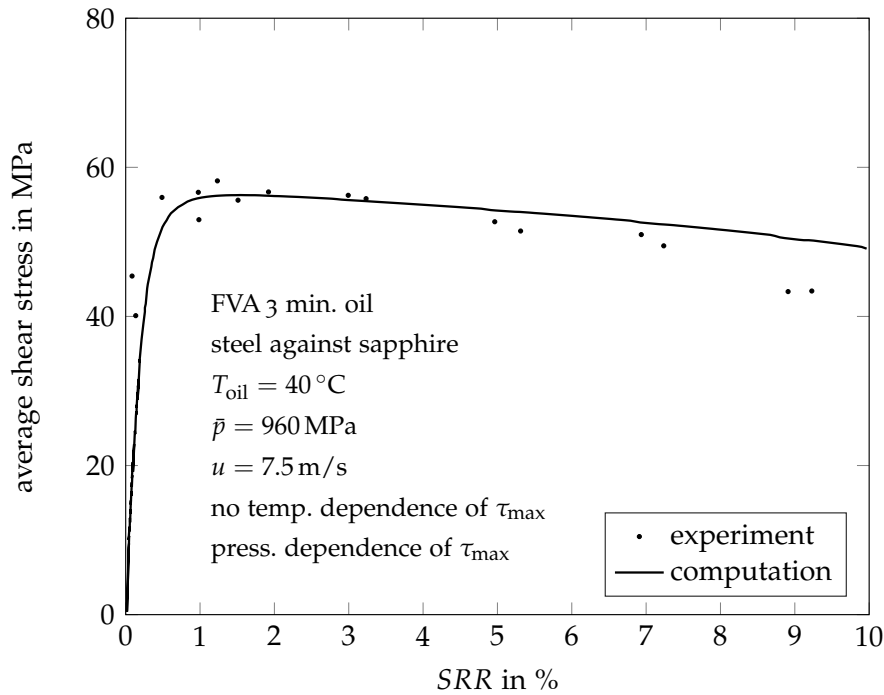
Figure 7.3.1: Comparison of thermal calculation with experimental data from the temperature experiments.

contact area is still reaching the limiting shear stress as for the iso-thermal calculation in Fig. 7.2.1. A decrease of the traction in both experiment and calculation, however, starts already at around 2 %. This can be attributed to the decreasing temperature dependent viscous shear stress in the remaining 10 % of the contact where τ_{lim} is not reached. Beyond 3 % this portion of the contact is rapidly increasing.

From these results it is deduced that the influence of temperature on the viscosity dominates any possible temperature influence on the limiting shear stress. The areas with a lower viscosity due to temperature increase do not reach the limiting shear stress any more and therefore lead to a total reduction of traction.

7.4   INFLUENCE OF VISCOSITY MODELS

As discussed in Sec. 2.3, several models for the physical properties of the lubricants exist, and these models yield quite notable differences for the fluid behaviour under EHL conditions. Therefore, a variation of implemented models was carried out. Furthermore, the observed effect that the viscosity variation with temperature dominates the reached traction at high SRR results in this region should heavily depend on the used lubricant models.
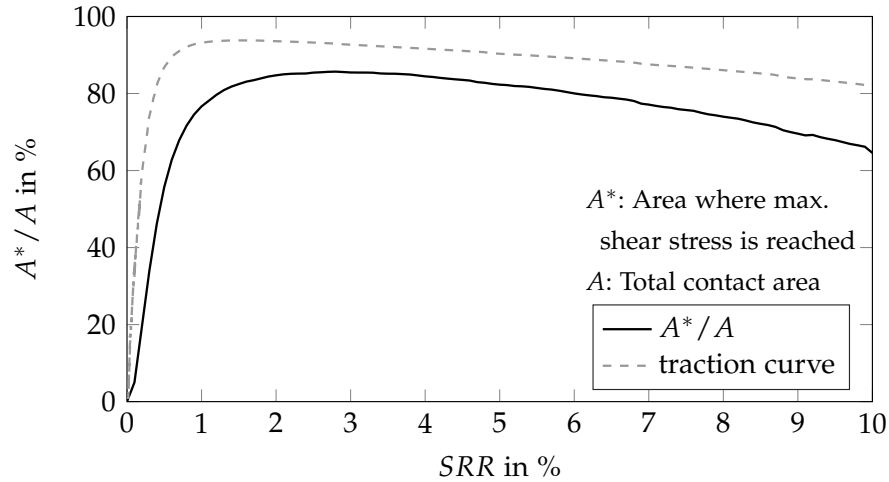
Figure 7.3.2: Area of contact (A^*) reaching max. shear stress τ_{max} according to calculation for calculation considering thermal effects.

Table 7.3.1: Parameters used for calculation.

FVA3		
Carreau exponent	n	0.35
kinematic viscosity	$\nu_{40\,°C}$	95 mm^2/s
kinematic viscosity	$\nu_{100\,°C}$	11,1 mm^2/s
density at 15 °C	$\rho_{15\,°C}$	896 kg/m^3
critical shear stress	τ_{crit}	6 MPa
Heat conductivity[†] (40 °C)	$\lambda_{40\,°C}$	0.145 W/m· K
Specific heat capacity[†] (40 °C)	$c_{p40\,°C}$	2258.8 J/kg· K

[†] data from (Bobach et al., 2015)

7.4.1 *Influence of pressure-viscosity model*

For one operating condition with the mineral reference oil FVA 3 the traction was calculated varying the viscosity model (Barus, Bode, Roelands, Yasutomi). The limiting shear stress model was not varied in these calculations. The shear thinning model used was the Carreau model. Figure 7.4.1 shows the resulting traction curves with the parameters for the pressure-viscosity models given in Tab. 7.4.1. Fluid properties are given in Tab. 7.3.1. It is clearly visible that the traction level is influenced by the choice of viscosity model.

The reason is that the limiting shear stress is reached in different portions of the contact depending on the viscosity model. Thus a model like the Barus equation, which underestimates the viscosity yields lower total traction as some regions have not reached a viscos-
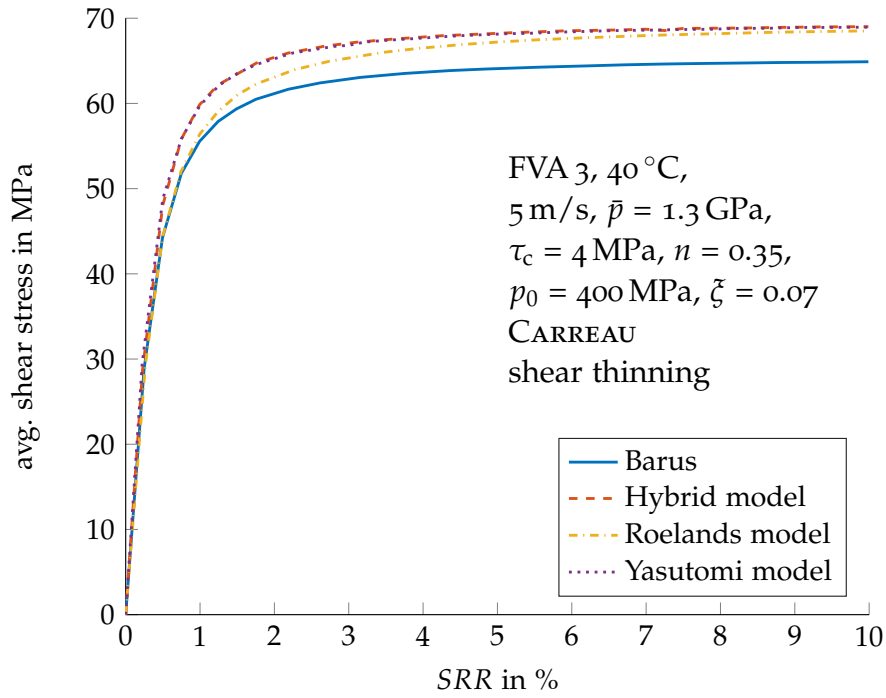
Figure 7.4.1: Influence of different pressure-viscosity models

ity which would in combination with the shear rate be greater than the limiting shear stress for that said pressure. Even the behaviour in the expected shear thinning area is different with the ROELANDS model yielding a shear thinning like behaviour. In conclusion the precise modeling of the pressure viscosity behaviour is of central importance for the results gained. Thus simulation of fluids is only feasible if the lubricant behaviour in the high pressure areas can be represented correctly.
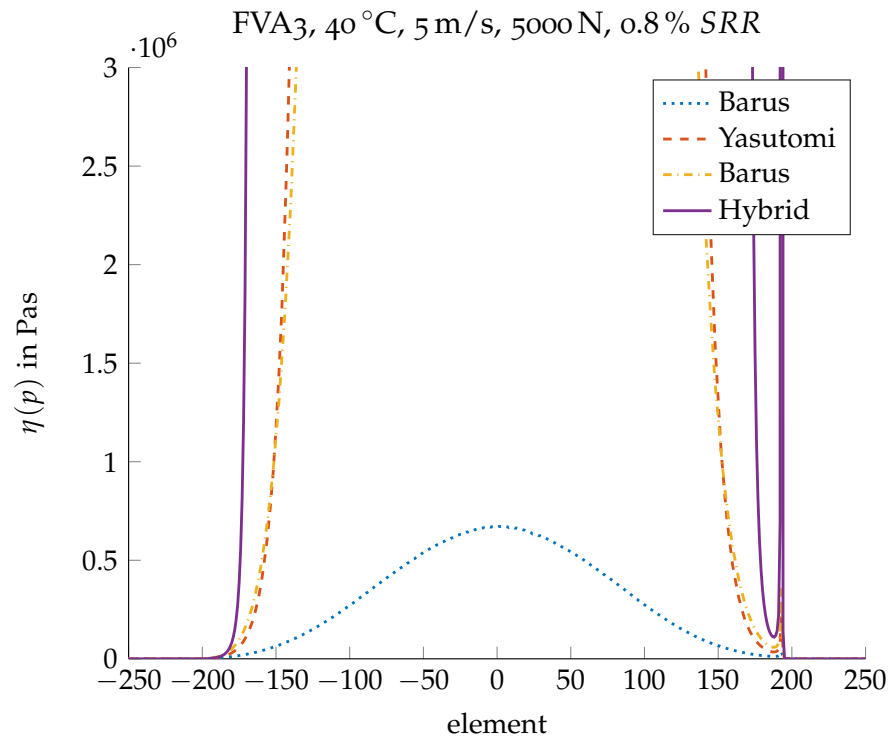
Figure 7.4.2: Difference of viscosity on contact middle plane using differ-
ent pressure-viscosity models. The shear thinning model is the
CARREAU model. Due to the differently calculated low shear
viscosity the presented relations are calculated. Notice the dif-
ferences in viscosity which will, assuming the shear rate to be
constant throughout the contact, lead to different shear stresses.
Thus the area reaching the limiting shear stress varies leading
to the different integral shear stresses, i. e., traction curves.

Table 7.4.1: Parameters of pressure-viscosity relations for FVA 3. Based on data from ITR or GTech (BAIR)

BARUS	Eq. 2.54
$\alpha_p = 2 \cdot 10^{-8}\,\mathrm{Pa}^{-1}$	

BARUS modified		Eq. 2.55
$\alpha_{00} = 0.0037\,\mathrm{bar}^{-1}$	$\alpha_{01} = -0.0093\,\mathrm{bar}^{\circ}\mathrm{C}$	
$\alpha_{10} = 5.09 \cdot 10^{-7}\,\mathrm{bar}^2$	$\alpha_{11} = -0.027\,\mathrm{bar}^{2\,\circ}\mathrm{C}$	

YASUTOMI		Eq. 2.70
$\mu_g = 1 \cdot 10^{12}\,\mathrm{Pas}$	$T_{g0} = -89.249\,^{\circ}\mathrm{C}$	
$A_1 = 161.781\,^{\circ}\mathrm{C}$	$A_2 = 0.833\,1/\mathrm{GPa}$	
$b_1 = 10.176\,1/\mathrm{Gpa}$	$b_2 = -0.295$	
$C_1 = 16.699$	$C_2 = 35.586\,^{\circ}\mathrm{C}$	

HYBRID		Eq. 2.73
$\mu_{\infty} = 0.0472\,\mathrm{mPas}$	$D_F = 5.833$	
$T_{\infty} = 176.368\,\mathrm{K}$	$e_0 = 8.137\,1/\mathrm{Gpa}$	
$e_1 = 318.9\,\mathrm{K}/\mathrm{Gpa}$	$e_2 = 1.02 \cdot 10^6\,\mathrm{K}^2/\mathrm{Gpa}$	
$f_0 = -13.111$	$f_1 = 6856\,\mathrm{K}$	
$C_F = D_F = 5.833$	$g_0 = 7.908\,\mathrm{Gpa}$	
$g_1 = -2021.555\,\mathrm{KGpa}$		

ROELANDS		Eq. 2.62
$\mu_p = 0.0631$	$\mu_R = 83.088\,\mathrm{mPas}$	
$Z = 0.630$	$S = 1.302$	
$P_p = 196\,\mathrm{MPa}$	$T_{\infty} = 138$	
$T_R = 40\,^{\circ}\mathrm{C}$		

7.5   INFLUENCE OF PARAMETERS IN THE MAXWELL MODEL

To investigate the influence of the parameters in the MAXWELL model the following variations were done. The elasticity of the fluid was not considered (i. e., $G = \infty$). Shear thinning was not considered ($\eta = f(p, T)$) and the limiting shear stress was ignored ($\tau_{\text{lim}} = \infty$). The results are shown in Fig. 7.5.1.

It can be observed that neglecting the elasticity causes a very steep increase of traction coefficient in the areas of low *SRR*, while a NEW-TONIAN lubricant behaviour leads to unreasonably high traction coefficients.

Neglecting the limiting shear stress yields curves similar to traction curves measured, however these curves do not reach the maximum from the experiment but overestimate the friction if temperature is taken into account. If the calculation is isothermal the traction CoF does not reach a maximum but increases with increasing *SRR*.
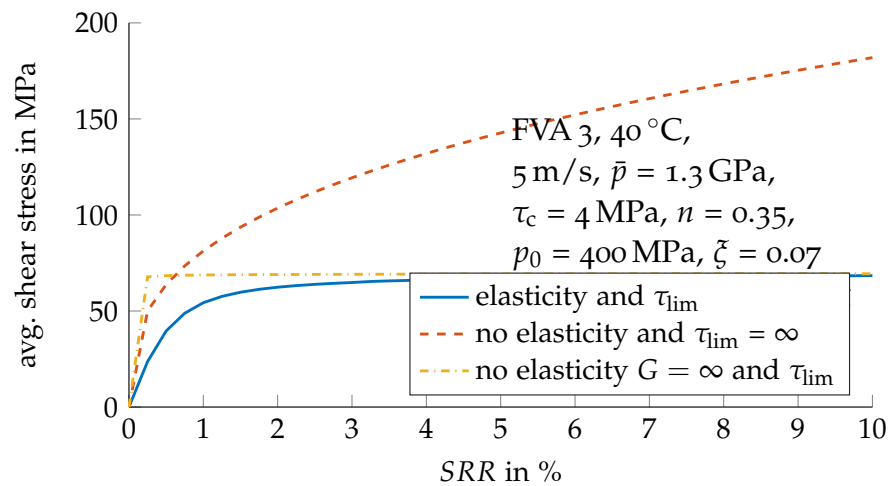
Figure 7.5.1: Influence of elasticity and limiting shear stress

DISCUSSION AND OUTLOOK

Several experimental results for gaining data associated with the lubricant behaviour were presented. It could be shown that the pressure dependence of the maximum shear stress $\bar{\tau}_{max}$ at medium and high contact pressures from traction experiments and HPC is similar for most investigated lubricants. Only polyglycol and a low viscosity diesel calibration fluid showed significantly differing results. However, the mechanism in the HPC experiments is not yet fully understood and it is unknown whether it is the same mechanism governing the limiting shear stress in an EHL contact.

Furthermore, a minor temperature influence on the maximum shear stress $\bar{\tau}_{max}$ derived from traction experiments could be detected. This was independent of speed and pressure.

However, the influence of temperature on viscosity already lowers the traction in a manner that a decent agreement between simulation and experiment can be achieved by keeping τ_{lim} constant independent of temperature.

A proposed bilinear approximation of the maximum shear stress may be used as well in calculations to determine traction curves. However, other models proposed for the limiting shear stress can be used and will differ only slightly under the experimental conditions that provided the parameters.

Therefore, the real behaviour can be explained by maintaining the assumption of τ_{lim} being independent of temperature as already stated by Habchi, Bair and Vergne (2013).

The extraction of local fluid properties by using integral measurements combined with local information of contact conditions may well be a step towards a better understanding of lubricant behaviour. Thus the aim is to understand the lubricant behaviour allowing these observations to then be applied to traction calculation.

The thermographic system was applied to a twin-disc experiment allowing simultaneous measurement of traction as well as temperature distribution in the contact. It is however limited to model systems using sapphire-steel contacts and cannot directly measure in steel-steel contacts. It is however useful as well to validate calculation models which can then be transferred engineering applications.

OUTLOOK

Whilst the model of the maximum shear stress, as well as the calculation, may be used to quantify the losses in EHL contacts, the aim must

be to also gain further insight into the fluid behaviour under EHL conditions. MARTINIE and VERGNE (2016) have noted that currently no rheometer exists which can accurately be used to gain data under the pressures, temperatures, timescopes, and shear rates needed to describe the lubricant behaviour. Thus an extraction of the lubricant properties, based on knowledge of the local contact conditions (i. e., pressure, temperature, shear rate), from traction experiments may be a feasible step towards a better understanding of the lubricant behaviour (ALBAHRANI et al., 2016).

It must be noted that at present the results gathered from the temperature measurements are not yet incorporated into the theoretical discussion in a satisfactory manner. The aim is to integrate the local temperature distributions of the contact partners into the determination of the limiting shear stress. To achieve this, the temperature of all partners, i. e., fluid and respective surfaces, will have to be determined based on a method proposed by REDDYHOFF, SPIKES and OLVER (2009b), REDDYHOFF, SPIKES and OLVER (2009a) and LU, REDDYHOFF and DINI (2017). This will be the focus of future work. Based on these results, the calculations will be refined making use, e. g. of methods proposed by GRIEVE and SPIKES (2002), CANN and SPIKES (1989) and GLOVNEA and SPIKES (1995). The implementation of a full system approach similar to work presented by LIU et al. (2007) might yield a further gain in precision of the calculation. It should be noted though, that the models implemented in this thesis were already chosen for physical plausibility based on primary laboratory data.

Hopefully, the use of traction experiments combined with local temperature measurements is a step towards a precise knowledge and identification of the real fluid properties, thus allowing the quantitative calculation of realistic local shear stresses based on temperature and pressure fields. This may be a move towards a better understanding of the real fluid behaviour and the physical mechanism at work from integral measurements and thus allow a better, physically sound, modeling of the losses in EHL contacts.

With four parameters I can fit an elephant,
and with five I can make him wiggle his trunk.
— Attributed to VON NEUMANN by ENRICO FERMI

as quoted by FREEMAN DYSON (DYSON, 2004)

BIBLIOGRAPHY

ASME Research Comittee on Lubrication (1953a). *Pressure–Viscosity Report, Vol. I*. Tech. rep. American Society of Mechanical Engineers, New York.

— (1953b). *Pressure–Viscosity Report, Vol. II*. Tech. rep. American Society of Mechanical Engineers, New York.

ASTM 341-93 (1998). *Standard viscosity-temperature charts for liquid petroleum products*. Standard. ASTM International.

ASTM D2502-14. *Standard test method for estimation of mean relative molecular mass of petroleum oils from viscosity measurements*. Standard. ASTM International.

Akyildiz, F., R. S. Jones and K. Walters (1990). 'On the spring-dashpot representation of linear viscoelastic behaviour'. In: *Rheologica Acta* 29.5, pp. 482–484. DOI: 10.1007/BF01376800.

Albahrani, S.M.B., D. Philippon, P. Vergne and J.M. Bluet (2016). 'A review of in situ methodologies for studying elastohydrodynamic lubrication'. In: *Proceedings of the Institution of Mechanical Engineers, Part J: Journal of Engineering Tribology* 230.1, pp. 86–110. DOI: 10.1177/1350650115590428.

Alsaad, M.M., Bair S.S., D.M. Sanborn and Winer W.O. (1978). 'Glass Transitions in Lubricants: Its Relation to Elastohydrodynamic Lubrication (EHD)'. In: *Journal of Lubrication Technology* 100 (3), pp. 404–416. DOI: 10.1115/1.3453197.

Alsaad, Mohammed Ahmed (1976). 'Light-Scattering Study of the Glass Transition and the Glassy State in Lubricating Oils'. PhD Thesis. Atlanta: Georgia Institute of Technology.

Andrade, Enda C. (1930). 'Viscosity of liquids'. In: *Nature* 125.3148, pp. 309–310.

— (1934). 'A theory of the viscosity of liquids – Part II'. In: *The London, Edinburgh, and Dublin Philosophical Magazine and Journal of Science* 17.113.

Anonymous (1972). 'MONSANTO'S HIGH TRACTION 'SANTOTRAC''. In: *Industrial Lubrication and Tribology* 24.1, pp. 43–44. DOI: 10.1108/eb053001.

Anuradha, Parinam and Punit Kumar (2011). 'New film thickness formula for shear thinning fluids in thin film elastohydrodynamic lubrication line contacts'. In: *Proceedings of the Institution of Mechanical Engineers, Part J: Journal of Engineering Tribology* 225.4, pp. 173–179. DOI: 10.1177/1350650111399520.

— (2013). 'New minimum film thickness formula for EHL rolling/sliding line contacts considering shear thinning behavior'. In: *Proceedings of the Institution of Mechanical Engineers, Part J: Journal of En-*

gineering Tribology 227.3, pp. 187–198. DOI: `10.1177/13506501124` `62173`.

ARCHARD, J. F. (1959). 'The temperature of rubbing surfaces'. In: *Wear* 2.6, pp. 438 –455. DOI: `10.1016/0043-1648(59)90159-0`.

ARRHENIUS, S. (1889). 'Über die Dissociationswärme und den Einfluss der Temperatur auf den Dissociationsgrad der Elektrolyte.' In: *Zeitschrift für Physikalische Chemie* 4, pp. 96–116. DOI: `10.1515/` `zpch-1889-0408`.

AUSHERMAN, V.K., H.S. NAGARAJ, D.M. SANBORN and Winer W.O. (1976). 'Infrared Temperature Mapping in Elastohydrodynamic Lubrication'. In: *Journal of Lubrication Technology* 98.2, pp. 236–242. DOI: `10.1115/1.3452806`.

BADER, N., D. WANG, L. BROUWER, H. SCHWARZE and G. POLL (2015). 'Comparison of maximum shear stress reached in traction tests with high pressure chamber measurements.' In: *Proceedings of 42nd Leeds-Lyon symposium on tribology*. Lyon.

BAIR, Scott S. (1990). 'High Shear Stress Rheology of Liquid Lubricants'. PhD Thesis. Atlanta: Georgia Institute of Technology.

— (2000). 'On the concentrated contact as a viscometer'. In: *Proceedings of the Institution of Mechanical Engineers, Part J: Journal of Engineering Tribology* 214.6, pp. 515–521. DOI: `10.1243/13506500015` `43386`.

— (2001). 'Ordinary shear-thinning behavior in liquids and its effect upon EHL traction'. In: *Tribology series* 39, pp. 733–742. DOI: `10.1` `016/S0167-8922(01)80154-1`.

— (2004a). 'A Rough Shear-Thinning Correction for EHD Film Thickness'. In: *Tribology Transactions* 47.3, pp. 361–365. DOI: `10.1080/05` `698190490455519`.

— (2004b). 'Roelands' missing data'. In: *Proceedings of the Institution of Mechanical Engineers, Part J: Journal of Engineering Tribology* 218.1, pp. 57–60. DOI: `10.1243/135065004322842834`.

— (2005). 'Shear thinning correction for rolling/sliding elastohydrodynamic film thickness'. In: *Proceedings of the Institution of Mechanical Engineers, Part J: Journal of Engineering Tribology* 219.1, pp. 69–74. DOI: `10.1243/135065005X9709`.

— (2007). *High pressure rheology for quantitative elastohydrodynamics*. Vol. 54. Elsevier.

— (2014). 'A critical evaluation of film thickness-derived pressure-viscosity coefficients'. In: *Lubrication Science*. DOI: `10.1002/ls.12` `84`.

— (2015). 'Choosing pressure-viscosity relations.' In: *High Temperatures – High Pressures* 44.6, pp. 415 –428.

— (2017). 'Comment on "The Relationship Between Friction and Film Thickness in EHD Point Contacts in the Presence of Longitudinal Roughness" by Guegan, Kadiric, Gabelli, & Spikes'. In: *Tribology Letters* 65.3, p. 83. DOI: `10.1007/s11249-017-0867-z`.

— (2018). 'Generalized Newtonian viscosity functions for hydrodynamic lubrication'. In: *Tribology International* 117.Supplement C, pp. 15 – 23. DOI: `10.1016/j.triboint.2017.08.014`.

BAIR, Scott S. and Ward O. WINER (1979a). 'A Rheological Model for Elastohydrodynamic Contacts Based on Primary Laboratory Data'. In: *Journal of Lubrication Technology* 101.3, pp. 258–264. DOI: `10.1115/1.3453342`.

— (1979b). 'Shear Strength Measurements of Lubricants at High Pressure'. In: *Journal of Lubrication Technology* 101.3, pp. 251–257. DOI: `10.1115/1.3453339`.

— (1992). 'The high pressure high shear stress rheology of liquid lubricants'. In: *Journal of tribology* 114.1, pp. 1–9. DOI: `10.1115/1.2920862`.

— (1997). 'A Simple Formula for EHD Film Thickness of Non-Newtonian Liquids'. In: *Elastohydrodynamics - '96 Fundamentals and Applications in Lubrication and Traction*. Ed. by D. DOWSON, C.M. TAYLOR, T.H.C. CHILDS, G. DALMAZ, Y. BERTHIER, L. FLAMAND, J.-M. GEORGES and A.A. LUBRECHT. Vol. 32. Tribology Series Supplement C. Elsevier, pp. 235 –241. DOI: `10.1016/S0167-8922(08)70452-8`.

BAIR, Scott, Jacek JARZYNSKI and Ward O. WINER (2001). 'The temperature, pressure and time dependence of lubricant viscosity'. In: *Tribology International* 34.7, pp. 461 –468. DOI: `doi.org/10.1016/S0301-679X(01)00042-1`.

BAIR, Scott and Mike KOTZALAS (2006). 'The Contribution of Roller Compliance to Elastohydrodynamic Traction'. In: *Tribology Transactions* 49.2, pp. 218–224. DOI: `10.1080/05698190600614817`.

BAIR, Scott, Yuchuan LIU and Q. WANG Jane (2006). 'The Pressure-Viscosity Coefficient for Newtonian EHL Film Thickness With General Piezoviscous Response'. In: *Journal of Tribology* 128.3, pp. 624–631. DOI: `10.1115/1.2197846`.

BAIR, Scott, Laetitia MARTINIE and Philippe VERGNE (2016). 'Classical EHL Versus Quantitative EHL: A Perspective Part II—Super-Arrhenius Piezoviscosity, an Essential Component of Elastohydrodynamic Friction Missing from Classical EHL'. In: *Tribology Letters* 63.3, p. 37. DOI: `10.1007/s11249-016-0725-4`.

BAIR, Scott and Clare MCCABE (2004). 'A study of mechanical shear bands in liquids at high pressure'. In: *Tribology International* 37.10, pp. 783–789. DOI: `10.1016/j.triboint.2004.05.002`.

BAIR, Scott and Farrukh QURESHI (2003). 'Ordinary shear thinning behavior and its effect upon EHL film thickness'. In: *Tribology Series* 41, pp. 693–699. DOI: `10.1016/S0167-8922(03)80182-7`.

BAIR, Scott, Farrukh QURESHI and Ward O. WINER (1993). 'Observations of Shear Localization in Liquid Lubricants Under Pressure'. In: *Journal of Triblogy* 115.3, pp. 507–513. DOI: `10.1115/1.2921667`.

BAIR, Scott, Ward O. WINER and Keith W. DISTIN (1993). 'Experimental Investigations Into Shear Localization in an Operating

EHD Contact'. In: *Thin Films in Tribology*. Ed. by D. Dowson, C.M. Taylor, T.H.C. Childs, M. Godet and G. Dalmaz. Vol. 25. Tribology Series Supplement C. Elsevier, pp. 383 –388. DOI: `10.1016/S0167-8922(08)70393-6`.

Bair, Scott, Charlotte Mary, Nathalie Bouscharain and Philippe Vergne (2013). 'An improved Yasutomi correlation for viscosity at high pressure'. In: *Proceedings of the Institution of Mechanical Engineers, Part J: Journal of Engineering Tribology* 227.9, pp. 1056–1060. DOI: `10.1177/1350650112474394`.

Baly, Hatem (2005). 'Reibung fettgeshmierter Wälzlager'. Dissertation. IMKT, Universität Hannover.

Barlow, A. J., A. Erginsavand and J. Lamb (1967). 'Viscoelastic relaxation of supercooled liquids. II'. In: *Proceedings of the Royal Society of London A: Mathematical, Physical and Engineering Sciences* 298.1455, pp. 481–494. DOI: `10.1098/rspa.1967.0116`. eprint: `http://rspa.royalsocietypublishing.org/content/298/1455/481.full.pdf`.

Barlow, A. J., J. Lamb and A. J. Matheson (1966). 'Viscous Behaviour of Supercooled Liquids'. In: *Proceedings of the Royal Society of London A: Mathematical, Physical and Engineering Sciences* 292.1430, pp. 322–342. DOI: `10.1098/rspa.1966.0138`.

Barlow, A. J., J. Lamb, A. J. Matheson, P. R. K. L. Padmini and J. Richter (1967). 'Viscoelastic relaxation of supercooled liquids. I'. In: *Proceedings of the Royal Society of London A: Mathematical, Physical and Engineering Sciences* 298.1455, pp. 467–480. DOI: `10.1098/rspa.1967.0115`. eprint: `http://rspa.royalsocietypublishing.org/content/298/1455/467.full.pdf`.

Bartel, Dirk (2001). 'Berechnung von Festkörper- und Mischreibung bei Metallpaarungen (Calculation of solid and mixed friction in metal pairs)'. Dissertation. Otto-von-Guericke Universität Magdeburg.

— (2010). *Simulation von Tribosystemen*. Vieweg + Teubner. ISBN: 978-3-8348-1241-4. DOI: `10.1007/978-3-8348-9656-8`.

Barus, Carl (1893). 'Isothermals, isopiestics and isometrics relative to viscosity'. In: *American Journal of Science* Series 3 Vol. 45.266, pp. 87–96. DOI: `10.2475/ajs.s3-45.266.87`.

Barz, Matthias (1996). 'Die Schmierfilmbildung in fettgeschmierten schnellaufenden Spindellagern'. Dissertation. IMKT, Hannover.

Baumann, H (1987). 'Measuring Surface Temperatures between Rolling Steel Cylinders Using Double-Layer Transducers'. In: *Proceedings of the Institution of Mechanical Engineers, Part C: Journal of Mechanical Engineering Science* 201.4, pp. 263–270. DOI: `10.1243/PIME\_PROC\_1987\_201\_119\_02`.

Beilicke, R., L. Bobach and D. Bartel (2016). 'Transient thermal elastohydrodynamik simulation of a DLC coated helical gear pair considering limiting shear stress behavior of the lubricant.' In: *Tri-*

bology International 97, pp. 136–150. DOI: `10.1016/j.triboint.20`
`15.12.046`.

Bell, J. C. (1962). 'Lubrication of Rolling Surfaces by a Ree-Eyring Fluid'. In: *A S L E Transactions* 5.1, pp. 160–171. DOI: `10.1080/056` `98196208972463`.

Bell, J. C., J. W. Kannel and C. M. Allen (1964). 'The Rheological Behavior of the Lubricant in the Contact Zone of a Rolling Contact System'. In: *Journal of Basic Engineering* 86.3, pp. 423–432. DOI: `10.1115/1.3653124`.

Blok, H. (1955). 'The dissipation of frictional heat'. In: *Applied Scientific Research, Section A* 5.2, pp. 151–181. DOI: `10.1007/BF031846` `15`.

— (1963). 'The flash temperature concept'. In: *Wear* 6.6, pp. 483 –494. DOI: `10.1016/0043-1648(63)90283-7`.

Bobach, Lars, Dirk Bartel, Ronny Beilicke, Josef Mayer, Klaus Michaelis, Karsten Stahl, Svenja Bachmann, Johann Schnagl and Holger Ziegele (2015). 'Reduction in EHL Friction by a DLC Coating'. In: *Tribology Letters* 60.1, p. 17. DOI: `10.1007/s11249-` `015-0594-2`.

Bode, B. (1984). 'Entwicklung eines Quarzviskosimeters für Messungen bei hohen Drücken'. Dissertation. Technische Universität Clausthal.

— (1989). 'Modell zur Beschreibung des Fließverhaltens von Flüssigkeiten unter hohem Druck'. In: *Tribologie und Schmierungstechnik* 36.4, pp. 182–189.

Bos, Johannes (1995). 'Frictional Heating of Tribological Contacts'. PhD Thesis. Twente: Universiteit Twente.

Brandão, J.A., M. Meheux, J.H.O. Seabra, F. Ville and M.J.D. Castro (2011). 'Traction curves and rheological parameters of fully formulated gear oils'. In: *Proceedings of the Institution of Mechanical Engineers, Part J: Journal of Engineering Tribology* 225.7, pp. 577–593. DOI: `10.1177/1350650111405111`.

Brewe, David E. and Bernard J. Hamrock (1977). 'Simplified Solution for Elliptical-Contact Deformation Between Two Elastic Solids'. In: *Journal of Lubrication Technology* 99.4, pp. 485–487. DOI: `10.111` `5/1.3453245`.

Brouwer, L., N. Bader and R. Beilicke (2016). *Tribologische Fluidmodelle für Nebenantriebsaggregate in Hybrid-und Elektrofahrzeugen.* Tech. rep. Heft 1092-2016. FVV.

Brouwer, Ludwig and Hubert Schwarze (2013). 'Bestimmung der Grenzschubspannung von Schmierstoffen aus Viskositätsmessungen *(Determination of Limiting Shear Stress from Viscosity Measurements)*'. In: *Reibung, Schmierung und Verschleiß*. Vol. 1. Aachen: Gesellschaft für Tribologie e.V., pp. 19/1–19/11.

Campos, A., A. Sottomayor and J. Seabra (2006). 'Non-newtonian thermal analysis of an EHD contact lubricated with MIL-L-23699 oil.' In: *Tribology International* 39.12. Interactions of Tribology and

the Operating Environment: Proceedings of the 32nd Leeds-Lyon Symposium on Tribology (Lyon, 2005), pp. 1732 –1744. DOI: `10.1016/j.triboint.2006.01.006`.

CANN, P., E. IOANNIDES, B. JACOBSON and A.A. LUBRECHT (1994). 'The lambda ratio – a critical re-examination'. In: *Wear* 175.1, pp. 177 –188. DOI: `10.1016/0043-1648(94)90181-3`.

CANN, P.M. and H.A. SPIKES (1989). 'Determination of the Shear Stresses of Lubricants in Elastohydrodynamic Contacts'. In: *Tribology Transactions* 32.3, pp. 414–422. DOI: `10.1080/10402008908981908`.

CARREAU, Pierre J. (1972). 'Rheological Equations from Molecular Network Theories'. In: *Transactions of the Society of Rheology* 16.1, pp. 99–127. DOI: `10.1122/1.549276`.

CARSLAW, H. S. and J. C. JAEGER (1959). *Conduction of Heat in Solids*. second. Oxford at the Clarendon Press.

CARTER, F. W. (1926). 'On the Action of a Locomotive Driving Wheel'. In: *Proceedings of the Royal Society of London. Series A, Containing Papers of a Mathematical and Physical Character* 112.760, pp. 151–157. DOI: `10.1098/rspa.1926.0100`.

CHANG, L. (2005). 'On the Shear Bands and Shear Localizations in Elastohydrodynamic Lubrication Films'. In: *Journal of Tribology* 127 (1), pp. 245–247. DOI: `10.1115/1.1843157`.

CHANG, L. and C. FARNUM (1992). 'A Thermal Model for Elastohydrodynamic Lubrication of Rough Surfaces'. In: *Tribology Transactions* 35.2, pp. 281–286. DOI: `10.1080/10402009208982119`.

CHAOMLEFFEL, J.-P., G. DALMAZ and P. VERGNE (2007). 'Experimental results and analytical film thickness predictions in EHD rolling point contacts'. In: *Tribology International* 40.10. Tribology at the Interface: Proceedings of the 33rd Leeds-Lyon Symposium on Tribology (Leeds, 2006), pp. 1543 –1552. DOI: `10.1016/j.triboint.2007.02.005`.

CHITTENDEN, R. J., D. Dowson, J. F. DUNN and C. M. TAYLOR (1985a). 'A Theoretical Analysis of the Isothermal Elastohydrodynamic Lubrication of Concentrated Contacts. I. Direction of Lubricant Entrainment Coincident with the Major Axis of the Hertzian Contact Ellipse'. In: *Proceedings of the Royal Society of London A: Mathematical, Physical and Engineering Sciences* 397.1813, pp. 245–269. DOI: `10.1098/rspa.1985.0014`.

— (1985b). 'A Theoretical Analysis of the Isothermal Elastohydrodynamic Lubrication of Concentrated Contacts. II. General Case, with Lubricant Entrainment along Either Principal Axis of the Hertzian Contact Ellipse or at Some Intermediate Angle'. In: *Proceedings of the Royal Society of London A: Mathematical, Physical and Engineering Sciences* 397.1813, pp. 271–294. DOI: `10.1098/rspa.1985.0015`.

COOPER, D. H. (1969). 'Hertzian contact-stress deformation coefficients'. In: *Journal of Applied Mechanics* 36.2, pp. 269–303. DOI: 10.1115/1.3564624.

COULOMB, Charles Augustin de (1821). *Théorie des machines simples.* Nouvelle éd. Paris: Bachelier.

CROOK, A. W. (1958). 'The lubrication of rollers'. In: *Philosophical Transactions of the Royal Society of London A: Mathematical, Physical and Engineering Sciences* 250.981, pp. 387–409. DOI: 10.1098/rsta.1958.0001.

— (1961a). 'The lubrication of rollers II. Film thickness with relation to viscosity and speed'. In: *Philosophical Transactions of the Royal Society of London A: Mathematical, Physical and Engineering Sciences* 254.1040, pp. 223–236. DOI: 10.1098/rsta.1961.0015.

— (1961b). 'The lubrication of rollers III. A theoretical discussion of friction and the temperatures in the oil film'. In: *Philosophical Transactions of the Royal Society of London A: Mathematical, Physical and Engineering Sciences* 254.1040, pp. 237–258. DOI: 10.1098/rsta.1961.0016.

— (1963). 'The lubrication of rollers IV. Measurements of friction and effective viscosity'. In: *Philosophical Transactions of the Royal Society of London A: Mathematical, Physical and Engineering Sciences* 255.1056, pp. 281–312. DOI: 10.1098/rsta.1963.0005.

CROUCH, R. F. and A. CAMERON (1961). 'Viscosity- temperature equations for lubricants'. In: *J. Inst. Petroleum* 47.453, pp. 307–313.

CUSSEAU, Pauline, Nathalie BOUSCHARAIN, Laetitia MARTINIE, David PHILIPPON, Philippe VERGNE and Fanny BRIAND (2017). 'Rheological considerations on polymer-based engine lubricants: viscosity index improvers versus thickeners – generalized Newtonian models'. In: *Tribology Transactions* 0.ja, pp. 0–0. DOI: 10.1080/10402004.2017.1346154.

DIN 51563:2011-04. *Prüfung von Mineralölen und verwandten Stoffen – Bestimmung des Viskosität-Temperatur-Verhaltens – Richtungskonstante m.* Standard. Beuth Verlag.

DAUBNER, O. (2001). 'Elastohydrodynamische Rollreibung in Stahl-Keramik-Kontakten (Elastohydrodynamic rolling friction in steel-ceramic contacts)'. Dissertation. Universität Karlsruhe.

DEALY, J. M. (2010). 'eissenberg and Deborah numbers–Their definition and use'. In: *Rheology Bulletin.*

DOOLITTLE, Arthur K. (1951a). 'Studies in Newtonian Flow. I. The Dependence of the Viscosity of Liquids on Temperature'. In: *Journal of Applied Physics* 22.8, pp. 1031–1035. DOI: 10.1063/1.1700096.

— (1951b). 'Studies in Newtonian Flow. II. The Dependence of the Viscosity of Liquids on Free-Space'. In: *Journal of Applied Physics* 22.12, pp. 1471–1475. DOI: 10.1063/1.1699894.

— (1952). 'Studies in Newtonian Flow. III. The Dependence of the Viscosity of Liquids on Molecular Weight and Free Space (in Ho-

mologous Series)'. In: *Journal of Applied Physics* 23.2, pp. 236–239. DOI: `10.1063/1.1702182`.

Dowson, D. and G. R. Higginson (1959). 'A Numerical Solution to the Elasto-Hydrodynamic Problem'. In: *Journal of Mechanical Engineering Science* 1.1, pp. 6–15. DOI: `10.1243/JMES\_JOUR\_1959 \_001\_004\_02`.

— (1966). *Elasto-hydrodynamic lubrication : the fundamentals of roller and gear lubrication*. Oxford; New York: Pergamon Press.

Dowson, Duncan (1962). 'A generalized Reynolds equation for fluid-film lubrication'. In: 4, pp. 159–170. DOI: `10.1016/S0020-7403(62 )80038-1`.

— (1998). *History of Tribology*. 2nd ed. Wiley. ISBN: 978-1-860-58070-3.

Dyson, A. (1965). 'Approximate calculations of Hertzian compressive stresses and contact dimensions'. In: *Journal of Mechanical Engineering Sciences* 7.2, pp. 224–227. DOI: `10.1243/JMES_JOUR_1965_00 7_031_02`.

— (1970). 'Frictional traction and lubricant rheology in elastohydrodynamic lubrication.' In: *Philosophical Transactions of the Royal Society of London, Series A* 266.1170, pp. 1–33.

Dyson, A., H. Naylor and A. R. Wilson (1965). 'Paper 10: The Measurement of Oil-Film Thickness in Elastohydrodynamic Contacts'. In: *Proceedings of the Institution of Mechanical Engineers, Conference Proceedings* 180.2, pp. 119–134. DOI: `10.1243/PIME\_CONF\_1965 \_180\_072\_02`.

Dyson, Freeman (2004). 'A meeting with Enrico Fermi'. In: *Nature* 427, p. 297. DOI: `10.1038/427297a`.

Evans, C. R. and K. L. Johnson (1986). 'The rheological properties of elastohydrodynamic lubricants'. In: *Proceedings of the Institution of Mechanical Engineers, Part C: Journal of Mechanical Engineering Science* 200.5, pp. 303–312. DOI: `10.1243/PIME\_PROC\_1986\_200 \_134\_02`.

Eyring, Henry (1936). 'Viscosity, Plasticity, and Diffusion as Examples of Absolute Reaction Rates'. In: *The Journal of Chemical Physics* 4.4, pp. 283–291. DOI: `10.1063/1.1749836`.

Fouad, Nabil A. and Torsten Richter (2012). *Leitfaden Thermografie im Bauwesen*. 4th ed. Fraunhofer IRB Verlag.

Fulcher, G.S. (1925). 'Analysis of recent measurements of the viscosity of glasses'. In: *Journal of American Ceramic Society* 8, pp. 339–355. DOI: `10.1111/j.1151-2916.1925.tb16731.x`.

Gattinoni, Chiara, David M. Heyes, Christian D. Lorenz and Daniele Dini (2013). 'Traction and nonequilibrium phase behavior of confined sheared liquids at high pressure'. In: *Phys. Rev. E* 88 (5), p. 052406. DOI: `10.1103/PhysRevE.88.052406`.

Gecim, B. and W. O. Winer (1980). 'Lubricant limiting shear stress effect on EHD film thickness'. In: *Journal of Tribology* 102.2, pp. 213–220.

GENIESSE, J. C. and T. G. DELBRIDGER (1932). 'Variation of Viscosity with Temperature'. In: *Proceedings American Petroleum, Institute-Section III, Refining* 13M, pp. 56–58.

GLOVNEA, R.P. and H.A. SPIKES (1995). 'Mapping Shear Stress in Elastohydrodynamic Contacts'. In: *Tribology Transactions* 38.4, pp. 932–940. DOI: 10.1080/10402009508983490.

GOHAR, Ramsey (1988). *Elastohydrodynamics*. Ellis Horwood Limited. ISBN: 0-85312-820-0.

GOKSEM, P. G. and R. A. HARGREAVES (1978a). 'The Effect of Viscous Shear Heating on Both Film Thickness and Rolling Traction in an EHL Line Contact—Part I: Fully Flooded Conditions'. In: *Journal of Lubrication Technology* 100.3, pp. 346–352. DOI: 10.1115/1.3453183.

— (1978b). 'The Effect of Viscous Shear Heating on Both Film Thickness and Rolling Traction in an EHL Line Contact—Part II: Starved Conditions'. In: *Journal of Lubrication Technology* 100.3, pp. 353–358. DOI: 10.1115/1.3453184.

GOLD, P. W., A. SCHMIDT, H. DICKE, J. LOOS and C. ASSMANN (2001). 'Viscosity–pressure–temperature behaviour of mineral and synthetic oils'. In: *Journal of Synthetic Lubrication* 18.1, pp. 51–79. DOI: 10.1002/jsl.3000180105.

GRAETZ, L. (1888). 'Ueber die Reibung von Flüssigkeiten'. In: *Annalen der Physik* 270.5, pp. 25–39. DOI: 10.1002/andp.18882700505.

GREENWOOD, J. A. and J. J. KAUZLARICH (1973). 'Inlet Shear Heating in Elastohydrodynamic Lubrication'. In: *Journal of Lubrication Technology* 95.4, pp. 417–423. DOI: 10.1115/1.3451844.

GRIEVE, R. and H.A. SPIKES (2002). 'Temperature and shear stress in rolling/sliding Elastohydrodynamic Contacts'. In: *Tribology and Interface Engineering Series* 38, pp. 511–522.

GRUBIN, A. N. (1949). 'Investigation of the contact of machine components (Ed. Kh. F. Ketova)'. In: *Central Scientific Research Institute for Technology and Mech- anical Engineering, Moscow) (DSIR translation 337)* 30.

GRUNTFEST, I. J. (1965). 'Apparent Departures from Newtonian Behavior in Liquids Caused by Viscous Heating'. In: *Transactions of the Society of Rheology* 9.1, pp. 425–441. DOI: 10.1122/1.548993. eprint: http://dx.doi.org/10.1122/1.548993.

GUEGAN, Johan, Amir KADIRIC, Antonio GABELLI and Hugh SPIKES (2017). 'Reply to the 'Comment on "The Relationship Between Friction and Film Thickness in EHD Point Contacts in the Presence of Longitudinal Roughness" by Guegan, Kadiric, Gabelli, & Spikes' by Scott Bair'. In: *Tribology Letters* 65.3, p. 91. DOI: 10.1007/s11249-017-0870-4.

GUO, Feng and Patrick L. WONG (2005). 'An anomalous elastohydrodynamic lubrication film – inlet dimple'. In: *Journal of Triblogy* 127.2, pp. 425–434. DOI: 10.1115/1.1866165.

Habchi, W., S. Bair and P. Vergne (2013). 'On friction regimes in quantitative elastohydrodynamics'. In: *Tribology International* 58, pp. 107 —117. doi: `10.1016/j.triboint.2012.10.005`.

Habchi, W. and J. S. Issa (2017). 'An Exact and General Model Order Reduction Technique for the Finite Element Solution of Elastohydrodynamic Lubrication Problems'. In: *Journal of Tribology* 139.5, p. 051501. doi: `10.1115/1.4035154`.

Habchi, W., P. Vergne, S. Bair, O. Andersson, D. Eyheramendy and G.E. Morales-Espejel (2010). 'Influence of pressure and temperature dependence of thermal properties of a lubricant on the behaviour of circular TEHD contacts'. In: *Tribology International* 43.10. 36th Leeds–Lyon Symposium Special Issue: Multi-facets of Tribology, pp. 1842 –1850. doi: `https://doi.org/10.1016/j.triboint.2009.10.002`.

Habchi, W., S. Bair, F. Qureshi and M. Covitch (2013). 'A Film Thickness Correction Formula for Double-Newtonian Shear-Thinning in Rolling EHL Circular Contacts'. In: *Tribology Letters* 50.1, pp. 59–66. doi: `10.1007/s11249-012-0078-6`.

Habchi, Wassim (2008). 'A Full-System Finite Element Approach to Elastohydrodynamic Lubrication Problems: Application to Ultra-Low-Viscosity Fluids'. PhD Thesis. Lyon: LaMCoS, INSA.

— (2014). 'A numerical model for the solution of thermal elastohydrodynamic lubrication in coated circular contacts'. In: *Tribology International* 73.Supplement C, pp. 57 –68. doi: `10.1016/j.triboint.2014.01.002`.

— (2015). 'Influence of thermo-mechanical properties of coatings on friction in elastohydrodynamic lubricated contacts'. In: *Tribology International* 90, pp. 113–122.

Hajishafiee, Alireza (2013). 'Finite-volume CFD modelling of fluid-solid interaction in EHL contacts'. PhD thesis. Tribology section Department of Mechanical Engineering Imperial College London.

Hamrock, B. J. (1991). *Fluid Film Lubrication*. Technical Report NASA-RP-1255. NASA, Washington, United States.

Hamrock, Bernard J. and Duncan Dowson (1976). 'Isothermal Elastohydrodynamic Lubrication of Point Contacts: Part 1–Theoretical Formulation'. In: *Journal of Lubrication Technology* 98.2, pp. 223–228. doi: `10.1115/1.3452801`.

— (1981). *Ball Bearing Lubrication*. John Wiley & Sons. isbn: 0-471-03553-X.

— (1983). *Film Thickness for Different Regimes of Fluid-Film Lubrication*. Tech. rep. NASA.

Harris, Tedric A. (1966). *Rolling Bearing Analysis*. Wiley.

— (1991). *Rolling Bearing Analysis*. 3rd. John Wiley & Sons Inc., New York.

Hartinger, Markus (2007). 'CFD Modelling of Elastohydrodynamic Lubrication'. PhD Thesis. London: Imperial College London.

HARTINGER, Markus, Marie-Laure DUMONT, Stathis IOANNIDES, David GOSMAN and Hugh SPIKES (2008). 'CFD Modeling of a Thermal and Shear-Thinning Elastohydrodynamic Line Contact'. In: *J. Tribol.* 130.4, p. 041503. DOI: 10.1115/1.2958077.

HERTZ, Heinrich (1881). 'Über die Berührung fester elastischer Körper'. In: *Journal für die reine und angewandte Mathematik* 92, pp. 156–171.

HIRST, W. and A. A. MOORE (1979). 'Elastohydrodynamic lubrication at high pressures II. Non-Newtonian behaviour'. In: *Proceedings of the Royal Society of London A: Mathematical, Physical and Engineering Sciences* 365.1723, pp. 537–565. DOI: 10.1098/rspa.1979.0033.

HIRST, W. and A. J. MOORE (1974). 'Non-Newtonian behaviour in elastohydrodynamic lubrication'. In: *Proceedings of the Royal Society of London A: Mathematical, Physical and Engineering Sciences* 337.1608, pp. 101–121. DOI: 10.1098/rspa.1974.0040.

HÖGLUND, E. (1984). 'Elastohydrodynamic lubrication, interferometric measurements, lubricant rheology and subsurface stresses.' Doctoral Thesis 32D. Luleå University.

HÖGLUND, E. and B. O. JACOBSON (1986). 'Experimental Investigation of the Shear Strength of Lubricants Subjected to High Pressure and Temperature'. In: *Journal of Tribology* 108.4, pp. 571–577. DOI: 10.1115/1.3261267.

HOUPERT, Luc (1980). 'Contribution a l'etude du frottement dans un contact elastohydrodynamic'. Thése de Docteuer no IDI 3-8019. I.N.S.A. Lyon.

HOUPERT, Luc, L. FLAMAND and D. BERTHE (1981). 'Rheological and Thermal Effects in Lubricated E. H. D. Contacts'. In: *ASME Journal of Lubrication Technology* 103, pp. 526–532. DOI: 10.1115/1.3251731.

HSIAO, Hsing-Sen S. and Bernard J. HAMROCK (1992). 'A Complete Solution for Thermal-Elastohydrodynamic Lubrication of Line Contacts Using Circular Non-Newtonian Fluid Model'. In: *Journal of Tribology* 114.3, pp. 540–551. DOI: 10.1115/1.2920916.

HUTTON, J. F. (1984). 'Reassessment of rheological properties of LVI 260'. In: *ASME Journal of Lubrication Technology* 106, pp. 536–537. DOI: 10.1115/1.3260978.

HUTTON, J. F. and M. C. PHILLIPS (1972). 'Shear Modulus of Liquids at Elastohydrodynamic Lubrication Pressures'. In: *Nature Physical Science*. DOI: 10.1038/physci238141b0.

IRVING, J. B. and A. J. BARLOW (1971). 'An automatic high pressure viscometer'. In: *Journal of Physics E: Scientific Instruments* 4.3, pp. 232–236.

JACOBSON, B. O. (1985). 'A High Pressure-Short Time Shear Strength Analyzer for Lubricants'. In: *Journal of Tribology*. DOI: 10.1115/1.3261024.

JACOBSON, B.O. (1991). *Rheology and elastohydrodynamic lubrication, Tribology series*. Vol. 54. Elsevier.

JACOBSON, B.O. (2006). 'High-pressure chamber measurements.' In: *Proc IMechE, Part J: J Engineering Tribology* 220.3, pp. 199–206. DOI: 10.1243/13506501JET133.

JAEGER, John Conrad (1942). 'Moving sources of heat and the temperature at sliding contacts'. In: *Journal and Proceedings of the Royal Society of New South Wales* 76.17, pp. 203–227.

JANG, J. Y., M. M. KHONSARI and Scott S. BAIR (2008). 'Correction Factor Formula to Predict the Central and Minimum Film Thickness for Shear-Thinning Fluids in EHL'. In: *Journal of Tribology* 130.2, pp. 024501–1–4. DOI: 10.1115/1.2842249.

JOHNSON, K. L. (1955). 'Surface interaction between elastically loaded bodies under tangential forces'. In: *Proceedings of the Royal Society of London A: Mathematical, Physical and Engineering Sciences* 230.1183, pp. 531–548. DOI: 10.1098/rspa.1955.0149.

— (1970). 'Regimes of Elastohydrodynamic Lubrication'. In: *Journal of Mechanical Engineering Science* 12.1, pp. 9–16. DOI: 10.1243/JMES_JOUR_1970_012_004_02.

— (1978). 'Introductory Review of Lubricant Rheology and Traction'. In: *Elastohydrodynamics and related topics: Proceedings of the 5th Leeds-Lyon Symposion on Tribology*. Ed. by D. DOWSON. V(i). Mechanical Engineering Publications for the Institute of Tribology, Leeds University and the Institut national des sciences appliquées de Lyon, pp. 155–161.

JOHNSON, K. L. and R. CAMERON (1967). 'Fourth Paper: Shear Behaviour of Elastohydrodynamic Oil Films at High Rolling Contact Pressures'. In: *Proceedings of the Institution of Mechanical Engineers* 182.1, pp. 307–330. DOI: 10.1243/PIME_PROC_1967_182_029_02.

JOHNSON, K. L. and J. A. GREENWOOD (1980). 'Thermal analysis of an Eyring fluid in elastohydrodynamic traction'. In: *Wear* 61.2, pp. 353–374. DOI: 10.1016/0043-1648(80)90298-7.

JOHNSON, K. L., J. A. GREENWOOD and S. Y. POON (1972). 'A simple theory of asperity contact in elastohydro-dynamic lubrication'. In: *Wear* 19.1, pp. 91 –108. DOI: 10.1016/0043-1648(72)90445-0.

JOHNSON, K.L. and A.D. ROBERTS (1974). 'Observations of Viscoelastic Behaviour of an Elastohydrodynamic Lubricant Film'. In: *Proceedings of the Royal Society of London A: Mathematical, Physical and Engineering Sciences* 337.1609, pp. 217–242. DOI: 10.1098/rspa.1974.0046.

JOHNSON, K.L. and J.L. TEVAARWERK (1977). 'Shear behaviour of elastohydrodynamic oil films.' In: *Proceedings of the Royal Society of London A: Mathematical, Physical and Engineering Sciences* 356, pp. 215–236. DOI: 10.1098/rspa.1977.0129.

KANETA, M., H. NISHIKAWA and K. KAMEISHI (1990). 'Observation of Wall Slip in Elastohydrodynamic Lubrication'. In: *Journal of Tribology* 112.3, pp. 447–452. DOI: 10.1115/1.2920280.

KANETA, M., H. NISHIKAWA, K. KAMEISHI, T. SAKAI and N. OHNO (1992). 'Effects of Elastic Moduli of Contact Surfaces in Elastohydrodynamic Lubrication'. In: *Journal of Tribology* 114.1, pp. 75–80. DOI: 10.1115/1.2920871.

KIM, H. J., P. EHRET, D. D. DOWSON and C. M. TAYLOR (2001). 'Thermal elastohydrodynamic analysis of circular contacts Part 1: Newtonian model'. In: *Proceedings of the Institution of Mechanical Engineers, Part J: Journal of Engineering Tribology* 215.4, pp. 339–352. DOI: 10.1243/1350650011543583.

KIM, Kyung Hoon and Farshid SADEGHI (1992). 'Three-Dimensional Temperature Distribution in EHD Lubrication: Part I–Circular Contact'. In: *Journal of Tribology* 114.1, pp. 32–41. DOI: 10.1115/1.2920864.

— (1993). 'Three-Dimensional Temperature Distribution in EHD Lubrication: Part II–Point Contact and Numerical Formulation'. In: *Journal of Tribology* 115.1, pp. 36–45. DOI: 10.1115/1.2920984.

KNEIZYS, F. X., G. P. ANDERSON, E.P. SHETTLE, W.O. GALLERY, L.W. ABREU, J.E.A. SELBY, J.H. CHETWYND and S.A. CLOUGH (1988). *Users Guide to LOWTRAN 7*. Environmental Research Papers, No. 1010 AFGL-TR-88-04 77. Air Force Geophysics Laboratory.

KREIL, O. (2007). *Viskositätsverhältnis Kappa, Bestimmung des Viskositätsverhältnisses κ in Wälzlagern*. Tech. rep. FVA, Forschungsvorhaben Nr. 418 Heft 812.

KUHLMANN, Jens (2009). 'Tribologische Eigenschaften von Wälzlagerschmierfetten bei dauerhaft niedrigen Betriebstemperaturen'. PhD thesis. Leibniz Universität Hannover, IMKT.

KUMAR, Punit and Parinam ANURADHA (2014). 'Elastohydrodynamic Lubrication Model With Limiting Shear Stress Behavior Considering Realistic Shear-Thinning and Piezo-Viscous Response'. In: *Journal of Tribology* 136.2, pp. 021503–021503–8. DOI: 10.1115/1.4026111.

KUMAR, Punit and M. M. KHONSARI (2008). 'EHL Circular Contact Film Thickness Correction Factor for Shear-Thinning Fluids'. In: *Journal of Tribology* 130.4, pp. 041506–1–7. DOI: 10.1115/1.2959115.

KUSS, E. (1982). *pVT-Daten und Druckviskosität von ausgesuchten Mineralölen*. Research Report Series Forschungsheft Nr. 198. Deutsch Gesellschaft für Mineralölwissenschaft und Kohlechemie e.V.

LE ROUZIC, Julian and Tom REDDYHOFF (2013). 'Development of Infrared Microscopy for Measuring Asperity Contact Temperatures'. In: *Journal of Tribology* 135.2, p. 021504. DOI: 10.1115/1.4023148.

LEEUWEN, H. J. van, H. A.; MEIJER and M. J. W. SCHOUTEN (1987). 'Elastohydrodynamic film thickness and temperature measurements in dynamically loaded concentrated contacts : eccentric cam-flat follower'. In: *Fluid film lubrication - Osborne Reynolds centenary : proceedings of the 13th Leeds-Lyon symposium, held in Boding-*

ton Hall, the University of Leeds, England, 8-12 September 1986. Ed. by D. Dowson, C. M. Taylor and M. Godet. Vol. 13. Tribology series. Amsterdam: Elsevier, pp. 611–625.

Leeuwen, Harry van (2009). 'The determination of the pressure-viscosity coefficient of a lubricant through an accurate film thickness formula and accurate film thickness measurements'. In: *Proceedings of the Institution of Mechanical Engineers, Part J: Journal of Engineering Tribology* 223.8, pp. 1143–1163. doi: 10.1243/13506501JET504.

Liu, Yuchuan, Q. Jane Wang, Scott Bair and Philippe Vergne (2007). 'A Quantitative Solution for the Full Shear-Thinning EHL Point Contact Problem Including Traction'. In: *Tribology Letters* 28.2, pp. 171–181. doi: 10.1007/s11249-007-9262-5.

Loewenthal, Stuart H. and Douglas A. Rohn (1983). *Regression Analysis of Traction Characteristics of Two Traction Fluids*. NASA Technical Paper 2154. NASA.

Lohner, Thomas, Klaus Michaelis and Karsten Stahl (2016). 'Limiting Shear Stress Formulation for TEHL Simulation'. In: doi: 10.7712/100016.1910.9225.

Lu, Jia, Tom Reddyhoff and Daniele Dini (2017). '3D Measurements of Lubricant and Surface Temperatures Within an Elastohydrodynamic Contact'. In: *Tribology Letters* 66.1, p. 7. doi: 10.1007/s11249-017-0953-2.

Lubrecht, A. A. (1987). 'The Numerical Solution of the Elastohydrodynamically Lubricated Line- and Point Contact Problem, Using Multigrid Techniques'. PhD thesis. Universiteit Twente.

Lugt, P. M. and G. E. Morales-Espejel (2011). 'A Review of Elasto-Hydrodynamic Lubrication Theory'. In: *Tribology Transactions* 54.3, pp. 470–496. doi: 10.1080/10402004.2010.551804.

Manning, R. E. (1974). 'Computational Aids for Kinematic Viscosity Conversions from 100 and 210 F to 40 and 100 °C '. In: *J. Testing Eval.* 2.6, pp. 522–528.

Martinie, Laetitia and Philippe Vergne (2016). 'Lubrication at Extreme Conditions: A Discussion About the Limiting Shear Stress Concept'. In: *Tribology Letters* 63.2, p. 21. doi: 10.1007/s11249-016-0709-4.

Marx, Johannes (2015). 'Weiterentwicklung und Inbetriebnahme eines Thermografiesystems zur Bestimmung der Temperatur in einem EHD-Kontakt'. unpublished Bachelors thesis.

Maxwell, J. Clerk (1867). 'On the Dynamical Theory of Gases'. In: *Philosophical Transactions of the Royal Society of London* 157, pp. 49–88.

Mayer, Josef (2013). 'Einfluss der Oberfläche und des Schmierstoffs auf das Reibungsverhalten im EHD-Kontakt'. Dissertation. Munich: Technical University of Munich.

Meyer, Carsten (2010a). *Reibung fettgeschmierter Wälzlager II*. Tech. rep. FVA.

—   (2010b). 'Reibung in hoch belasteten EHD-Wälzkontakten (*Friction in highly loaded EHL contacts*)'. Dissertation. Leibniz Universität Hannover, IMKT.

MINDLIN, R. D. (1949). 'Compliance of Elastic Bodies in Contact'. In: *ASME Journal of Applied Mechanics*.

MORGADO, P Lafont, J Echávarri OTERO, J B Sánchez-Peñuela LEJARRAGA, J L Muñoz SANZ, A Díaz LANTADA, J M MUNOZ-GUIJOSA, H Lorenzo YUSTOS, P Leal WIÑA and J Muñoz GARCÍA (2009). 'Models for predicting friction coefficient and parameters with influence in elastohydrodynamic lubrication'. In: *Proceedings of the Institution of Mechanical Engineers, Part J: Journal of Engineering Tribology* 223.7, pp. 949–958. DOI: `10.1243/13506501JET599`.

MURCH, L. E. and W. R. D. WILSON (1975). 'A thermal elastohydrodynamic inlet zone analysis'. In: *Journal of Lubrication Technology* 97.2, pp. 212–216. DOI: `10.1115/1.3452559`.

MURNAGHAN, Francis D. (1951). *Finite Deformation of an Elastic Solid*. New York: John Wiley & Sons, London: Chapman & Hall Limited.

NAGARAJ, H.S., D.M. SANBORN and W.O. WINER (1979). 'Surface Temperature Measurements in Rolling and Sliding EHD Contacts'. In: *A S L E Transactions* 22.3, pp. 277–285. DOI: `10.1080/05698197908 982925`.

NDIAYE, S.-N. (2017). 'Ultimate behavior of confined fluids under very high pressure and shear stress'. PhD thesis. INSA Lyon.

NDIAYE, S.-N., L. MARTINIE, D. PHILIPPON, N. DEVAUX and P. VERGNE (2017). 'A Quantitative Friction-Based Approach of the Limiting Shear Stress Pressure and Temperature Dependence'. In: *Tribology Letters* 65.4, p. 149. DOI: `10.1007/s11249-017-0929-2`.

NEUBAUER, Timo (2007). 'Untersuchung des elastischen Schlupfs im Wälzkontakt mit der FE-Methode'. Student Thesis, –unpublished. Hannover: Leibniz Universitaet Hannover.

OLDROYD, J. G. (1950). 'On the formulation of rheological equations of state'. In: *Proceedings of the Royal Society of London A: Mathematical, Physical and Engineering Sciences* 200.1063, pp. 523–541. DOI: `10.1 098/rspa.1950.0035`.

PAREDES, Xavier, Olivia FANDIÑO, Alfonso S. PENSADO, María J.P. COMUÑAS and Josefa FERNÁNDEZ (2012). 'Experimental density and viscosity measurements of di(2ethylhexyl)sebacate at high pressure'. In: *The Journal of Chemical Thermodynamics* 44.1, pp. 38 –43. DOI: `https://doi.org/10.1016/j.jct.2011.07.005`.

PATIR, Nadir and H. S. CHENG (1978). 'An Average Flow Model for Determining Effects of Three-Dimensional Roughness on Partial Hydrodynamic Lubrication'. In: *Journal of Lubrication Technology*. DOI: `10.1115/1.3453103`.

PATIR, Nadir and H. S. CHENG (1979). 'Application of Average Flow Model to Lubrication Between Rough Sliding Surfaces'. In: *Journal of Lubrication Technology*. DOI: 10.1115/1.3453329.

PEEKEN, H., P. AYANOGLU, G. KNOLL and G. WELSCH (1990). 'Measurement of lubricating film thickness, temperature and pressure in gear contacts with surface topography as a parameter'. In: *Lubrication Science* 3.1, pp. 33–42. DOI: 10.1002/ls.3010030103.

PEIRAN, Yang and Wen SHIZHU (1990a). 'A Generalized Reynolds Equation for Non-Newtonian Thermal Elastohydrodynamic Lubrication'. In: *Journal of Tribology* 112.4, pp. 631–636. DOI: 10.1115/1.2920308.

— (1990b). 'A generalized Reynolds equation based on non-Newtonian flow in lubrication mechanics'. In: *Acta Mechanica Sinica* 6.4, pp. 289–295. DOI: 10.1007/BF02486885.

PEKLENIK, J. (1967). 'Paper 24: New Developments in Surface Characterization and Measurements by Means of Random Process Analysis'. In: *Proceedings of the Institution of Mechanical Engineers, Conference Proceedings* 182.11, pp. 108–126. DOI: 10.1243/PIME_CONF_1967_182_309_02.

PHAN THIEN, Nhan (1978). 'A Nonlinear Network Viscoelastic Model'. In: *Journal of Rheology* 22.3, pp. 259–283.

PHAN THIEN, Nhan and Roger I. TANNER (1977). 'A new constitutive equation derived from network theory'. In: *Journal of Non-Newtonian Fluid Mechanics* 2.4, pp. 353 –365. DOI: https://doi.org/10.1016/0377-0257(77)80021-9.

PITENIS, Angela A., Duncan DOWSON and Gregory W. SAWYER (2014). 'Leonardo da Vinci's Friction Experiments: An Old Story Acknowledged and Repeated'. In: *Tribology Letters* 56.3, pp. 509–515. DOI: 10.1007/s11249-014-0428-7.

PLINT, M. A. (1967). 'Third Paper: Traction in Elastohydrodynamic Contacts'. In: *Proceedings of the Institution of Mechanical Engineers* 182.1, pp. 300–306. DOI: 10.1243/PIME_PROC_1967_182_028_02.

POLL, G. and Ding WANG (2012). 'Fluid rheology, traction/creep relationships and friction in machine elements with rolling contacts.' In: *Proc IMechE, Part J: J Engineering Tribology* 226.6, pp. 481–500. DOI: 10.1177/1350650111431790.

POLL, Gerhard (1983). 'Der Einfluss der realen Systemeigenschaften auf die Kraftschlussgesetze bei wälzender Relativbewegung (*Influence of system properties on traction in rolling/sliding motion*)'. Dissertation. Rheinisch-Westfälische Technische Hochschule Aachen.

POOLE, R. J. (2012). 'The Deborah and Weissenberg numbers'. In: *British Society of Rheology, Rheology Bulletin*.

QURESHI, Farrukh (1992). 'Kinematics of Shear Deformation of Materials Under High Pressure and Shear Stress'. PhD Thesis. Atlanta: Georgia Institute of Technology.

RAMAN, C. V. (1923). 'A theory of the viscosity of liquids'. In: *Nature (London)* 111, pp. 532–533. DOI: `10.1038/111532b0`.

RAMESH, K. T. (1989). 'On the Rheology of a Traction Fluid'. In: *Journal of Tribology*. DOI: `10.1115/1.3261985`.

REDDYHOFF, T., H.A. SPIKES and A.V. OLVER (2009a). 'Compression Heating and Cooling in Elastohydrodynamic Contacts'. In: *Tribology Letters* 36.1, pp. 69–80. DOI: `10.1007/s11249-009-9461-3`.

— (2009b). 'Improved infrared temperature mapping of elastohydrodynamic contacts'. In: *Proceedings of the Institution of Mechanical Engineers, Part J: Journal of Engineering Tribology* 223.8, pp. 1165–1177. DOI: `10.1243/13506501JET499`.

REE, Taikyue and Henry EYRING (1955). 'Theory of Non-Newtonian Flow. I. Solid Plastic System'. In: *Journal of Applied Physics* 26.7, pp. 793–800. DOI: `10.1063/1.1722098`.

REINER, M. (1964). 'The Deborah Number'. In: *Physics Today* 17.1, pp. 62–62. DOI: `10.1063/1.3051374`.

RESHTOV, D. N. and S. V. GRYAZIN (1990). 'Estimation of Friction Forces with the Limit Shear Stress in the Lubricant Taken Into Account'. In: *Design, Testing and Reliability of Machines, Englisch translation of Vestnik Mashinostroeniya* 70.3, pp. 8–10.

REYNOLDS, Osborne (1876). 'On Rolling-Friction'. In: *Philosophical Transactions of the Royal Society of London* 166, pp. 155–174.

— (1886). 'On the Theory of Lubrication and Its Application to Mr. Beauchamp Tower's Experiments, Including an Experimental Determination of the Viscosity of Olive Oil'. In: *Phil. Trans. R. Soc. Lond.* 177, pp. 157–234. DOI: `10.1098/rstl.1886.0005`.

ROELANDS, Cornelius Julianus Adrianus (1966). 'Correlational aspects of the viscosity–temperature–pressure relationship of lubricating oils'. PhD Thesis. Delft University of Technology, Netherlands.

SCHIPPER, D. J., P. H. VROEGOP, A. W. J. de GEE and R. BOSMA (1990). 'Micro-EHL in Lubricated Concentrated Contacts'. In: *Journal of Tribology* 112.2, pp. 392–397. DOI: `10.1115/1.2920269`.

SCHIRRU, Michele M. and Rob S. DWYER-JOYCE (2016). 'A model for the reflection of shear ultrasonic waves at a thin liquid film and its application to viscometry in a journal bearing'. In: *Proceedings of the Institution of Mechanical Engineers, Part J: Journal of Engineering Tribology* 230.6, pp. 667–679. DOI: `10.1177/1350650115610357`.

SCHMELZ, Friedrich and Christoph MÜLLER (2001). *Sechsstellige Hilfswerte nach Heinrich Hertz, Daraus berechnet die vierstelligen elliptischen Koeffizienten*. Polygon-Verlag. ISBN: 978-3-928671-31-6.

SCHMIDT, K., S. BAIR and J.P.M. TRUSLER (2016). 'The viscosity of Squalane Revisited – An Updated Reference Model'. In: *16th Meeting of the International Association for Transport Properties*.

SCHMIDT, Uwe (1985). 'Die Schmierfilmbildung in Elastohydrodynamisch beanspruchten Wälzkontakten unter Berücksichtigung der Oberflächenrauheit'. PhD thesis. Universität Hannover.

Seeton, Christopher J. (2006). 'Viscosity-temperature correlation for liquids'. In: *Tribology Letters* 22.1, pp. 67–78. DOI: 10.1007/s11249-006-9071-2.

Shieh, Jinn an and Bernard J. Hamrock (1991). 'Film Collapse in EHL and Micro-EHL'. In: *Journal of Tribology* 113.2, pp. 372–377. DOI: 10.1115/1.2920631.

Shirzadegan, Mohammad (2015). 'Elastohydrodynamic Lubrication of Cam and Roller Follower'. PhD Thesis. Luleå: Luleå University of Technology.

Shirzadegan, Mohammad, Marcus Björling, Andreas Almqvist and Roland Larsson (2016). 'Low degree of freedom approach for predicting friction in elastohydrodynamically lubricated contacts'. In: *Tribology International* 94.Supplement C, pp. 560 –570. DOI: 10.1016/j.triboint.2015.10.010.

Slotte, K. F. (1881). 'Ueber die innere Reibung der Lösungen einiger Chromate'. In: *Annalen der Physik* 250.9, pp. 13–22. DOI: 10.1002/andp.18812500903.

Smith, F. W. (1960). 'Lubricant Behavior in Concentrated Contact–Some Rheological Problems'. In: *A S L E Transactions* 3.1, pp. 18–25. DOI: 10.1080/05698196008972381.

So, B. Y. C. and E. E. Klaus (1980). 'Viscosity-Pressure Correlation of Liquids'. In: *A S L E Transactions* 23.4, pp. 409–421. DOI: 10.1080/05698198008982986.

Sottomayor, A. (2002). 'Reologia de um lubrificante não-Newtoniano no interior de um contacto termoelastohidrodinâmico. Determinação dos parâmetros reológicos de um lubrificante'. Tese de Doutoramento. DEMEGI, Faculdade de Engenharia da Universidade do Porto.

Šperka, P., I. Křupka and M. Hartl (2014). 'Evidence of Plug Flow in Rolling–Sliding Elastohydrodynamic Contact'. In: *Tribology Letters* 54.2, pp. 151–160. DOI: 10.1007/s11249-014-0320-5.

Spikes, H. A. (1997). 'Mixed lubrication – an overview'. In: *Lubrication Science* 9.3, pp. 221–253. DOI: 10.1002/ls.3010090302.

Spikes, H. A. and A. V. Olver (2003). 'Basics of mixed lubrication'. In: *Lubrication Science* 16.1, pp. 1–28. DOI: 10.1002/ls.3010160102.

Spikes, Hugh and Zhang Jie (2014). 'History, Origins and Prediction of Elastohydrodynamic Friction'. In: *Tribology Letters* 56.1, pp. 1–25. DOI: 10.1007/s11249-014-0396-y.

Srirattayawong, Sutthinan (2014). 'CFD Study of Surface Roughness Effects on the Thermo-Elastohydrodynamic Lubrication Line Contact Problem'. PhD thesis. Engineering Department University of Leicester.

Ståhl, Jonas and B.O. Jacobson (2003). 'A non-Newtonian model based on limiting shear stress and slip planes-parametric studies'. In: *Tribology International* 36.11, pp. 801–806. DOI: 10.1016/s0301-679x(03)00096-3.

TANNER, Roger I. (1960). 'Full-film lubrication theory for a maxwell liquid'. In: *International Journal of Mechanical Sciences* 1.2, pp. 206–215. DOI: https://doi.org/10.1016/0020-7403(60)90040-0.

— (1965). 'Some Illustrative Problems in the Flow of Viscoelastic Non-Newtonian Lubricants'. In: *A S L E Transactions* 8.2, pp. 179–183. DOI: 10.1080/05698196508972091.

— (2000). *Engineering Rheology*. second. Oxford Engineering Science Series. OUP Oxford. ISBN: 9780199590160.

TEVAARWERK, J. and K.L. JOHNSON (1975). 'A simple non-linear constitutive equation for elastohydrodynamic oil films'. In: *Wear* 35.2, pp. 345 –356. DOI: https://doi.org/10.1016/0043-1648(75)90081-2.

TOLKIEN, John R. R. (1954). *The Fellowship of the Ring*. George Allen & Unwin.

VENNER, C. H. (1991). 'Multilevel Solution of the EHL Line and Point Contact Problems'. PhD thesis. Universiteit Twente.

VENNER, Cornelis Henricus and Antonius Adrianus LUBRECHT (2000). *Multi-level methods in lubrication*. Ed. by Duncan DOWSON. Vol. 37. Elsevier. ISBN: 978-0-444-50503-3.

VERGNE, Philippe and Scott BAIR (2014). 'Classical EHL Versus Quantitative EHL: A Perspective Part I—Real Viscosity-Pressure Dependence and the Viscosity-Pressure Coefficient for Predicting Film Thickness'. In: *Tribology Letters* 54.1, pp. 1–12. DOI: 10.1007/s11249-014-0302-7.

VOGEL, H. (1921). 'Das temperature-abhängigketsgesetz der viskosität von flüssigkeiten. (*The law of the relationship between viscosity of liquids and the temperature*)'. In: *Physikalische Zeitschrift* 22, pp. 645–646.

VOLLMER, M. and K. P. MÖLLMANN (2011). *Infrared Thermal Imaging: Fundamentals, Research, and Applications*. second. Weinheim: Wiley VHC.

WALBECK, Thomas (2004). 'Das Viskositätsverhalten und die Schmierfilmbildung von Schmierstoffen in Abhängigkeit von Druck und Temperatur'. Dissertation. Aachen: RWTH Aachen.

WALTHER, C. (1928). 'The variation of viscosity with temperature'. In: *Erdöl und Teer* 4, 510, 529 and 614.

— (1931). 'The variation of viscosity with temperature'. In: *Erdöl und Teer* 7, p. 382.

WAN, G.T.Y. and P.L. WONG (2010). 'Pressure Dependence of the Limiting Shear Stress Coefficient of Liquid Lubricants'. In: *Advanced Tribology: Proceedings of CIST2008 & ITS-IFToMM2008*. Ed. by Jianbin LUO, Yonggang MENG, Tianmin SHAO and Qian ZHAO. Berlin, Heidelberg: Springer Berlin Heidelberg, pp. 206–210. ISBN: 978-3-642-03653-8. DOI: 10.1007/978-3-642-03653-8_68.

Wang, D. and G. Poll (2013). 'Prediction of traction in EHL contacts.' In: *Proceedings of the 5th world tribology congress*. Palaolimpico Torino, Italy.

Wang, Ding (2015). 'Berechnung der Wälzlagerreibung aufgrund weiterentwickelter rheologischer Fluidmodelle (*Calculation of bearing friction using extended rheological fluid models)'*. Dissertation. IMKT, Leibniz Universität Hannover.

Ward, A. G. (1937). 'The viscosity of Pure Liquids'. In: *Transactions of the Faraday Society* 33, pp. 88–97.

Wheeler, Jean-David, Philippe Vergne, Nicolas Fillot and David Philippon (2016). 'On the relevance of analytical film thickness EHD equations for isothermal point contacts: Qualitative or quantitative predictions?' In: *Friction* 4.4, pp. 369–379. doi: `10.1007/s4 0544-016-0133-7`.

Wikström, Victoria and Erik Höglund (1994). 'Investigation of Parameters Affecting the Limiting Shear Stress-Pressure Coefficient: A New Model Incorporating Temperature'. In: *ASME Journal of Tribology* 116.3, pp. 612–620. doi: `10.1115/1.2928889`.

Williams, Malcolm L., Robert F. Landel and John D. Ferry (1955). 'The Temperature Dependence of Relaxation Mechanisms in Amorphous Polymers and Other Glass-forming Liquids'. In: *Journal of American Chemical Society* 77.14, pp. 3701–3707. doi: `10.1021/ja0 1619a008`.

Winer, W. O. and H. S. Cheng (1980). 'Wear Control Handbook'. In: ed. by M. B. Peterson and W. O. Winer. ASME Research Committee on Lubrication. Chap. Film Thickness, Contact Stress and Surface Temperatures.

Workel, M.F., D. Dowson, P. Ehret and C.M. Taylor (2000). 'The influence of mean contact pressure on the friction coefficient of a traction fluid at high pressure'. In: *Proceedings of the Institution of Mechanical Engineers, Part C: Journal of Mechanical Engineering Science* 214.2, pp. 309–312. doi: `10.1243/0954406001522976`.

Wright, W. A. (1969). In: *J. Mater. JMLSA* 4.11, p. 19.

Xi, Yinhu, Marcus Björling, Yijun Shi, Junhong Mao and Roland Larsson (2016). 'Traction formula for rolling-sliding contacts in consideration of roughness under low slide to roll ratios'. In: *Tribology International* 104.Supplement C, pp. 263 –271. doi: `10.1016 /j.triboint.2016.09.006`.

Yagi, Kazuyuki, Keiji Kyogoku and Tsunamitsu Nakahara (2006). 'Measurements of Temperature Distributions around Longitudinally Grooved Rough Surfaces in Sliding Elastohydrodynamic Point Contacts'. In: *Tribology Transactions* 49.4, pp. 482–489. doi: `10.1080/10402000600843778`.

Yasuda, K., R. C. Armstrong and R. E. Cohen (1981). 'Shear flow properties of concentrated solutions of linear and star branched

polystyrenes'. In: *Rheologica Acta* 20.2, pp. 163–178. DOI: 10.1007/BF01513059.

YASUTOMI, S., S. BAIR and W. O. WINER (1984a). 'An application of a free volume model to lubricant rheology 1 – dependence of viscosity on temperature and pressure'. In: *Journal of tribology* 106.2, pp. 291–302. DOI: 10.1115/1.3260907.

— (1984b). 'An application of a free volume model to lubricant rheology 2 –Variation in Viscosity of Binary Blended Lubricants'. In: *Journal of Tribology* 106.2, pp. 304–311. DOI: 10.1115/1.3260911.

YOKOYAMA, F. and H. A. SPIKES (2000). 'Film-Forming Properties of Polyol Esters, Polyphenyl Ethers and Their Mixtures Over a Wide Range of Temperature'. In: *Tribology Transactions* 43.1, pp. 130–136. DOI: 10.1080/10402000008982322.

ZHANG, Bo (2015). 'A Novel Model of the Equivalent Viscosity of Simple Viscoelastic Fluids'. In: *Journal of Tribology* 138.2, p. 021802. DOI: 10.1115/1.4031751.

ZHANG, Yongbin and Shizhu WEN (2002a). 'An Analysis of Elastohydrodynamic Lubrication with Limiting Shear Stress: Part I–Theory and Solutions'. In: *Tribology Transactions* 45.2, pp. 135–144. DOI: 10.1080/10402000208982532.

— (2002b). 'An Analysis of Elastohydrodynamic Lubrication with Limiting Shear Stress: Part II – Load Influence'. In: *Tribology Transactions* 45.2, pp. 211–216. DOI: 10.1080/10402000208982542.

ZHU, Dong and Q Jane WANG (2012). 'On the λ ratio range of mixed lubrication'. In: *Proceedings of the Institution of Mechanical Engineers, Part J: Journal of Engineering Tribology* 226.12, pp. 1010–1022. DOI: 10.1177/1350650112461867.

CURRICULUM VITAE

Norbert Fritz Bader

Geboren am 01.05.1985 in Pretoria

BERUFSTÄTIGKEIT

2012–2018 Wissenschaftlicher Mitarbeiter am Institut für Maschinenkonstruktion und Tribologie der Leibniz Universität Hannover

AUSBILDUNG

2006–2012 Studium des Maschinenbaus an der Leibniz Universität Hannover

Abschluss mit Dipl.-Ing. in den Schwerpunkten Mechanik und Konstruktion sowie Mechatronische Systeme

ZIVILDIENST

2005–2006 Im Bereich Naturschutz

SCHULE

2002–2005 Gymnasium Großburgwedel, Abschluss Abitur

1993–2001 Deutsche Internationale Schule Pretoria